

The Pennsylvania State University  
The Graduate School  
College of Engineering

**COMPARISON OF WATER, HELIUM, AND CARBON DIOXIDE  
AS COOLANTS FOR NEXT GENERATION POWER PLANTS  
USING TRACE**

A Thesis in  
Nuclear Engineering  
by  
Grant Garrett

© 2018 Grant Garrett

Submitted in Partial Fulfillment  
of the Requirements  
for the Degree of

Master of Science

May 2018

The thesis of Grant Garrett was reviewed and approved\* by the following:

Justin K. Watson

Associate Research Professor and Associate Professor of Nuclear Engineering  
Thesis Advisor

Fan-Bill Cheung

George L. Guillet Professor Mechanical and Nuclear Engineering

Arthur T. Motta

Chair and Professor in the Nuclear Engineering Program

\*Signatures are on file in the Graduate School.

# Abstract

The purpose of this study is to compare the use of water, helium, and carbon dioxide as coolants for Generation IV and fusion power plants. The Symbolic Nuclear Analysis Package (SNAP) was used to create input files for the TRAC/RELAP Advanced Computational Engine (TRACE) thermal hydraulics and neutronics coupled code representing this phenomenon. In addition, TRACE was used to perform simulations comparing how Helium, Carbon Dioxide, and water perform as coolants for power plant systems.

To start, a TRACE model was built for each coolant of this study that represented a 600  $MW_{th}$  fusion Field Reversed Configuration (FRC) power plant. The vessel and power source were the same for each model of this study. The TRACE models include all components of the primary side of a Rankin cycle power plant, including pumps, heat exchangers, a reactor vessel, pipes, coolant channels, etc. The reactor vessel in the TRACE models represented a hollow cylinder at vacuum with a fusion FRC power source inside this hollow cylinder. The materials that comprised the cylinder wall were chosen based on thermal conductivity, attenuation coefficients, and other factors. Part of the cylinder wall was coolant channels with the coolant flowing through it. Besides flow through the steam generators, most of the secondary side components were represented by a control system that calculated the turbine output work. Once the model for each coolant was built, simulations were performed to ensure the models reached steady state.

After the models prove to reach steady state, parameters were changed to optimize the performance of the systems for each coolant based on the various system requirements. The final water cooled model operated at similar conditions to those of a PWR. The final helium and carbon dioxide cooled models operated at conditions based on AGRs, GFRs, and other similar gas cooled systems. Simulations were performed, and the results were used to analyze how each coolant performs for the power system analyzed in this study. Before performing analysis based on the TRACE predicted results, verification was performed for helium and carbon dioxide in TRACE because TRACE is only verified and validated with water as the fluid in simulations.

To ensure the results from the helium cooled and carbon dioxide cooled TRACE models were reliable, the method of manufactured solutions was used to perform verification for various test cases. The TRACE results were compared to hand calculated results for identical test cases. The verification process determined the TRACE predicted results from the helium and carbon dioxide models were reliable for the range of conditions of each respective model. Further verification and validation can be performed for helium and carbon dioxide as fluids in TRACE models and simulations.

After performing the tasks mentioned in the previous paragraphs, analysis was performed based on the TRACE predicted results for each coolant. Based on the system requirements and the results from the TRACE simulations, it was determined that water was the best coolant for the system analyzed in this study. For the operating conditions used in this research, water was able to keep the temperature of certain materials below their maximum temperatures much easier than the helium and carbon dioxide cooled systems. Specifically, beryllium was used as a material in the system and was determined to have a maximum temperature of 800°C for its applications in this study. Additionally, this temperature limit restricts the efficiency and capabilities of the helium and carbon dioxide cooled systems. There is also uncertainty associated with the turbine efficiencies used in this study. This introduces uncertainty into the overall efficiency of the system for each coolant. So, the overall efficiency is not as important of a parameter in determining the best coolant for the system in this study as other parameters. Theoretically, the helium and carbon dioxide cooled systems should have a higher efficiency than the water cooled model. Modifications that could be made to the system of this study and their resulting potential impacts are considered and analyzed.

# Table of Contents

List of Figures	viii
List of Tables	xi
List of Symbols	xiii
Acknowledgments	xvi
<b>Chapter 1</b>	
Introduction	1
<b>Chapter 2</b>	
<b>TRACE Solution Methods</b>	<b>5</b>
2.1 Introduction . . . . .	5
2.2 TRACE Fluid Field Equations . . . . .	5
2.2.1 Finite Volume Thermal Hydraulic Equations . . . . .	6
2.2.2 Stability Enhancing Two-Step (SETS) Method . . . . .	10
2.2.2.1 Semi-Implicit Step Equations . . . . .	11
2.2.2.2 Stabilizer Step Equations . . . . .	15
2.3 Discretized Heat Transfer Equations . . . . .	18
2.4 External Property Table (XPTB) for Carbon Dioxide . . . . .	21
<b>Chapter 3</b>	
<b>Modeling</b>	<b>25</b>
3.1 Introduction . . . . .	25
3.2 Vessel . . . . .	26
3.2.1 Vessel Design . . . . .	27
3.2.2 Plasma Power Source . . . . .	30
3.3 Pumps . . . . .	32

3.3.1	Pumping Power . . . . .	32
3.4	Turbine . . . . .	33
3.5	Overall System Efficiency . . . . .	35
3.6	Water Cooled TRACE Model . . . . .	35
3.6.1	U-tube Steam Generator . . . . .	35
	3.6.1.1 U-tube Steam Generator Mesh Size Error Analysis	40
3.6.2	Pressurizer . . . . .	43
	3.6.2.1 Pressurizer TRACE Model . . . . .	44
3.6.3	Complete Water Cooled Model . . . . .	46
3.6.4	Water Cooled Model Operating Conditions . . . . .	47
3.7	Helium and Carbon Dioxide Cooled Models . . . . .	48
3.7.1	Helical Coil Steam Generator . . . . .	49
	3.7.1.1 Helical Coil Steam Generator Mesh Size Error Analysis . . . . .	52
3.7.2	Complete Helium and Carbon Dioxide Models . . . . .	53
3.7.3	Helium Cooled Model Operating Conditions . . . . .	54
3.7.4	Carbon Dioxide Cooled Model Operating Parameters . . . . .	55
3.8	Summary of Operating Conditions . . . . .	56

## Chapter 4

	<b>Verification of Helium and Carbon Dioxide in TRACE</b>	<b>57</b>
4.1	Introduction . . . . .	57
4.2	TRACE Model . . . . .	58
4.3	Hand Calculations . . . . .	60
4.4	Results . . . . .	62
4.4.1	Helium Verification Test Results . . . . .	62
	4.4.1.1 Horizontal Adiabatic Verification Case Results . . . . .	62
	4.4.1.2 Horizontal Non-Adiabatic Verification Case Results . . . . .	63
	4.4.1.3 Vertical Adiabatic Verification Case Results . . . . .	64
	4.4.1.4 Vertical Non-Adiabatic Verification Case Results . . . . .	65
4.4.2	Carbon Dioxide Verification Test Results . . . . .	67
	4.4.2.1 Horizontal Adiabatic Verification Case Results . . . . .	67
	4.4.2.2 Horizontal Non-Adiabatic Verification Case Results . . . . .	68
	4.4.2.3 Vertical Adiabatic Verification Case Results . . . . .	69
	4.4.2.4 Vertical Non-Adiabatic Verification Case Results . . . . .	70
	4.4.2.5 Carbon Dioxide XPTB Verifiaction . . . . .	71
4.5	Chapter Conclusion . . . . .	73

<b>Chapter 5</b>	
<b>Results</b>	<b>74</b>
5.1 Introduction . . . . .	74
5.1.1 Coolant Pressure Drop in Vessel . . . . .	74
5.1.2 Coolant Axial Density Profile in Vessel . . . . .	76
5.1.3 Coolant Axial Temperature Profile in Vessel . . . . .	78
5.1.4 Axial Coolant Velocity Profiles in Vessel . . . . .	82
5.1.5 Heat Transfer Coefficient in Coolant Channels . . . . .	84
5.1.6 Beryllium Axial Temperature Profile in Vessel . . . . .	85
5.1.7 Overall Efficiency . . . . .	87
5.2 Analysis . . . . .	88
<b>Chapter 6</b>	
<b>Conclusions and Future Work</b>	<b>94</b>
<b>Appendix A</b>	
<b>Input File For TRACE Water Cooled Model</b>	<b>96</b>
A.1 Introduction . . . . .	96
A.2 TRACE Water Cooled Model Input File . . . . .	96
<b>Appendix B</b>	
<b>Input File For TRACE Helium Cooled Model</b>	<b>110</b>
B.1 Introduction . . . . .	110
B.2 TRACE Helium Cooled Model Input File . . . . .	110
<b>Appendix C</b>	
<b>Input File For TRACE Carbon Dioxide Cooled Model</b>	<b>130</b>
C.1 Introduction . . . . .	130
C.2 TRACE Carbon Dioxide Cooled Model Input File . . . . .	130
<b>Appendix D</b>	
<b>Chapter 5 Plots Values</b>	<b>149</b>
D.1 Introduction . . . . .	149
D.2 Chapter 5 Plot Results . . . . .	149
<b>Bibliography</b>	<b>164</b>

# List of Figures

2.1	Staggered Mesh Example for the Finite Volume Method used in TRACE . . . . .	6
2.2	Cylindrical Wall Geometry . . . . .	19
2.3	XPTB Column Structure . . . . .	24
2.4	NISTPROPGEN Executable Prompt . . . . .	24
3.1	Basic Design of Power Plant System used in this Study . . . . .	26
3.2	Axial Section of Vessel . . . . .	27
3.3	Vessel Cross Section (Figure not to scale) . . . . .	28
3.4	Example Cross Section of a FRC Plasma . . . . .	31
3.5	Pump 70 Pumping Power Control System for the TRACE Water Cooled Model . . . . .	33
3.6	Water Cooled Model Turbine Control System . . . . .	35
3.7	U-tube Steam Generator . . . . .	36
3.8	TRACE U-tube Steam Generator Model . . . . .	39
3.9	U-tube Steam Generator Feedwater Controller . . . . .	40
3.10	U-tube Liquid Velocity vs Time at 12.157594 m from the entrance of the u-tubes. Mesh Length=2.242406 m. . . . .	41
3.11	U-tube Liquid Velocity vs Time at 12.157594 m from the entrance of the u-tubes. Mesh Length=1.121203 m. . . . .	41
3.12	U-tube Liquid Velocity vs Time at 12.157594 m from the entrance of the u-tubes. Mesh Length= 0.560601 m. . . . .	41
3.13	Cutaway of a Pressurizer . . . . .	44
3.14	Pressurizer Geometry . . . . .	45
3.15	TRACE Pressurizer Model . . . . .	46
3.16	TRACE Water Cooled complete model . . . . .	47
3.17	Cutaway of a Helical Coil Steam Generator . . . . .	49
3.18	TRACE Helical Coil Steam Generator Model . . . . .	50
3.19	TRACE Helium and Carbon Dioxide Cooled Model . . . . .	54
4.1	Horizontal Verification TRACE model . . . . .	59
4.2	Vertical Verification TRACE model . . . . .	59



4.3	Helium Velocity Horizontal Adiabatic Verification Test Case . . . . .	62
4.4	Helium Pressure Horizontal Adiabatic Verification Test Case . . . . .	63
4.5	Helium Temperature Horizontal Non-Adiabatic Verification Test Case	63
4.6	Helium Velocity Horizontal Non-Adiabatic Verification Test Case . .	64
4.7	Helium Pressure Horizontal Non-Adiabatic Verification Test Case .	64
4.8	Helium Velocity Vertical Adiabatic Verification Test Case . . . . .	65
4.9	Helium Pressure Vertical Adiabatic Verification Test Case . . . . .	65
4.10	Helium Temperature Vertical Non-Adiabatic Verification Test Case	66
4.11	Helium Velocity Vertical Non-Adiabatic Verification Test Case . . .	66
4.12	Helium Pressure Vertical Non-Adiabatic Verification Test Case . . .	66
4.13	Carbon Dioxide Velocity Horizontal Adiabatic Verification Test Case	67
4.14	Carbon Dioxide Pressure Horizontal Adiabatic Verification Test Case	67
4.15	Carbon Dioxide Temperature Horizontal Non-Adiabatic Verification Test Case . . . . .	68
4.16	Carbon Dioxide Velocity Horizontal Non-Adiabatic Verification Test Case . . . . .	68
4.17	Carbon Dioxide Pressure Horizontal Non-Adiabatic Verification Test Case . . . . .	69
4.18	Carbon Dioxide Velocity Vertical Adiabatic Verification Test Case .	69
4.19	Carbon Dioxide Pressure Vertical Adiabatic Verification Test Case .	70
4.20	Carbon Dioxide Temperature Vertical Non-Adiabatic Verification Test Case . . . . .	70
4.21	Carbon Dioxide Velocity Vertical Non-Adiabatic Verification Test Case . . . . .	71
4.22	Carbon Dioxide Pressure Vertical Non-Adiabatic Verification Test Case . . . . .	71
5.1	Coolant Loop 1 Axial Pressure Profile at Steady State . . . . .	75
5.2	Coolant Loop 2 Axial Pressure Profile at Steady State . . . . .	75
5.3	Coolant Loop 3 Axial Pressure Profile at Steady State . . . . .	76
5.4	Coolant Loop 1 Axial Density Profile at Steady State . . . . .	77
5.5	Coolant Loop 2 Axial Density Profile at Steady State . . . . .	77
5.6	Coolant Loop 3 Axial Density Profile at Steady State . . . . .	77
5.7	Coolant Loop 1 Coolant Axial Temperature Profile at Steady State	78
5.8	Coolant Loop 2 Coolant Axial Temperature Profile at Steady State	79
5.9	Coolant Loop 3 Coolant Axial Temperature Profile at Steady State	79
5.10	Coolant Loop 1 Axial Velocity Profile at Steady State . . . . .	83
5.11	Coolant Loop 2 Axial Velocity Profile at Steady State . . . . .	83
5.12	Coolant Loop 3 Axial Velocity Profile at Steady State . . . . .	83
5.13	Heat Transfer Coefficients Axial Profile in Vessel at Steady State . .	85

5.14 Beryllium Axial Temperature Profile in Vessel at Steady State . . . 86

# List of Tables

3.1	U-tube Steam Generator Richardson Extrapolation Results and Values Used . . . . .	42
3.2	Pressurizer Operating Conditions . . . . .	46
3.3	Water Cooled Model Primary Side Operating Conditions . . . . .	48
3.4	Water Cooled Model Secondary Side Operating Conditions . . . . .	48
3.5	Helical Coil Steam Generator Richardson Extrapolation Results and Values Used . . . . .	53
3.6	Helium Cooled Model Primary Side Operating Conditions . . . . .	55
3.7	Helium Cooled Model Secondary Side Operating Conditions . . . . .	55
3.8	Carbon Dioxide Cooled Model Primary Side Operating Conditions . . . . .	56
3.9	Carbon Dioxide Cooled Model Secondary Side Operating Conditions . . . . .	56
3.10	Primary Side Operating Conditions . . . . .	56
3.11	Secondary Side Operating Conditions . . . . .	56
4.1	Helium Verification Model Boundary Conditions . . . . .	60
4.2	Carbon Dioxide Verification Model Boundary Conditions . . . . .	60
4.3	Carbon Dioxide Cell 5 XPTB Verification Test . . . . .	72
4.4	Carbon Dioxide Cell 10 XPTB Verification Test . . . . .	72
5.1	Mass Flow Rates for a Single Coolant Loop TRACE Models . . . . .	80
5.2	Specific Heat Coolant Loop 1 . . . . .	80
5.3	Specific Heat Coolant Loop 2 . . . . .	80
5.4	Specific Heat Coolant Loop 3 . . . . .	80
5.5	Overall System Efficiencies . . . . .	88
D.1	Coolant Loop 1 Axial Pressure Profile at Steady State . . . . .	150
D.2	Coolant Loop 2 Axial Pressure Profile at Steady State . . . . .	151
D.3	Coolant Loop 3 Axial Pressure Profile at Steady State . . . . .	152
D.4	Coolant Loop 1 Density Pressure Profile at Steady State . . . . .	153
D.5	Coolant Loop 2 Density Pressure Profile at Steady State . . . . .	154
D.6	Coolant Loop 3 Density Pressure Profile at Steady State . . . . .	155
D.7	Coolant Loop 1 Coolant Axial Temperature Profile at Steady State . . . . .	156

D.8	Coolant Loop 2 Coolant Axial Temperature Profile at Steady State	157
D.9	Coolant Loop 3 Coolant Axial Temperature Profile at Steady State	158
D.10	Coolant Loop 1 Axial Velocity Profile at Steady State . . . . .	159
D.11	Coolant Loop 2 Axial Velocity Profile at Steady State . . . . .	160
D.12	Coolant Loop 3 Axial Velocity Profile at Steady State . . . . .	161
D.13	Heat Transfer Coefficients Axial Profile in Vessel at Steady State . .	162
D.14	Beryllium Axial Temperature Profile in Vessel at Steady State . . .	163

# List of Symbols

## Independent Variables

- $t$  Time
- $x$  Cartesian coordinate x direction
- $y$  Cartesian coordinate y direction
- $z$  Cartesian coordinate z direction

## Thermal-Hydraulic Variables

- $P$  Pressure
- $\alpha$  Void fraction
- $a_i$  Interfacial area concentration
- $T$  Temperature
- $V$  Velocity
- $f$  Force per unit volume
- $\rho$  Density
- $\Gamma$  Interfacial mass-transfer rate (positive from liquid to gas)
- $\vec{g}$  Gravity vector
- $e$  internal energy
- $q$  Heat transfer rate per unit volume
- $C$  Shear coefficient

$\Gamma^-$  Minimum of  $\Gamma$  and zero

$\Gamma^+$  Maximum of  $\Gamma$  and zero

$h$  Heat transfer coefficient

$h_l$  Liquid enthalpy of the bulk liquid if the liquid is vaporizing or the liquid saturation enthalpy if vapor is condensing

$h_v$  Vapor enthalpy of the bulk vapor if the vapor is condensing or the vapor saturation enthalpy if vapor is vaporizing

$h_{lv}$  Latent heat of of vaporization

### **Thermal-Hydraulic Subscripts**

$w$  wall

$l$  liquid

$g$  gas

$i$  Interfacial

$wl$  Wall-to-liquid

$wg$  Wall-to-gas

$dg$  Direct-to-gas

$dl$  Direct-to-liquid

$wsat$  Wall-to-saturated mixture

$ig$  Interfacial-to-gas

$j$  Cell centered index

### **Thermal-Hydraulic Superscripts**

$n$  Current time quantity

$n + 1$  New-time quantity

### **Heat Conduction Variables**

$k$  Thermal Conductivity  
 $q'''$  Volumetric heat-generation rate  
 $T$  Temperature  
 $\rho$  Density  
 $C_p$  Specific heat  
 $\Delta r$  Volume length in the radial direction  
 $\Delta z$  Volume length in the z direction  
 $h$  Heat transfer coefficient

### Heat Conduction Subscripts

$i$  Nodal index in the radial direction  
 $j$  Nodal index in the z direction  
 $l$  Liquid  
 $g$  Gas  
 $w$  Wall

### Heat Conduction Superscripts

$n$  Current-time quantity  
 $n + 1$  New-time quantity  
 $p$  Predicted new-time values

### Geometric Variables

$D_i$  Inner diameter of object  
 $A$  Cross section area of object

# Acknowledgments

I would like to thank Dr. Justin Watson for his technical contribution and mentoring throughout my master's education. He was willing to be my new advisor after my advisor from my first year of graduate school took a job as the head of the nuclear engineering department at a different university. He was also willing and eager to work with me to help me complete my thesis in an abbreviated time frame. His technical knowledge and willingness to help me proved vital to the completion of this study.

Furthermore, I would like to thank Mr. Alex Cheung and TAE technologies for letting me continue some of my work from my summer 2017 internship as parts of my thesis. The work I did while at TAE technologies served as a starting point for my thesis.

Finally, I would also like to thank The Pennsylvania State University department of Mechanical and Nuclear Engineering for providing financial support through the entirety of my master's education by providing me the opportunity to serve as a teaching assistant for every semester of my master's education.



# Chapter 1 | Introduction

Water, helium, and carbon dioxide are amongst the various coolants being considered to achieve power balance for Generation IV nuclear reactors and fusion reactors. It is important to be able to compare how these coolants perform in a power system. The complexity of reactor systems necessitates the use of numerical methods instead of an analytical approach, and there is a wide range of software packages that model various aspects of reactor systems. The TRAC/RELAP Advanced Computational Engine (TRACE - formerly called TRAC-M) is the latest in a series of advanced, best-estimate reactor systems codes developed by the United States Nuclear Regulatory Commission (NRC) for analyzing transient and steady-state neutronic-thermal-hydraulic behavior in power systems. TRACE combines the capabilities of the NRC's four main systems codes (TRAC-P, TRAC-B, RELAP5 and RAMONA) into one modernized computational tool [1]. TRACE has the ability to perform simulations to predict the behavior of power systems under various conditions. TRACE can perform simulations with various fluids, including water, helium, and carbon dioxide.

There is a bigger history of water being used as a coolant for nuclear power systems than helium or carbon dioxide. Most of today's water cooled reactors trace their ancestry back to the USS Nautilus, the world's first nuclear submarine, launched in 1954 [2]. Also, as of January 2018, water cooled reactors make up 92.9% of the nuclear reactors commercially operational or operable in the world [3]. Carbon dioxide is used as a coolant in Advanced Gas Cooled Reactors (AGRs). The first AGR, Calder Hall, a MAGNOX station, was developed in 1956 in the United Kingdom [4]. As of January 2018, AGRs comprise 3.1% of the nuclear reactors commercially operational or operable in the world [3]. Although helium has not

been used in a commercial nuclear power plant, it is in consideration as a coolant for Generation IV and fusion reactors.

Helium and carbon dioxide are being considered as coolants for Generation IV and fusion reactors for multiple reasons. One reason is to increase the power cycle efficiency compared to a water cooled system. In a helium or carbon dioxide cooled system, the coolant can safely reach a much higher temperature than water in a water cooled system. For example, most AGRs have an efficiency around 40% [4] while Light Water Reactors (LWRs) have an efficiency around 33% [5]. A higher temperature coolant will also allow for a power plant to perform more chemical processes at potentially higher efficiencies. Another advantage of a helium or carbon dioxide cooled system over a water cooled system is that helium and carbon dioxide are less corrosive than water [6, 7]. Carbon dioxide is not corrosive to metals or alloys [7]. Helium and carbon dioxide are also less reactive than water [8, 9]. In addition, helium is chemically inert [8].

Due to the interest in various coolants for Generation IV reactors, many existing thermal hydraulic codes have expanded their capabilities to be able to perform simulations with the coolants of interest for these systems. Gas Cooled Fast Reactors (GFRs) are a Generation IV reactor that are of interest for multiple reasons including high theoretical efficiency, and for high efficiency hydrogen production [10]. Helium or carbon dioxide are the coolants being considered for GFR systems [10]. Various simulation tools have been used to analyze GFR systems. A project by the Idaho National Engineering and Environmental Laboratory used RELAP5/ATHENA to perform simulations to analyze decay heat removal processes for GFRs under accident scenarios [11]. Another study used RELAP-3D to analyze the same accident scenario for GFRs [12]. Both studies concluded that the GFRs of their respective studies can't be 100% passively cooled for a loss of coolant accident (LOCA). TRACE and CATHARE have also been used to analyze GFR systems for various conditions and transient scenarios [13]. A challenge for any thermal hydraulic simulation tool for most Generation IV reactors is that most are theoretical and have no experimental data. A modified version of TRACE was validated for a range of conditions for a Molten Salt Reactor (MSR) previously operated by Oakridge National Laboratory (ONL) [14]. Various thermal hydraulic codes have been used and further developed for every type of Generation IV reactor [15], [16], [17], [18], [19].

Various thermal hydraulic codes have been used to perform analysis of fusion reactors. For example, RELAP/SCDAPSIM/MOD4.0 was used to build and run various simulations for accident analysis on a helium cooled fusion reactor system by ITER [20]. This code has also been used to analyze lead lithium eutectic liquid metal as a coolant for fusion reactors [21]. These are just a couple of examples of thermal hydraulic codes that have been used to perform analysis for fusion devices. ITER uses a tokamak style fusion reactor. There has been little thermal hydraulic analysis performed for field reversed configuration (FRC) fusion systems. This study used TRACE to build and perform simulations for a FRC fusion system that is cooled by either water, helium, or carbon dioxide. The purpose of this study is to analyze the performance of each coolant and determine the best coolant for the system of this study. The results and analysis of this study are relevant for Generation IV reactors too.

TRACE capabilities have expanded over the lifetime of the code to improve the code. Recently, there have been advancements in the capabilities of TRACE to allow the code to accurately model and simulate systems like Generation IV reactors. One feature of interest for Generation IV and fusion reactors is a helical coil steam generator. One primary advantage of a helical coil steam generator over heat exchanger designs with straight tubes is that the mechanical effects from thermal expansion are much less [22]. This signifies the importance for these heat exchangers in helium or carbon dioxide cooled Rankine systems because these coolants can safely reach a much higher temperature than water. In a Rankine cycle power system with water as the secondary side coolant, a higher temperature primary side coolant will make it easier for the secondary side water to be superheated and reach higher superheated temperatures. Assuming the secondary side coolant remains in the superheated phase throughout the turbine, it will cause less damage than a saturated steam because no condensate will form. Also, the superheating steam increases the maximum temperature of the rankine cycle, therefore increasing the overall efficiency of the system without increasing the boiler pressure [23]. In 2014, the NRC introduced a curved pipe component into TRACE that allows the code to accurately model and perform simulations for helical coil pipes [24]. The TRACE curved pipe was used to model the secondary side helical coil pipes for a helical coil steam generator in the helium and carbon dioxide cooled models of this study.

For most of TRACE's history simulations could only be performed for its built

in fluids of water, heavy water, helium, sodium, lead bismuth, nitrogen, and air. In 2012 the NRC made an addition to TRACE to allow it to perform simulations for other fluids by reading equations of state from a user defined External Property Table (XPTB) [24]. This capability should be used carefully though because TRACE is only verified and validated for water in simulations [24]. For this study, TRACE's built in equations of state for water and helium were used, and an external property table was generated for carbon dioxide to provide its equations of state to be read and used by TRACE. The method of manufactured solutions was used to verify the use of helium and carbon dioxide in TRACE for the range of conditions in the models for each respective coolant. Also, the physical properties used by TRACE were compared to known values. These tests verified using helium and carbon dioxide in TRACE for the range of conditions in each coolant's respective TRACE model.

Chapter 2 of this document reviews the fluid field equations and heat transfer equations solved for in TRACE and the final sets of discretized equations solved for in TRACE. Chapter 3 of this document reviews the modeling process for the various components of the TRACE models used in this study, and the complete TRACE models for the various systems of this study. A unique TRACE model representing the complete system was built for each coolant analyzed. Chapter 4 performs verification tests for the helium and carbon dioxide cooled models using the method of manufactured solutions because these fluids are not verified or validated for use in TRACE. Chapter 5 compares the steady state results of the systems in this study. Chapter 5 also includes a discussion of the results for the different coolants analyzed in this study and future work that can be performed related to this research. Chapter 6 provides a summary of this study and the future work suggested.

# Chapter 2 | TRACE Solution Methods

## 2.1 Introduction

Partial differential equations (PDEs) are used to describe the phenomena that occurs in a physical problem. TRACE solves PDEs by discretizing the time and spacial domains and using numerical approximations to evaluate integral and differential quantities. This chapter provides a brief overview of the fluid and heat transfer equations used in TRACE and the discrete forms of the field equations used in TRACE. TRACE has built in equations of state for water, heavy water, helium, sodium, lead bismuth, nitrogen, and air. Carbon dioxide is a fluid analyzed in this research and its properties are not built into TRACE. The carbon dioxide properties are supplied to TRACE by an external property table (XPTB). The process for creating and using an XPTB in TRACE is summarized in section 2.4. The finite volume method is used to discretize the fluid field PDEs in TRACE, and the finite difference method is used to discretize the heat transfer PDEs in TRACE [24]. Section 2.2 reviews the fluid field equations used by TRACE and section 2.3 reviews the heat transfer equations used by TRACE.

## 2.2 TRACE Fluid Field Equations

In this section I will present an overview of the fluid field equations used by TRACE. This section does not provide the complete derivation of the fluid field equations, but rather provides a brief summary of the derivation process and provides the final set of fluid field equations used by TRACE. For a more detailed description of

the fluid field equations and the derivation process to arrive at the final set of fluid field equations used in TRACE, refer to the TRACE V5.0 PATCH 5 THEORY MANUAL [24].

### 2.2.1 Finite Volume Thermal Hydraulic Equations

TRACE finite volume methods differ slightly from the finite volume methods of most contemporary thermal hydraulic solution methods. In modern thermal-hydraulic solutions it is common to have all of the variables collocated on the same mesh. TRACE uses a staggered mesh technique that staggers the mesh for the momentum conservation equation relative to the mesh that is used for the mass and energy conservation equations. An example of a staggered mesh is shown in figure 2.1. The principle advantage of a staggered mesh is improved coupling between velocities and pressure. Without the staggered mesh arrangement, oscillations can occur in the pressure and velocity fields [25].

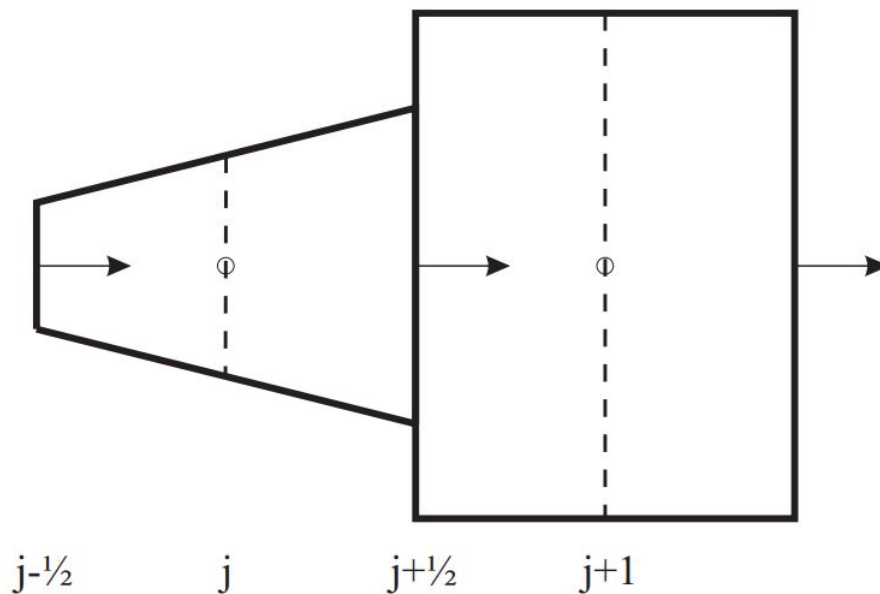


**Figure 2.1.** Staggered Mesh Example for the Finite Volume Method used in TRACE [24]

Figure 2.1 provides an example of a staggered finite volume discretization from the TRACE Theory Manual [24]. For figure 2.1, TRACE evaluates the unknowns in the mass and energy equations at nodes  $j$  and  $j+1$  and the unknowns for the momentum equation at node  $j+1/2$ . The faces of the control volumes for the mass and energy finite volumes are located at the center of the finite volume for the momentum conservation equations, and vice versa.

The staggered mesh approach nullifies the need for interpolation schemes to approximate the velocity at finite volume edges for flux terms in the mass and energy thermal hydraulic equations. In a collocated mesh for thermal hydraulic equations, interpolation is needed to approximate velocity at the boundaries of the finite volumes to calculate the flux term. However, in a staggered mesh, the velocity variable coincides with the surface of the mass or energy conservation equation volume. So, no interpolation is needed. When state variables are needed for the surface integrals in the mass and energy conservation equations, the values are taken from the nearest upstream finite volume center as determined by the fluid velocity contained in the surface integral. This is a first order accurate method in space [24].

The process for discretizing the momentum equations is more difficult than the process used for the mass and energy equations. First, there can be discontinuity in flow area on the edges of the mass and energy conservation finite volumes, which coincides with the center of the conservation of momentum finite volumes. Also, because of the staggered mesh arrangement, there are different thermodynamic state variables on either side of the center of the momentum volume because the thermodynamic properties are considered constant over the mass and energy conservation finite volumes. To handle these complexities, the mass conservation equations are manipulated for the left and right halves of the momentum conservation finite volume and keeping constant volumetric flow on either side of the momentum conservation finite volume. This process and detailed derivation are described in more detail in the TRACE Theory Manual [24].

Derivation of the fluid field equation set used in TRACE starts with single phase Navier-Stokes equations in each phase, and jump conditions between the phases. Time averaging is applied to this combination of equations, to obtain a useful set of two-fluid, two-phase conservation equations. Gauss' Theorem is first utilized to transform the equations into integral form before writing the discrete form of the

finite volume equations. Finite volume averaging is applied to the equations along with applicable assumptions to cut down computer cost and arrive at the final set of fluid field equations [24].

Although the TRACE fluid field equations derived are fully conservative, the equations are rearranged for solution in TRACE to cut complexity and computer time of the numerical solution. The fully conservative energy and momentum equations are rearranged to arrive at internal energy and motion equations [24]. Use of motion equations, rather than fully conservative momentum equations, generally works very well in TRACE. An internal energy conservation equation (gas or liquid) is obtained by taking the dot product of the corresponding momentum equation with its velocity and subtracting the results from the fully conservative energy equation [24]. Equation 2.1 provides the gas internal energy equations used by TRACE. A similar operation is performed on the liquid energy equation, but rather than using it in that form, the result is added to the gas energy equation to produce a mixture energy conservation equation. This mixture energy conservation equation is given by equation 2.2.

#### Gas Internal Energy Conservation Equation

$$\begin{aligned} & \frac{\partial (\alpha \rho_g e_g)}{\partial t} + \nabla \cdot (\alpha \rho_g e_g \vec{V}_g) \\ & = -P \frac{\partial \alpha}{\partial t} - P \nabla \cdot (\alpha \vec{V}_g) + q_{wg} + q_{dg} + q_{ig} + \Gamma h_{v'} \end{aligned} \quad (2.1)$$

#### Mixture Energy Conservation Equation

$$\begin{aligned} & \frac{\partial [(1 - \alpha) \rho_l e_l + \alpha \rho_g e_g]}{\partial t} + \nabla \cdot [(1 - \alpha) \rho_l e_l \vec{V}_l + \alpha \rho_g e_g \vec{V}_g] \\ & = -P \nabla \cdot [(1 - \alpha) \vec{V}_l + \alpha \vec{V}_g] + q_{wl} + q_{wsat} + q_{wg} + q_{dl} + q_{dg} \end{aligned} \quad (2.2)$$



When included in the finite volume equation solution, the mixture energy equation makes it easier to deal with transitions from two-phase to single-phase flow during a step in the time integration. To fully achieve this advantage during a transition, a pair of gas and mixture mass equations, equations 2.3 and 2.4 respectively, must be used in the actual solution [24].

Gas Mass Equation

$$\frac{\partial (\alpha \rho_g)}{\partial t} + \nabla \cdot [\alpha \rho_g \vec{V}_g] = \Gamma \quad (2.3)$$

Mixture Mass Equation

$$\frac{\partial [(1 - \alpha) \rho_l + \alpha \rho_g]}{\partial t} + \nabla \cdot [(1 - \alpha) \rho_l \vec{V}_l + \alpha \rho_g \vec{V}_g] = 0 \quad (2.4)$$

The liquid and gas motion equations are derived by multiplying the mass conservation equation for a phase by that phase's velocity, subtracting it from the corresponding momentum conservation equation, and dividing the result by the appropriate macroscopic density [24]. These intermediate steps and equations are not included in this paper, but the complete derivation process can be found in the TRACE Theory Manual [24].

Liquid Equation of motion

$$\frac{\partial \vec{V}_l}{\partial t} + \vec{V}_l \cdot \nabla \vec{V}_l = -\frac{1}{\rho_l} \nabla P + \frac{[f_i - \Gamma (\vec{V}_i - \vec{V}_l) + f_{wl}]}{(1 - \alpha) \rho_l} + \vec{g} \quad (2.5)$$

## Gas Equation of Motion

$$\frac{\partial \vec{V}_g}{\partial t} + \vec{V}_g \cdot \nabla \vec{V}_g = -\frac{1}{\rho_g} \nabla P + \frac{[f_{wg} - f_i - \Gamma (\vec{V}_g - \vec{V}_i)]}{\alpha \rho_g} + \vec{g} \quad (2.6)$$

For the helium cooled TRACE model of this research, helium is modeled as an ideal noncondensable gas. In TRACE, a noncondensable gas or gas mixture is assumed to be in thermal equilibrium with any steam that is present and move with the same velocity as the steam (mechanical equilibrium). Hence, only a single gas momentum equation (equation 2.6) and a single gas energy equation (equation 2.1) are needed. Mass conservation is provided with a total noncondensable mixture mass equation for TRACE [24], shown in equation 2.7.

## Noncondensable Gas Mass Equation

$$\frac{\partial \alpha \rho_a}{\partial t} + \nabla \cdot (\alpha \rho_a \vec{V}_g) = 0 \quad (2.7)$$

### 2.2.2 Stability Enhancing Two-Step (SETS) Method

There are multiple time integration methods that can be applied to solve the fluid field equations in TRACE. The time solution method used in this study was the Stability Enhancing Two-Step (SETS) method. The SETS method involves two steps, a semi-implicit step and a stabilizer step. Each step has its own sets of equations for mass, momentum, and energy and the final equations solved for in TRACE are the difference between the stabilizer equations and their corresponding equations from the semi-implicit step. For mass and energy equations, the first step is the semi-implicit step followed by the stabilizer step. The motion equations

first evaluate the momentum-stabilizer equation, then evaluate the semi-implicit equations. The SETS method has the advantage of avoiding Courant stability limits on time-step size but the disadvantage of relatively high numerical diffusion. This section provides the final set of discretized equations solved for in TRACE using the SETS method. The complete derivation process for these equations and the intermediate equations can be found in the TRACE V5.0 PATCH 5 THEORY MANUAL [24].

### 2.2.2.1 Semi-Implicit Step Equations

This section provides the final set of equations used by TRACE in the semi-implicit step of the SETS method. For these equations, a tilde above a variable indicates that it is a first estimate of the new-time value. Actual new-time variables have a superscript “ $n + 1$ ” and no tilde. As explained in section 2.2.1, a spatially first order accurate upwind method is used to determine the state variable values used for the surface integrals in the mass and energy conservation equations.

Combined Gas Mass Equation

$$\frac{[\tilde{\alpha}_j^{n+1} \tilde{\rho}_{gj}^{n+1} - (\alpha \rho_g)_j^n]}{\Delta t} + \nabla_j \cdot [(\alpha \rho_g)^n V_g^{n+1}] = \tilde{\Gamma}^{n+1} \quad (2.8)$$

Noncondensable Gas Mass Equation

$$\frac{[\tilde{\alpha} \tilde{\rho}_a]_j^{n+1} - [\alpha \rho_a]_j^n}{\Delta t} + \nabla_j \cdot [(\alpha \rho_a)^n \vec{V}_g^{n+1}] = 0 \quad (2.9)$$

Liquid Mass Equation

$$\frac{|(1 - \tilde{\alpha}_j^{n+1}) \tilde{\rho}_l^{n+1} - [(1 - \alpha) \rho_l]^n|}{\Delta t} + \nabla_j \cdot [(1 - \alpha) \rho_l]^n V_l^{n+1} = -\tilde{\Gamma}^{n+1} \quad (2.10)$$

Mixture Gas Equation of Motion

$$\begin{aligned} & \frac{(V_g^{n+1} - V_g^n)}{\Delta t} + V_g^n \nabla_{j+1/2} \tilde{V}_g^{n+1} + \beta (V_g^{n+1} - V_g^n) \nabla_{j+1/2} \tilde{V}_g^n \\ & - \frac{f_i^{n+1} + \frac{\partial f_i}{\partial V_g} \delta V_g + \frac{\partial f_i}{\partial V_l} \delta V_l}{\langle \alpha \rho_g \rangle_{j+1/2}^n} \\ & + \frac{1}{\langle \rho_g \rangle_{j+1/2}^n} \frac{(\tilde{P}_{j+1}^{n+1} - \tilde{P}_j^n)}{\Delta x_{j+1/2}} + \frac{\tilde{\Gamma}_{j+1/2}^{n+1}}{\langle \alpha \rho_g \rangle_{j+1/2}^n} (V_g^{n+1} - V_l^{n+1}) \\ & + \frac{C_{wg}}{\langle \alpha \rho_g \rangle_{j+1/2}^n} (2V_g^{n+1} - V_g^n) |V_g^n| + g \cos \theta = 0 \end{aligned} \quad (2.11)$$

Liquid Equation of Motion

$$\begin{aligned}
& \frac{(V_l^{n+1} - V_l^n)}{\Delta t} + V_l^n \nabla_{j+1/2} \tilde{V}_l^{n+1} + \beta (V_l^{n+1} - V_l^n) \nabla_{j+1/2} \tilde{V}_l^n \\
& \quad + \frac{f_i^{n+1} + \frac{\partial f_i}{\partial V_g} \delta V_g + \frac{\partial f_i}{\partial V_l} \delta V_l}{\langle (1 - \alpha) \rho_l \rangle_{j+1/2}^n} \\
& + \frac{1}{\langle \rho_l \rangle_{j+1/2}^n} \frac{(\tilde{P}_{j+1}^{n+1} - \tilde{P}_j^n)}{\Delta x_{j+1/2}} - \frac{\tilde{\Gamma}_{j+1/2}^{-n}}{\langle (1 - \alpha \rho_l) \rangle_{j+1/2}^n} (V_l^{n+1} - V_g^{n+1}) \\
& \quad + \frac{C_{wl}}{\langle (1 - \alpha) \rho_l \rangle_{j+1/2}^n} (2V_l^{n+1} - V_l^n) |V_l^n| + g \cos \theta = 0
\end{aligned} \tag{2.12}$$

Combined Gas Equation of Energy

$$\begin{aligned}
& \frac{[\tilde{\alpha}_j^{n+1} \tilde{\rho}_{gj}^{n+1} \tilde{e}_{gj}^{n+1} - (\alpha \rho_g e_g)_j^n]}{\Delta t} + \nabla_j \cdot [(\alpha \rho_g e_g)^n V_g^{n+1}] \\
& \quad + \tilde{P}^{n+1} \left[ \frac{(\tilde{\alpha}^{n+1} - \alpha^n)}{\Delta t} + \nabla_j \cdot (\alpha^n V_g^{n+1}) \right] \\
& \quad = \tilde{q}_{wg}^{n+1} + q_{dg}^n + \tilde{q}_{ig}^{n+1} + \tilde{\Gamma}^{n+1} \tilde{h}_{sg}^{n+1}
\end{aligned} \tag{2.13}$$

Total Fluid (Liquid and Gas) Equation of Energy

$$\begin{aligned}
& \frac{\left\{ \tilde{\alpha}_j^{n+1} \tilde{\rho}_{gj}^{n+1} \tilde{e}_{gj}^{n+1} + (1 - \tilde{\alpha}_{gj}^{n+1}) \tilde{\rho}_{gj}^{n+1} \tilde{e}_j^{n+1} - [(\alpha \rho_g e_g)_j^n + (1 - \alpha) \rho_l e_l]_j^n \right\}}{\Delta t} \\
& + \nabla_j \cdot \left\{ (\alpha \rho_g e_g)^n V_g^{n+1} + [(1 - \alpha) \rho_l e_l]^n V_l^{n+1} \right\} \\
& + \tilde{P}^{n+1} \nabla_j \cdot \left[ (1 - \alpha)^n V_l^{n+1} + \alpha^n V_g^{n+1} \right] \\
& = \tilde{q}_{wg}^{n+1} + \tilde{q}_{wl}^{n+1} + \tilde{q}_{wsat}^{n+1} + q_{dl}^n + q_{dg}^n
\end{aligned} \tag{2.14}$$

Source Terms

$$\tilde{q}_{wl}^{n+1} = h_{wl}^n a_w (T_w^n - \tilde{T}_l^{n+1}) \tag{2.15}$$

$$\tilde{q}_{wsat}^{n+1} = h_{wsat}^n a_w (T_w^n - \tilde{T}_{sat}^{n+1}) \tag{2.16}$$

$$\tilde{q}_{wg}^{n+1} = h_{wg}^n a_w (T_w^n - \tilde{T}_g^{n+1}) \tag{2.17}$$

$$\tilde{\Gamma}^{n+1} = \frac{-\left(\tilde{q}_{ig}^{n+1} + \tilde{q}_{il}^{n+1}\right)}{(h'_v)^{n+1} - (h'_l)^{n+1}} \tag{2.18}$$

where

$$\tilde{q}_{ig}^{n+1} = h_{ig}^n a_i (\tilde{T}_{sat}^{n+1} - \tilde{T}_g^{n+1}) \tag{2.19}$$

and

$$\tilde{q}_{il}^{n+1} = h_{il}^n a_i \left( \tilde{T}_{sat}^{n+1} - \tilde{T}_l^{n+1} \right) \quad (2.20)$$

### 2.2.2.2 Stabilizer Step Equations

This section provides the final set of equations used by TRACE in the stabilizer step of the SETS method. Similar to the semi-implicit step equations, for these equations a tilde above a variable also indicates that it is a first estimate of the new-time value. Actual new-time variables have a superscript “ $n + 1$ ” and no tilde. Again, a first order accurate upwind difference scheme is used to determine the state variable values used for the surface integrals in the mass and energy conservation equations.

Combined Gas Mass Equation

$$\frac{[(\alpha\rho_g)_j^{n+1} - \tilde{\alpha}_j^{n+1} \tilde{\rho}_{gj}^{n+1}]}{\Delta t} + \nabla_j \cdot [(\alpha\rho_g)^{n+1} V_g^{n+1}] = \nabla_j \cdot [(\alpha\rho_g)^n V_g^{n+1}] \quad (2.21)$$

Noncondensable Gas Mass Equation

$$\frac{[(\alpha\rho_a)_j^{n+1} - \tilde{\alpha}_j^{n+1} \tilde{\rho}_{gj}^{n+1}]}{\Delta t} + \nabla_j \cdot [(\alpha\rho_a)^{n+1} V_g^{n+1}] = \nabla_j \cdot [(\alpha\rho_a)^n V_g^{n+1}] \quad (2.22)$$

Liquid Mass Equation

$$\frac{[(1 - \alpha) \rho_l]_j^{n+1} - (1 - \tilde{\alpha}_j^{n+1}) \tilde{\rho}_{lj}^{n+1}}{\Delta t} + \nabla_j \cdot \{[(1 - \alpha) \rho_l]^{n+1} V_l^{n+1}\} = \nabla_j \cdot \{[(1 - \alpha) \rho_l]^n V_l^{n+1}\} \quad (2.23)$$

Combined Gas Energy Equation

$$\frac{[(\alpha \rho_g e_g)_j]^{n+1} - \tilde{\alpha}_j^{n+1} \tilde{\rho}_{gj}^{n+1} \tilde{e}_{gj}}{\Delta t} + \nabla_j \cdot [(\alpha \rho_g e_g)^{n+1} V_g^{n+1}] = \nabla_j \cdot [(\alpha \rho_g e_g)^n V_g^{n+1}] \quad (2.24)$$

Liquid Energy Equation

$$\frac{\{[(1 - \alpha) \rho_l e_l]_j^{n+1} - (1 - \tilde{\alpha}_j^{n+1}) \tilde{\rho}_{lj}^{n+1} \tilde{e}_l\}}{\Delta t} + \nabla_j \cdot \{[(1 - \alpha) \rho_l e_l]^{n+1} V_l^{n+1}\} = \nabla_j \cdot \{[(1 - \alpha) \rho_l e_l]^n V_l^{n+1}\} \quad (2.25)$$



### Mixture Gas Equation of Motion

$$\begin{aligned}
& \frac{(\tilde{V}_g^{n+1} - V_g^n)}{\Delta t} + V_g^n \nabla_{j+1/2} \tilde{V}_g^{n+1} + \beta (\tilde{V}_g^{n+1} - V_g^n) \nabla_{j+1/2} \tilde{V}_g^n \\
& \quad - \frac{f_i^{n+1} + \frac{\partial f_i}{\partial V_g} \delta \hat{V}_g + \frac{\partial f_i}{\partial V_l} \delta \hat{V}_l}{\langle \alpha \rho_g \rangle_{j+1/2}^n} \\
& \quad + \frac{1}{\langle \rho_g \rangle_{j+1/2}^n} \frac{(P_{j+1}^{n+1} - P_j^n)}{\Delta x_{j+1/2}} + \frac{\Gamma_{j+1/2}^{+n}}{\langle \alpha \rho_g \rangle_{j+1/2}^n} (\hat{V}_g^{n+1} - \hat{V}_l^{n+1}) \\
& \quad + \frac{C_{wg}}{\langle \alpha \rho_g \rangle_{j+1/2}^n} (2\tilde{V}_g^{n+1} - V_g^n) |V_g^n| + g \cos \theta = 0
\end{aligned} \tag{2.26}$$

### Liquid Equation of Motion

$$\begin{aligned}
& \frac{(\tilde{V}_l^{n+1} - V_l^n)}{\Delta t} + V_l^n \nabla_{j+1/2} \tilde{V}_l^{n+1} + \beta (\tilde{V}_l^{n+1} - V_l^n) \nabla_{j+1/2} \tilde{V}_l^n \\
& \quad + \frac{f_i^{n+1} + \frac{\partial f_i}{\partial V_l} \delta \hat{V}_l + \frac{\partial f_i}{\partial V_g} \delta \hat{V}_g}{\langle (1 - \alpha) \rho_l \rangle_{j+1/2}^n} \\
& \quad + \frac{1}{\langle \rho_l \rangle_{j+1/2}^n} \frac{(P_{j+1}^{n+1} - P_j^n)}{\Delta x_{j+1/2}} - \frac{\Gamma_{j+1/2}^{-n}}{\langle (1 - \alpha) \rho_l \rangle_{j+1/2}^n} (\hat{V}_l^{n+1} - \hat{V}_g^{n+1}) \\
& \quad + \frac{C_{wl}}{\langle (1 - \alpha) \rho_l \rangle_{j+1/2}^n} (2\tilde{V}_l^{n+1} - V_l^n) |V_l^n| + g \cos \theta = 0
\end{aligned} \tag{2.27}$$

## 2.3 Discretized Heat Transfer Equations

This section provides a brief summary of the discretized heat transfer equations used by TRACE. This section will only cover the discretized heat transfer equations for cylindrical coordinates using the finite difference method for one dimensional components because all of the heat structures used in the TRACE models for this study were cylindrical heat structures attached to one dimensional components and used the finite difference method to solve the heat transfer equations. First, the derivation process is briefly summarized. Then, the final discretized heat transfer equations used in TRACE are provided. The governing heat conduction equation used by TRACE uses Fourier's law of conduction, which states, "the heat flux resulting from thermal conduction is proportional to the magnitude of the temperature gradient and opposite to it in sign" [26]. The governing heat conduction equation used by TRACE for an arbitrary geometry is shown in equation 2.28.

$$\rho c_p \frac{\partial T}{\partial t} = \nabla \cdot (k \nabla T) + q''' \quad (2.28)$$

In one-dimensional cylindrical coordinates, the divergence of the temperature gradient is shown in the first term on the right hand side of equation 2.29. Equation 2.29 is Fourier's law of conduction in cylindrical coordinates.

$$\rho c_p \frac{\partial T}{\partial t} = \frac{1}{r} \left[ \frac{\partial}{\partial r} \left( r k \frac{\partial T}{\partial r} \right) \right] + q''' \quad (2.29)$$

The temperature distribution within the walls of the one dimensional components is obtained from a finite-volume approximation to equation 2.29. To arrive at the final set of discretized heat transfer equations, the differential form of the heat conduction equations are integrated to reduce the order of the derivative of the temperature field. This complete process and derivation can be found in the TRACE theory manual [24]. To better understand the discretized heat transfer equations, figure 2.2 provides an example of a computational mesh for a cylindrical wall geometry.

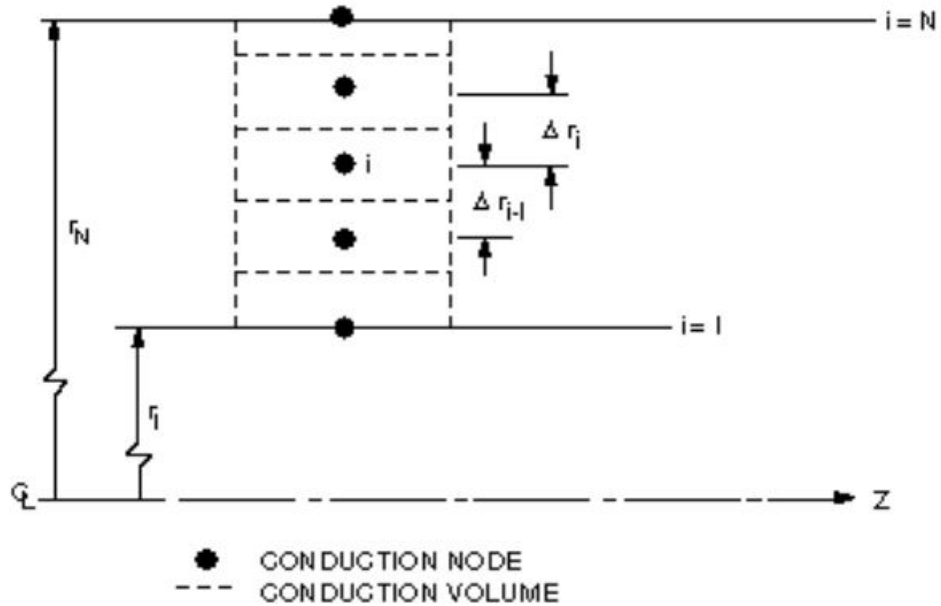


**Figure 2.2.** Cylindrical Wall Geometry [24]

The general form of the discrete heat transfer equation in the  $i^{th}$  interior volume ( $1 < i < N$ ) is given in equation 2.30. Equation 2.30 is implicit in the radial direction and explicit in the axial direction.

$$\begin{aligned}
& \frac{r_{i-1/2}k_{i-1/2}}{\Delta r_{i-1}}T_{i-1}^{n+1} - \left\{ \frac{r_{i-1/2}k_{i-1/2}}{\Delta r_{i-1}} + \frac{r_{i+1/2}k_{i+1/2}}{\Delta r_i} \right. \\
& \left. + \frac{1}{2\Delta t} \left[ \left( r_i\Delta r_{i-1} - \frac{\Delta r_{i-1}^2}{4} \right) (\rho c_p)_{i-1/2} + \left( r_i\Delta r_i - \frac{\Delta r_i^2}{4} \right) (\rho c_p)_{i+1/2} \right] \right\} T_i^{n+1} \\
& \frac{r_{i+1/2}k_{i+1/2}}{\Delta r_i}T_{i+1}^{n+1} = -\frac{1}{2} \left\{ \left( r_i\Delta r_{i-1} - \frac{\Delta r_{i-1}^2}{4} \right) \left[ \frac{(\rho c_p)_{i-1/2}}{\Delta t}T_i^n + q''' \right] \right. \\
& \left. \left( r_i\Delta r_i - \frac{\Delta r_i^2}{4} \right) \left[ \frac{(\rho c_p)_{i+1/2}}{\Delta t}T_i^n + q''' \right] \right\}
\end{aligned} \tag{2.30}$$

For the case of a fluid volume adjacent to the inner surface ( $i = 1$ ) of figure 2.2, the conduction solution effectively treats the boundary condition as a time-dependent heat flux.

$$-k \left. \frac{\partial T}{\partial r} \right|_{i=1} = -q_{total,I}^{n+1} \tag{2.31}$$

For example, application of this boundary condition to the inner surface ( $i = 1$ ) yields a discrete approximation to the conduction equation, shown in equation 2.32.

$$\begin{aligned}
& - \left\{ \frac{r_{3/2}k_{3/2}}{\Delta r_1} + \frac{1}{2} \left[ r_1\Delta r_1 + \frac{\Delta r_1^2}{4} \right] \frac{(\rho c_p)_{3/2}}{\Delta t} \right\} T_1^{n+1} + \frac{r_{3/2}k_{3/2}}{\Delta r_1} T_2^{n+1} \\
& = -\frac{1}{2} \left( r_1\Delta r_1 + \frac{\Delta r_1^2}{4} \right) \left[ \frac{(\rho c_p)_{3/2}}{\Delta t} T_1^n + q''' \right] + r_1 q_{total,I}^{n+1}
\end{aligned} \tag{2.32}$$

## 2.4 External Property Table (XPTB) for Carbon Dioxide

This section reviews the process for creating an XPTB for carbon dioxide equations of state that TRACE can read and apply to its equation sets. Due to the length of the complete carbon dioxide XPTB used for this research, it is not included in this document. Unlike water and helium equations of state, carbon dioxide equations of state are not built-in to TRACE. TRACE does have the ability to read fluid properties from a user created External Property Table (XPTB). TRACE source distribution provides a tool called “NISTPROPGEN” that is used to create XPTBs from fluids in the National Institute of Standards and Technology (NIST) REFPROP database [27]. NISTPROPGEN was used to create a XPTB for carbon dioxide that was used in this study. Once created and saved to the appropriate location, TRACE reads the carbon dioxide properties from the XPTB and applies these properties to the TRACE fluid field equations. XPTBs created by NISTPROPGEN include the liquid phase, saturation, and vapor phase properties, along with the properties corresponding to the triple point and critical point. The main focus of the external property table was the vapor phase properties because the carbon dioxide cooled system of this study operates in a range of conditions where this is the only fluid phase present.

The process for creating the carbon dioxide XPTB was rather tedious because NISTPROPGEN would generate a XPTB, but use a single value for the viscosity and thermal conductivity for all conditions in the XPTB. For this reason, the correct values for these properties had to be manually input into the XPTB for the range of condition in the XPTB. I wasn’t unable to confirm the source of this error, but found a solution to change the XPTB’s viscosity and thermal conductivity values for all conditions of the XPTB. This process is explained later in this section in chronological order of when the task was performed.

First, the NIST REFPROP database was downloaded to my computer. There is a free sample version of REFPROP called miniREFPROP that includes a small sample of fluids from the REFPROP database including carbon dioxide. This was the version I downloaded on to my computer. The properties for carbon dioxide are under the “CO2.fld” file in REFPROP. Next, to allow the NISTPROPGEN tool to

access REFPROP properties for carbon dioxide, the “CO2.fld” file was copied into the same folder as the NISTPROPGEN executable. Next, the NISTPROPGEN executable was opened. Figure 2.4 shows the prompt used in NISTPROPGEN to generate the XPTB for carbon dioxide used in this research. The first thing the executable asks is for the user to enter the fluid name (the name before the .fld file for the fluid of interest). So, “CO2” was entered in this field and I hit enter. After this, the user is prompted to define the number of pressure and temperature values and the lower and upper bounds for these parameters of the XPTB. The units for NISTPROPGEN are  $Pa$  and  $K$  for pressure and temperature respectively. 100 values were selected for both pressure and temperature with the pressure bounds selected to be  $1.1 \times 10^7 Pa$  and  $1.4 \times 10^7 Pa$ . The temperature bounds were selected to be  $500 K$  and  $1000 K$ . These bounds were selected to cover the operating conditions for the carbon dioxide cooled TRACE model. After the maximum temperature was entered, I hit “enter” on my keyboard and the NISTPROPGEN generated a XPTB for carbon dioxide. For each pressure value of the XPTB, the fluid properties are evaluated for every temperature value.

As explained earlier in this section, NISTPROPGEN used a single value for the viscosity and thermal conductivity respectively for all conditions in the XPTB. So, accurate values for these parameters were manually implemented into the XPTB. Only the properties for the vapor phase were updated because carbon dioxide is only in the vapor phase for the conditions of the carbon dioxide cooled model. The XPTB is organized in a way that the first two columns of values are the pressure and temperature values respectively. The remaining columns are the values of the fluid properties corresponding to the conditions from the first two columns. Figure 2.3 provides an example of the column order for the first 8 columns of the vapor phase properties for the carbon dioxide XPTB. So, to update the viscosity and thermal conductivity values, I needed to input accurate values in every row their respective columns. First, I opened the XPTB with notepad++ and copied the fluid properties into an excel sheet so that I could fill in the values for the viscosity and thermal conductivity in their respective columns. Using an excel sheet was a mean to make the process go faster, I could’ve theoretically typed in each value one by one in notepad++. Then I used miniREFPROP to generate a table with the proper viscosity and thermal conductivity for the same pressure and temperature values in the XPTB. MiniREFPROP allows up to 1,000 rows for

a given table. Since 100 pressure and 100 temperature values were used for the XPTB, there were 10,000 rows of data that needed to be updated for both the vapor phase viscosity and thermal conductivity. The miniREFPROP was ran 10 times to generate all of the proper viscosity and thermal conductivity values. The proper values from miniREFPROP were copied and pasted into the appropriate columns and rows after each miniREFPROP run. After all of the vapor phase viscosity and thermal conductivity values of the XPTB were updated, the entire set of values from the excel sheet were copied and pasted over the previous values in the XPTB. The entire set of parameters had to be copied and pasted because I was using notepad ++ to access the XPTB and data can't be pasted as a single column in notepad ++, unless it is the only data in all of the rows that column occupies. Next, the carbon dioxide XPTB was saved in the TRACE working directory. This allows TRACE to read the carbon dioxide properties from its corresponding XPTB. During simulations, TRACE reads the XPTB table data and interpolates linearly in the pressure-temperature grid [24]. Chapter 4 reviews the verification process for determining that the values of the XPTB were reliable, TRACE read the correct values, and TRACE properly applied the carbon dioxide parameters to its sets of equations.

10225	Vapor	P (Pa),	T (K),	dPdT (Pa/K),	Int Energy (J/kg),	dedT (J/kg/K),	dedP (J/kg/Pa),	Density (kg/m3),	drhodT (kg/m3/K),
10226	1.10000000000000E+07,	5.00000000000000E+02,	1.6474126160508E+05,	5.7270634149111E+05,	9.3438886623564E+02,	-2.6450022645184E-03,	1.2505582284698E+02,	-3.4742747608106E-01,	
10228	1.10000000000000E+07,	5.0505050505051E+02,	1.6474126160508E+05,	5.7742323915517E+05,	9.3354071613678E+02,	-2.5876551311145E-03,	1.2333166977467E+02,	-3.3545977898270E-01,	
10229	1.10000000000000E+07,	5.1010101010101E+02,	1.6474126160508E+05,	5.8213641270607E+05,	9.3291064835338E+02,	-2.5328902579303E-03,	1.2166615506990E+02,	-3.2419630853340E-01,	
10230	1.10000000000000E+07,	5.1515151515152E+02,	1.6474126160508E+05,	5.8684691288710E+05,	9.3247895488739E+02,	-2.4805294214709E-03,	1.2005587337953E+02,	-3.1357825470289E-01,	
10231	1.10000000000000E+07,	5.2020202020202E+02,	1.6474126160508E+05,	5.9155569615993E+05,	9.3222796302638E+02,	-2.4304108508297E-03,	1.1849770011499E+02,	-3.0355309808080E-01,	
10232	1.10000000000000E+07,	5.2525252525253E+02,	1.6474126160508E+05,	5.9626363433356E+05,	9.3214178440183E+02,	-2.3823873369079E-03,	1.1698876178852E+02,	-2.9407379753531E-01,	
10233	1.10000000000000E+07,	5.3030303030303E+02,	1.6474126160508E+05,	6.0097152301973E+05,	9.3220610014404E+02,	-2.3363246001210E-03,	1.1552641013302E+02,	-2.8509810078822E-01,	
10234	1.10000000000000E+07,	5.3535353535354E+02,	1.6474126160508E+05,	6.0586008908175E+05,	9.3240797621076E+02,	-2.2920998758563E-03,	1.1410819944431E+02,	-2.7659795445133E-01,	
10235	1.10000000000000E+07,	5.4040404040404E+02,	1.6474126160508E+05,	6.1038999721647E+05,	9.3273570405629E+02,	-2.2496006841809E-03,	1.1273186667912E+02,	-2.685900067622E-01,	
10236	1.10000000000000E+07,	5.4545454545455E+02,	1.6474126160508E+05,	6.1510185578699E+05,	9.3317866267445E+02,	-2.2087237561064E-03,	1.1139531391846E+02,	-2.6083014099050E-01,	
10237	1.10000000000000E+07,	5.5050505050505E+02,	1.6474126160508E+05,	6.1981622200565E+05,	9.3372719874537E+02,	-2.1693740934147E-03,	1.1009659286913E+02,	-2.5352316367351E-01,	
10238	1.10000000000000E+07,	5.5555555555556E+02,	1.6474126160508E+05,	6.2453360655155E+05,	9.3437252217573E+02,	-2.1314641428559E-03,	1.0883389112715E+02,	-2.4656241818634E-01,	

**Figure 2.3.** XPTB Column Structure (not all columns are included due to the large number of columns)

```

C:\Users\Grant Garrett\Desktop\TRACE-V50P5-Exe\TRACE-V50P5-Exe\Executables\NIST-Prop-Gen\nistPropGen.exe
Enter fluid name (left side of *.FLD file name) : CO2
NIST REFPROP database successfully initialized for:
Fluid: carbon diox
      carbon dioxide      !full name
CAS # 124-38-9
      0.044                ! Molecular Mass
      517964., 216.592, 1178.463, 13.761, ! Triple Point: P, T, rho
      7377300., 304.128, 467.600 ! Critical Point: P, T, rho
      517964., 216.592      ! DB pMin, tMin
      800000000., 2000.000  ! DB pMax, tMax

Input Table Range:
Default values are (nP=200 pMin-4*pCrit), (nT=50 tMin-2*tCrit)
Enter number of pressure values on table : 100
Enter minimum pressure (Pa) : 11000000
Enter maximum pressure (Pa) : 14000000
Enter number of temperature values on table: 100
Enter minimum temperature (K) : 500
Enter maximum temperature (K) : 1000

```

**Figure 2.4.** NISTPROGEN Executable Prompt



# Chapter 3 | Modeling

## 3.1 Introduction

This chapter presents the models used in this analysis. It also provides the modeling process for various components used in the water cooled, helium cooled, and carbon dioxide cooled reactor systems. There are similarities and differences between the different reactor subsystems based on coolant type. First, the common components between all three models are described, along with how these components were modeled in TRACE. Next, the complete models for each fluid are described, including the unique components to each system and the modeling process for these unique components.

Before getting into specifics, it is important to understand the basic design of the power systems used in this study. This basic design is common for all coolants studied. Each system has three coolant loops that pump coolant through the system. Part of each coolant loops is a section of coolant channels that flow through the vessel. Energy from the source is deposited into the coolant channel pipe walls. So, when the coolant flows through the coolant channels, the energy deposited into the pipe walls from the source is transferred to the coolant by direct heating. After exiting the coolant channels in the vessel, the primary side coolant from all three coolant loops will mix and enter the same steam generator. As the primary side coolant passes through the steam generator, it will transfer its energy to the secondary side fluid. The steam generators for each model are described in sections 3.6.1 and 3.7.1 for the water cooled model and for the helium and carbon dioxide cooled models respectively. The primary side coolant, after exiting the

steam generator, will diverge three ways and be pumped back through the three individual coolant loops. This process is constantly repeated. Figure 3.1 shows the general design of the system and the flow pattern of the coolant.

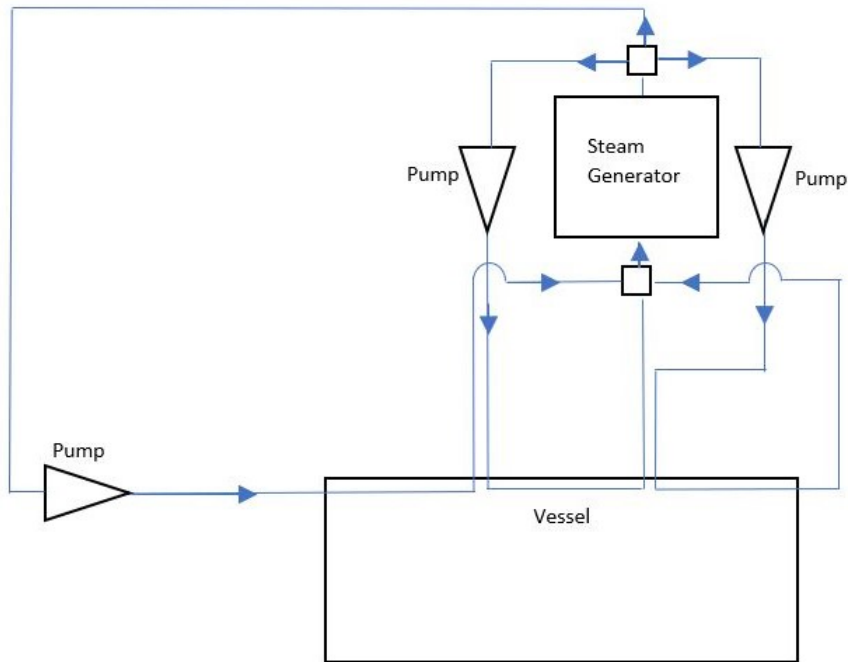


**Figure 3.1.** Basic Design of Power Plant System used in this Study

## 3.2 Vessel

The vessel used in this research is based off a conceptual design for a fusion reactor. The same vessel design is used for all three fluids in this analysis. It is assumed that there is a steady state Field Reversed Configuration (FRC) plasma inside the vessel that has a constant power of 600 MW. It is assumed that all of the power from the plasma is due to gamma rays emitted from the plasma. The energy from these gammas is assumed to be deposited uniformly to the coolant channel walls. This phenomenon is explained further in section 3.2.1. This section describes the design of the vessel, the power source, and how these two features were modeled in TRACE.

### 3.2.1 Vessel Design

The vessel is 39 m long with a 4 m inner diameter. There are three coolant loops in total for the vessel. Figures 3.2 and 3.3 show an axial view and a radial cross section of the vessel respectively. The vessel contains an armor layer of beryllium 5 mm thick between the power source and the coolant channels. The coolant channels are circular cross section pipes that are 3 cm in inner diameter and have a wall thickness of 1 mm. The coolant channel wall material is inconel 600. There are 359 13 m long coolant channels in each of the three coolant loops. The coolant channels are equally spaced apart azimuthally around the vessel. The azimuthal space between the inner surface of each coolant channel is 5.2 mm. After the coolant channels, relative to the radial direction of the vessel, is 4 mm of tungsten. The purpose of the low z to high z material transition is to have the source gammas deposit their energy uniformly to the coolant channels. A low z material was chosen for the armor layer so that the source gamma rays can pass through this region with minimal interactions. It is assumed that none of the source gamma ray energy is deposited into the beryllium armor layer. Beryllium has been among the top choices as an armor layer material for fusion applications [28]. The vessel material after the tungsten layer will depend on shielding applications and other specifics that are beyond the scope of this study.

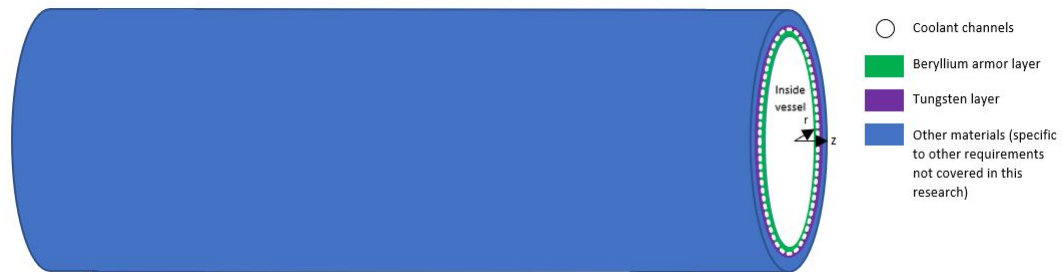


**Figure 3.2.** Axial Section of Vessel

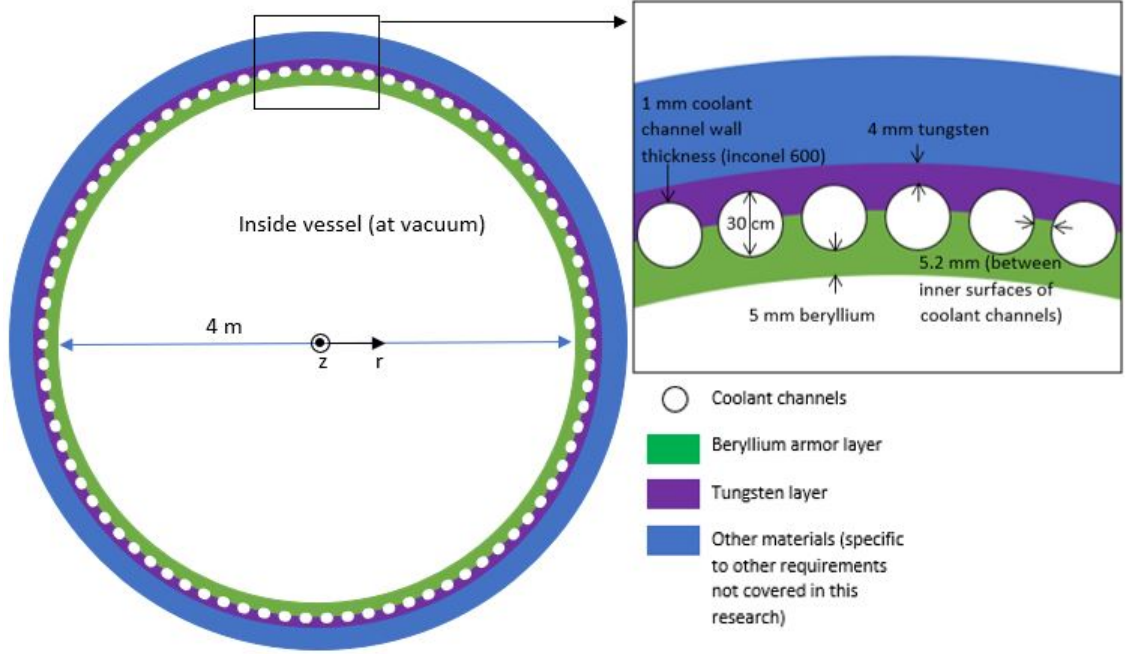


**Figure 3.3.** Vessel Cross Section (Figure not to scale)

Pipes 180, 200, and 210 represent coolant loops 1, 2, and 3 respectively for each TRACE model analyzed in this study. These pipes are geometrically identical for each TRACE model of this study. Cells 1 through 13 of each coolant loop represent the "cold leg" of the coolant loops. Cells 14 through 26 of of the coolant loops represent the three sections of coolant channels that flow through the vessel for each respective coolant loop. The sections of coolant channels for each coolant loop are modeled by setting the flow area and hydraulic diameter of these cells to represent 359 pipes with an inner diameter of 3 cm. Cells 27 through 39 of the coolant loops represent the "hot leg" of each respective coolant loop. The pipes representing the coolant loops in the TRACE models are labeled for the water cooled model in figure 3.16, and labeled for the helium and carbon dioxide cooled models in figure 3.19. It is worth referring to these figures to get an idea about the layout and components for each system.

$$single\ coolant\ channel\ flow\ area = \pi \times \frac{D_i^2}{4} = 7.06858 \times 10^{-4} m^2 \quad (3.1)$$

$$\begin{aligned}
& \text{Single loop coolant channels total flow area} = \\
& \text{single coolant channel flow area} \times \text{number of coolant channels} = \quad (3.2)
\end{aligned}$$

$$\frac{7.06858 \times 10^{-4} \text{ m}^2}{\text{single pipe}} \times 359 \text{ pipes} = 2.538 \times 10^{-1} \text{ m}^2$$

Cells 14 through 26 of the 3 coolant loops are each 1 m long cells that in total represent 3 13 m long sections of coolant channels flowing through the 39 m long vessel. The flow area and hydraulic diameter of cells 14 through 26 of each coolant loop are  $2.538 \times 10^{-1} \text{ m}^2$  and 3 cm respectively to accurately represent 359 3 cm inner diameter coolant channels. The flow area for every cell of every coolant loop is the same. For the hot and cold legs, the cells not representing the vessel coolant channels, the hydraulic diameter is set to  $5.684 \times 10^{-1} \text{ m}$ . This allows the hot and cold legs for a given coolant loop to represent a single circular cross section pipe with an equivalent flow area to the sum of the flow area of the coolant channels in said coolant loop. This was done to reduce the frictional pressure drop of the primary side coolant. The cells of all the hot and cold legs are each 1 m long. As stated in the previous paragraph, cells 1 through 13 of the coolant loops represent the cold leg for each coolant loop and cells 27 through 39 of the coolant loops represent the hot leg of each coolant loop. So, the cold legs account for 13 m that the coolant must travel from the exit of the pump to the entrance of the coolant channels in the vessel and the hot leg represents 13 m of distance the coolant travels from the exit of the coolant channels in the vessel to the converging tee where the coolants from each coolant loop mix before entering passing through the steam generator. The 13 m lengths for the cold and hot leg are arbitrarily selected values, and these lengths may change in a real system. The converging tee is represented by pipe 1090 in the TRACE models and is labeled for the water cooled TRACE model in figure 3.16, and labeled for the helium and carbon dioxide cooled models in figure 3.7. The converging tee is a 1 m long single cell pipe component and has an equivalent flow area to the sum of the flow areas of all 3 coolant loops. Cell

edge 40 of each coolant loop is connected to the converging tee in cross flow at 90°.

*Cold and Hot Leg Diameter =*

$$\sqrt{\frac{4 \times \text{Total Flow Area of coolant channels}}{\pi}} = \quad (3.3)$$

$$\sqrt{\frac{4 \times 2.538 \times 10^{-1} \text{ m}^2}{\pi}} = 5.684 \times 10^{-1} \text{ m}$$

The entrance and exit of the coolant channels to and from the vessel are represented by cell edges 14 and 27 for each coolant loop respectively. Irrecoverable losses associated with the flow configurations making up these entrance and exit regions to and from the vessel in each coolant loop are modeled using k-factors. The k-factor calculated assumed these flow configurations are 359 90 degree bends in parallel. Using a single 90 elbow k-factor of 0.75 [29], the total k-factor for all 359 parallel 90 degree bends is  $2.089 \times 10^{-3}$ .

*k – factor for entrance and exit to vessel =*

$$\left(\frac{1}{0.75} \times 359 \text{ pipes}\right)^{-1} = 2.089 \times 10^{-3} \quad (3.4)$$

### 3.2.2 Plasma Power Source

In an FRC plasma, the plasma source will spin inside a vessel that is at nearly zero pressure. The research into specific FRC plasma sources is limited. For the purpose of this study, it is assumed that all of the energy from the plasma source is due to gamma rays and their energy is deposited uniformly into the coolant channel walls

as explained in section 3.2.1. It is also assumed that there is no conduction from the plasma because the vessel is at vacuum [30].

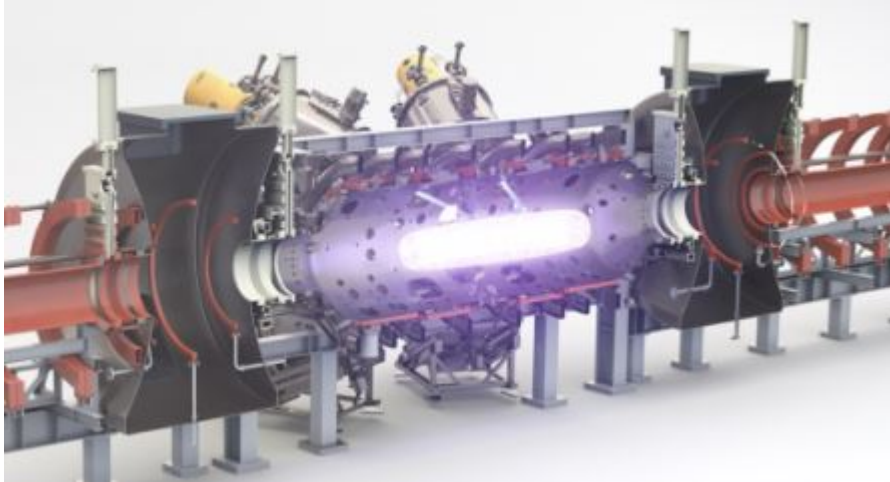


**Figure 3.4.** Example Cross Section of a FRC Plasma [31]

Heat structure 90 is used to represent the coolant channels pipe walls in each coolant loop and to model the power generated by the gamma source. This heat structure is attached to the 359 coolant channels in each coolant loop and has a total prescribed constant power of  $600 MW_{th}$ , or  $200 MW_{th}$  for each coolant loop. Heat structure 90 is a hollow inconel 600 cylinder with an inner diameter of 3 cm and a wall thickness of 1 mm, corresponding to the geometry of a single coolant channel. There are 39 1 m long cells in total for heat structure 90. The surface multiplier of heat structure 90 is set to 359 to represent the pipe wall for the 359 coolant channels of each coolant loop in the vessel. The inner surfaces of cells 1 to 13 of heat structure 90 are attached to cells 14 to 26 of coolant loop 1. The inner surfaces of cells 14 to 26 of heat structure 90 is attached to cells 14 to 26 of coolant loop 2. The inner surfaces of cells 27 to 39 of heat structure 90 is attached to cells 14 to 26 of coolant loop 3.

## 3.3 Pumps

The pumps used for all three coolants in this study are geometrically identical. The pumps differ between each model with respect to the pump impeller rotational speed. This is because each fluid analyzed has different properties and required different mass flow rates to meet the system requirements. The pumps were modeled using TRACE built in pump components. The specifics of the pumps used in this study are not relevant because the only purpose of the pumps is to provide a constant mass flow rate for each coolant loop in each TRACE model for the respective coolant analyzed. The component numbers for the pumps in coolant loops 1, 2, and 3 are 70, 170, and 270 respectively. A pump efficiency of 85% is assumed.

### 3.3.1 Pumping Power

The pumping power was calculated by modeling equation 3.5 using a control system in TRACE. The unit for the pumping power calculated is  $W$ , the volumetric flow rate,  $Q$ , is in units of  $\frac{m^3}{s}$ , and the Pressure difference,  $\Delta P$ , is in units of  $Pa$ .

$$Pumping\ Power = Q \times \Delta P \quad (3.5)$$

The only difference in the control systems used to model the pumping power from pump 70, 170, and 270 for a given system is the control block numbers. The control system will vary between models with respect to using liquid phase properties vs gas phase properties for the water and the helium and carbon dioxide cooled models of this study respectively. Figure 3.5 provides the control system implemented in TRACE to calculate the pumping power for pump 70 in the water cooled model for this study. Signal variable 530 read the pressure from cell 2 of pipe 40, the last cell before pump 70. Signal variable 531 read the pressure from cell 1 of pipe 180, the first cell after pump 70. Control block -21 calculated the pressure difference between these two cells, representing the  $\Delta P$  term in equation 3.5. To solve for the volumetric flow rate,  $Q$ , in equation 3.5, the mass flow rate of



the water through the pump is divided by the density of the coolant in the pump. To represent this in the control system for the pumping power, signal variable 528 reads the mass flow rate across cell edge 3 of pump 70, the last cell edge of pump 70, signal variable 529 reads the density of the water in cell 2 of pump 70, the last cell of pump 70, and control block -24 divides these values accordingly. Control block -22 calculates the pumping power by multiplying the pressure difference across pump 70, calculated by control block -21, by the volumetric flow rate through pump 70, calculated by control block -24.

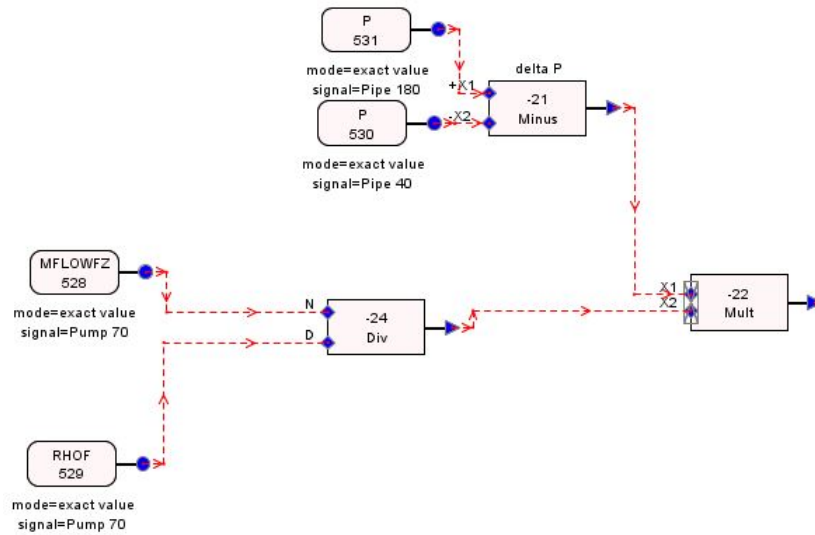


**Figure 3.5.** Pump 70 Pumping Power Control System for the TRACE Water Cooled Model

### 3.4 Turbine

The only output from the turbine desired for this study is the turbine output work. Turbine output work can be predicted by equation 3.6.

$$W_{turbine} = \sum_{in} \dot{m}h - \sum_{out} \dot{m}h \quad (3.6)$$

The turbine output work for the TRACE models used in this study was predicted by creating a control system that modeled equation 3.6. The value for the mass flow rate "in" and "out" was taken at the last cell edge of the steam generator for each respective model. This was the only mass flow rate used in the control system because the secondary side of the power plant is a closed loop. So, the mass flow rate out of the steam generator to the turbine will equal the mass flow rate into the steam generator from the condenser. The value for the enthalpy "in" was taken at the last cell of the steam generator for each respective model. The value for the enthalpy "out" was taken at the fill component of the steam generator for each respective model. This value for enthalpy "out" is not truly representative of the enthalpy at the exit of the low pressure turbine because the fill component for the secondary side of the steam generators represents the fluid after it has passed through the condenser. So, the fluid properties will at this point will be different from those at the exit of the low pressure turbine.

The only differences between the water cooled model turbine control system and the turbine control system used for the helium and carbon dioxide models are the component numbers referenced for the signal variables, and the turbine efficiency. As an example, the turbine control system for the water cooled model is shown in figure 3.6. Signal variable 105 reads the mass flow rate across the last cell edge of the steam generator. Signal variable 106 reads the enthalpy in the last cell of the steam generator. Signal variable 109 reads the enthalpy from the fill component representing the steam generator feedwater. Control block -150 is the turbine efficiency. Control block -120 calculates the difference in enthalpy between the last cell of the steam generator and the fill component representing the steam generator feedwater. Control Block -130 multiplies the difference in enthalpy calculated by control block -120 by the mass flow rate from signal variable 105. Control block -140 multiplies the turbine efficiency by the result from control block -130 to calculate the turbine output work.

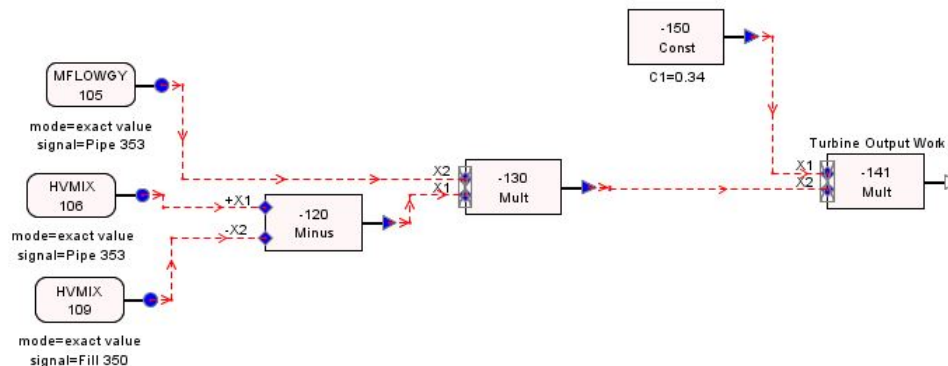


Figure 3.6. Water Cooled Model Turbine Control System

### 3.5 Overall System Efficiency

The overall efficiency of the models analyzed in this study were calculated by subtracting the power for all components of the system from the power produced by the turbine. This is modeled in TRACE for all of the models used in this study by control block -8. Control block -8 subtracted the sum of the pumping powers of pumps 70, 170, and 270, calculated by control block -17, from the turbine output power, calculated by control block -141.

### 3.6 Water Cooled TRACE Model

Water was the first coolant analyzed in this process. Water has been used in power plant applications throughout history. This section describes the additional components used in the water cooled model, how they were modeled in TRACE, and the entire water cooled model in TRACE. The additional components to the vessel and pumps include the steam generator and the pressurizer.

#### 3.6.1 U-tube Steam Generator

The steam generator in the water model is modeled after a U-tube steam generator. This section briefly presents how a u-tube steam generator functions, then describe the modeling process in TRACE.

A u-tube steam generator consists of a primary and secondary side. Primary side water, after passing through the vessel coolant channels, enters the steam

generator lower plenum. After this, the coolant enters the u-tubes where energy is transferred to the secondary side water by conduction through the u-tube pipe walls. The secondary side pressure is lower than the primary side pressure, so the secondary side water will boil to create a saturated steam. The high-pressure steam will pass through a separator and dryer to ensure it is 100 % vapor before exiting the steam generator and entering the turbine. Any liquid removed by the separator and dryer will flow through the downcomer and re-enter the system to attempt to become vapor again. The internal energy of the high-pressure steam exiting the steam generator is converted to rotational kinetic energy by expansion across the turbine blades. After exiting the turbine, the steam passes through a condenser and is condensed back into a liquid. After exiting the condenser, the single-phase liquid water pumped back into the steam generator to become steam again. The closed loop cycle is constantly repeated. Figure 3.7 shows the basic design of a u-tube steam generator and its important features.

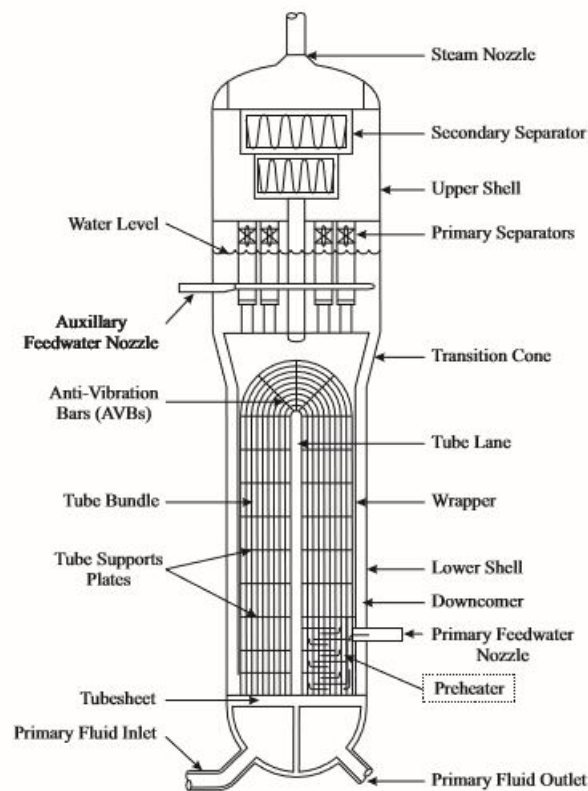


**Figure 3.7.** U-tube Steam Generator [32]

The specific u-tube steam generator modeled consists of 4570 u-tubes with an average tube length of 16 m. Each u-tube has an inner diameter of 1.6886 cm. Each u-tube has a wall thickness of 1.092 mm. The u-tube wall material is inconel 600.

The primary side lower plenum, tubesheet, and u-tubes are modeled by two pipe components in TRACE, pipes 311 and 320. The u-tubes are represented by cells 2 through 14 of pipes 311 and 320. The cell averaged flow area and cell edge flow area for each cell representing the u-tubes was calculated by finding the flow area of one u-tube and multiplying by the total number of u-tubes.

$$U - tube \text{ single pipe flow area} = \pi \times \frac{D_i^2}{4} = 2.2395 \times 10^{-4} \text{ m}^2 \quad (3.7)$$

$$\begin{aligned} & \text{Pipe 311 and 320 total flow area} = \\ & \text{single pipe flow area} \times \text{number of pipes} = \end{aligned} \quad (3.8)$$

$$\frac{2.2395 \times 10^{-4} \text{ m}^2}{\text{single pipe}} \times 4570 \text{ pipes} = 1.0234 \text{ m}^2$$

Cell one of pipes 311 and 320 represented the lower plenum. A loss coefficient is added to the cell edges between the cells representing the u-tube and lower plenum, cell edge 2 in each pipe component, to account for the minor loss due to the tubesheet. Two identical heat structures, heat structures 381 and 390, are used to represent an average steam generator tube wall. A surface multiplier is used to extend their representation to all 4570 tubes. Heat structures 381 and 390 are cylindrical inconel 600 tubes with an inner diameter of 1.6886 cm and a wall thickness of 1.092 mm. The length of each heat structure is equal to half of the average total u-tube length, 8 m.

The surface multiplier for heat structures 381 and 390 is 4570. This means that there are 4570 of these heat structures that represented the 4570 u-tubes of the steam generator. The inner surfaces of heat structures 381 and 390 are attached

to cells 2 through 14 of pipes 311 and 320 respectively, the cells representing the u-tubes. The outer surfaces of these heat structures are attached to fluid volumes that represent the boiler region of the steam generator, cells 2 through 5 of pipe 353. This allowed the energy from the primary side coolant to be transferred to the secondary side coolant through the heat structures representing the u-tube pipe walls.

The steam generator housing and relevant secondary side components are represented by multiple pipe components, a fill component, and a break component in TRACE. Pipe 353 is used to represent the steam generator boiler, separator, and drier. There are 10 cells in total for pipe 353. Cell 1 represented where secondary side liquid water and liquid water separated from steam that passed through the separator and drier re-enters the steam generator to attempt to become vapor again. Cells 2 through 5 represented where the u-tubes pass through the steam generator and transfer energy from the primary side coolant to the secondary side water. Cells 6 through 10 represent the separator and drier. There is a minor loss factor added at cell 9 to represent the minor loss due to the separator and dryer. Break 355 is attached to cell 10 of pipe 353 to set the steam line pressure boundary conditions. The transition cone is represented by pipe 354. The transition cone pipe is attached to the first cell of the downcomer pipe, pipe 352. Attached to cell 2 of the pipe representing the downcomer is a pipe component representing the feedwater nozzle, pipe 351. Attached to the feedwater nozzle is fill 350 that represents liquid water after it has passed through the condenser. The last cell of the pipe 352 is attached to the first cell of the pipe 353. This allows liquid water that has been separated from the steam after passing through the separator and drier and liquid water that has formed after steam has passed through the turbine and condenser to re-enter the steam generator to attempt to become vapor again. The TRACE u-tube Steam generator model is shown in figure 3.8.

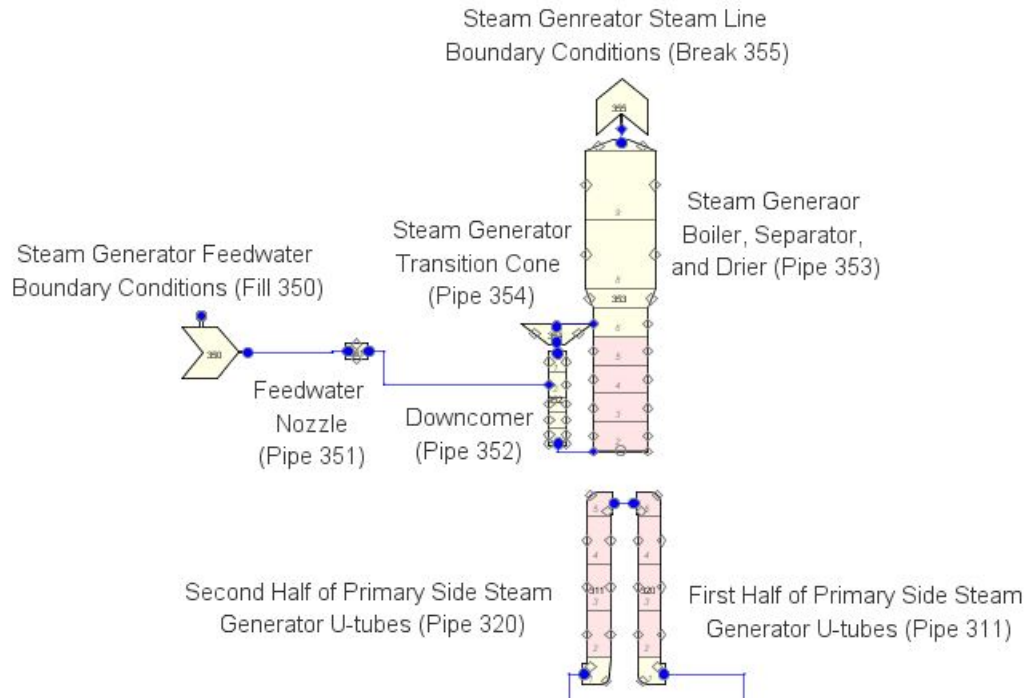


**Figure 3.8.** TRACE U-tube Steam Generator Model

A control system is used to keep the water level consistent in the steam generator, even with power transients. The controller measures the collapsed liquid level in the boiler region and adjusts the feedwater mass flow rate to maintain a constant level in the steam generator. The controller implemented first used a user set fill mass flow rate for the first 30 seconds of simulation time. After this, the controller set the fill mass flow rate to equal the mass flow rate exiting the steam generator at cell edge 11. The control system is shown in figure 3.9.

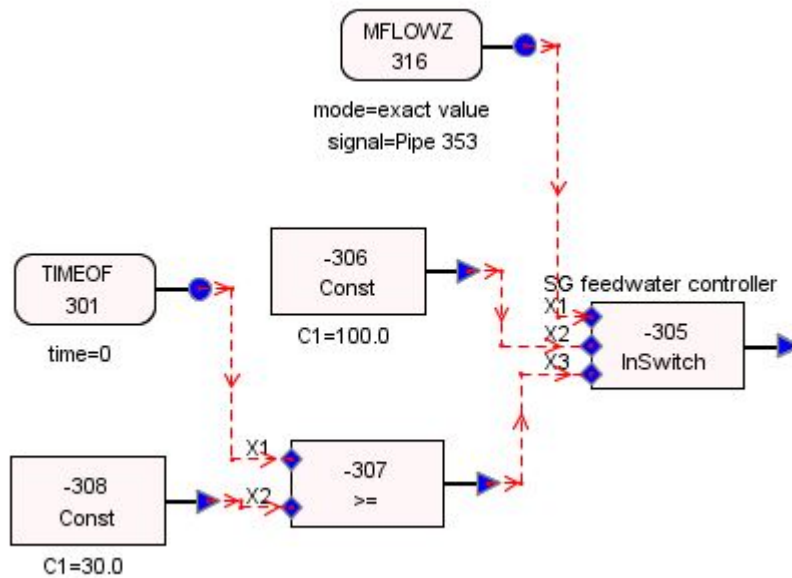


**Figure 3.9.** U-tube Steam Gnerator Feedwater Controller

### 3.6.1.1 U-tube Steam Generator Mesh Size Error Analysis

Richardson Extrapolation was used to quantify the error associated with the mesh size of the u-tube pipes. To perform this analysis, the components of the u-tube steam generator was isolated from the rest of the system, but a fill and break component were used to represent the boundary conditions of the u-tube pipes. The fill and break component used the steady state conditions from the model for the fluid volume before and after the u-tube u-tube pipes respectively. The mesh sizes were changed for the vertically straight sections of the u-tubes. The three mesh sizes used in this analysis were 2.242406 m, 1.121203 m, and 0.560601 m. The parameter chosen for the analysis was the liquid velocity at 12.157594 m from the entrance of the primary side water into the u-tubes at 190 seconds of simulation time. This was plenty of time for the model to reach steady state conditions. This was confirmed by plotting and examining the results for various parameters vs time. Figures 3.10, 3.11, and 3.12 show the liquid velocity vs time at 12.157594 m from the beginning of the u-tubes for the three different mesh sizes used in this analysis from largest to smallest respectively.



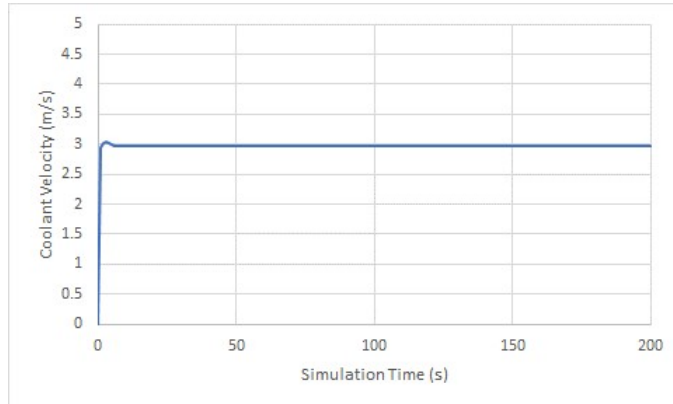


**Figure 3.10.** U-tube Liquid Velocity vs Time at 12.157594 m from the entrance of the u-tubes. Mesh Length=2.242406 m.

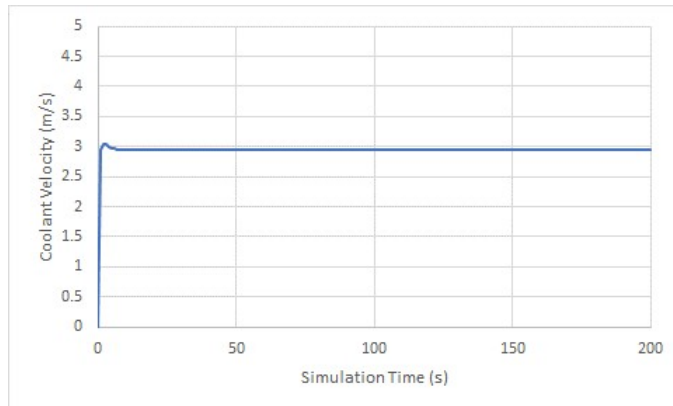


**Figure 3.11.** U-tube Liquid Velocity vs Time at 12.157594 m from the entrance of the u-tubes. Mesh Length=1.121203 m.

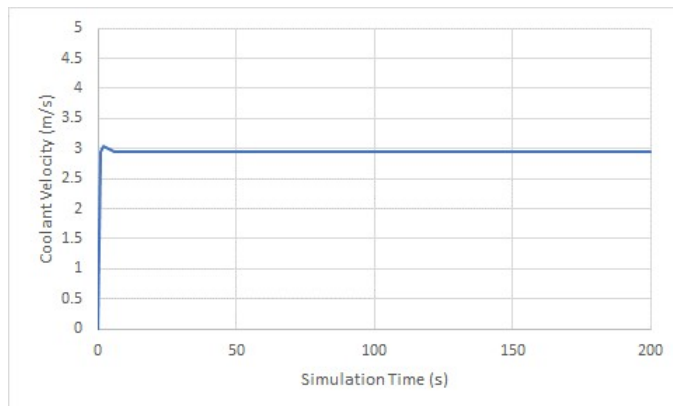


**Figure 3.12.** U-tube Liquid Velocity vs Time at 12.157594 m from the entrance of the u-tubes. Mesh Length= 0.560601 m.

After confirming the model had reached steady state, the liquid velocity in the u-tubes at 12.157594 m from the beginning of the u-tubes at 190 seconds of simulation time for all three mesh sizes was used to determine the error associated with the finest mesh. For equations 3.9, 3.10, and 3.11, the subscript numbers correspond to ranking of the mesh size from smallest to largest. i.e.  $f_1$  corresponds to the liquid velocity at 12.157594 m from the start of the u-tubes at 190 seconds for the finest mesh.

**Table 3.1.** U-tube Steam Generator Richardson Extrapolation Results and Values Used

h (mesh length in m)	r	p	$f_{computed} \frac{m}{s}$	$f_{exact} \frac{m}{s}$	error finest mesh $\frac{m}{s}$
0.560601	2	0.809233	2.941597	2.931653	0.009944
1.121203	2		2.949078		
2.242406			2.962186		

$$r = \frac{h_3}{h_2} = \frac{h_2}{h_1} = 2 \quad (3.9)$$

$$p = \frac{\ln(\frac{f_3 - f_2}{f_2 - f_1})}{\ln(r)} = 0.809233 \quad (3.10)$$

$$\epsilon_1 = f_1 - f_{exact} = \frac{f_2 - f_1}{r^p - 1} = 0.009944 \frac{m}{s} \quad (3.11)$$

### 3.6.2 Pressurizer

A pressurizer was modeled and used for the water cooled model in this study. This section provides a brief description of a pressurizer functions, then describes how this component was modeled in the water cooled TRACE model for this study. Only one pressurizer is needed to regulate the pressure of the entire water cooled model because there are no isolated coolant loops. Regardless of the number of coolant loops in a PWR, there is usually only one pressurizer because pressurizers are relatively difficult to control [33].

A pressurizer has a large volume that is partially filled with a fluid and contains a heater and condensing spray. In a PWR system, a pressurizer is typically 60% filled with liquid water and 40% filled with steam [34]. For the water cooled model of this study, the fluid in the pressurizer is water. In a pressurized water cooled system, a pressurizer is attached to the primary side used to pressurize the system, to regulate and maintain the pressure in the primary loop constant, and to manage any volume changes in the primary loop due to thermal expansion/contraction during any transient conditions. A pressurizer can also serve as safety component [5]. The heater in a pressurizer is used to increase the pressure of the system by vaporizing some of the liquid phase water inside the pressurizer. Conversely, the condensing spray is used to condense the vapor in the pressurizer and decrease the pressure of the system [32]. A Cutaway of a pressurizer is shown in figure 3.13.

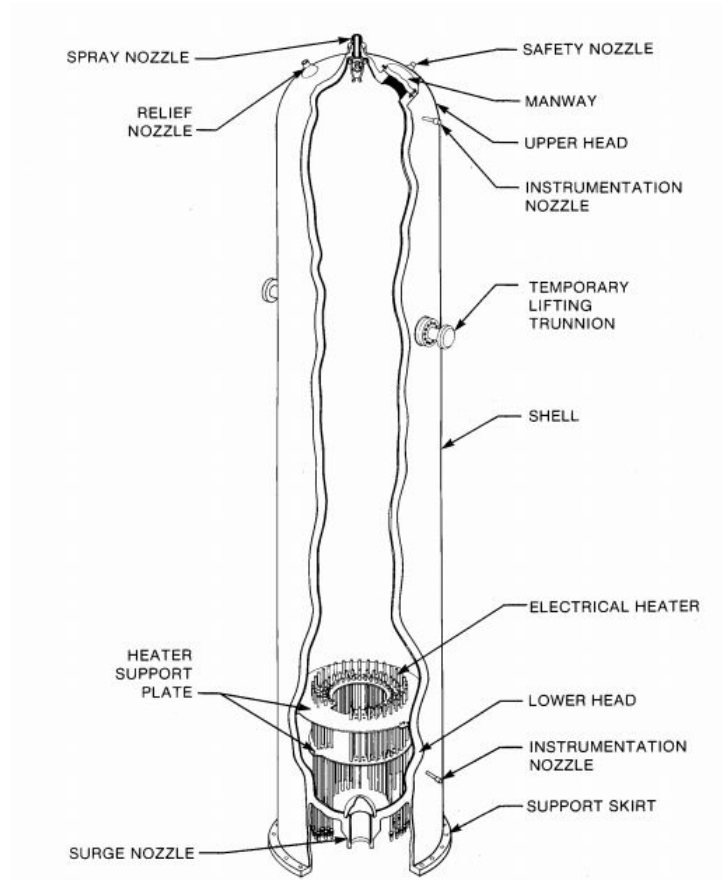


**Figure 3.13.** Cutaway of a Pressurizer [34]

### 3.6.2.1 Pressurizer TRACE Model

The pressurizer in the water cooled model of this study, pressurizer 611, was modeled using TRACE's built in pressurizer component. The pressurizer contained 6 cells and had a heater/sprayer maximum power of 1.8 MW. This is the same power used for pressurizers in Westinghouse four loop PWRs [34]. This means that at maximum/minimum power, the pressurizer can add/remove 1.8 MW from the water inside the pressurizer to heat it up and increase the system pressure or condense vapor and decrease the system pressure, respectively [1]. Pipe 46 modeled the surge line of the pressurizer. Cell edge 7 of pressurizer 611 is attached to cell edge 1 of pipe 46. Cell edge 3 of pipe 46 is attached to cell 30 of pipe 180 in cross flow at 90°. Valve 110 and break 140 are used to model safety relief valves for the pressurizer. This valve is included in the model, but not used. A summary of the

pressurizer geometry is provided in figure 3.14. The operating conditions for the pressurizer are summarized in table 3.2. The TRACE pressurizer model for the water cooled system is shown in figure 3.15.

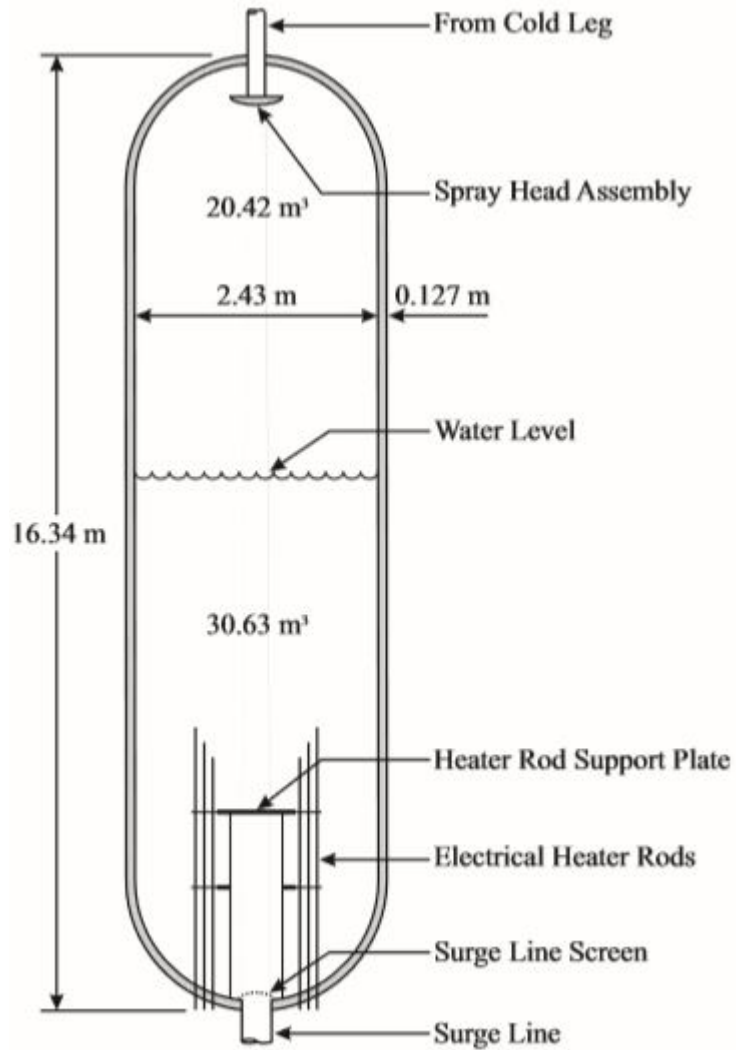


**Figure 3.14.** Pressurizer Geometry [32]

**Table 3.2.** Pressurizer Operating Conditions

Pressure Setpoint (MPa)	Heater/Sprayer Power (MW)	Liquid Volume at Steady State( $m^3$ )	Vapor Volume at Steady State ( $m^3$ )
15.5	1.8	30.63	20.42

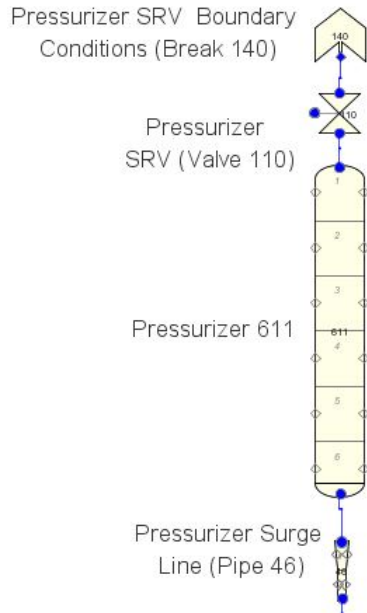


**Figure 3.15.** TRACE Pressurizer Model

### 3.6.3 Complete Water Cooled Model

This section provides the complete water cooled TRACE model, followed by the operating conditions for the water cooled TRACE model.

The water cooled TRACE model includes the various components described in the preceding sections. Water is pumped via pumps 70, 170, and 270 through coolant loops 1, 2, and 3 respectively. As stated in section 3.2.1, cells 14 through 26 of the coolant loops represent three 13 m long sections of coolant channels in the 39 m long vessel where the energy from the source is transferred to the coolant. After passing through the coolant loops, the water from each coolant loop will converge in the converging tee before passing through the steam generator u-tubes where its energy will be transferred to the secondary side water in the steam generator to create steam to spin the turbine via conduction through the steam generator

u-tube walls. After passing through the steam generator primary side components, the primary side water enters the diverging tee where the mass flow rate is split evenly between pipes 40, 50, and 60. After passing through pipes 40, 50, and 60, the coolant enters pumps 70, 170, and 270 respectively to be pumped back through the three coolant loops. This cycle is constantly repeated. The complete water cooled TRACE model is shown in figure 3.16.

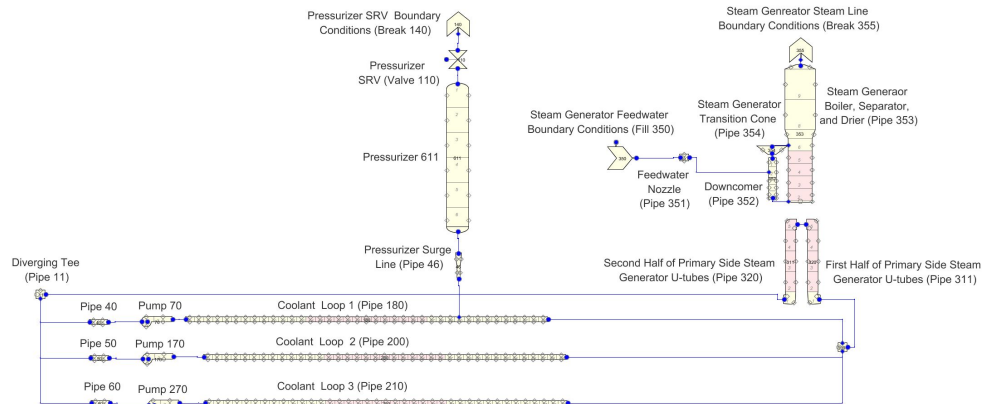


**Figure 3.16.** TRACE Water Cooled complete model

### 3.6.4 Water Cooled Model Operating Conditions

This section provides the operating parameters for the water cooled system and why these parameters were chosen. There were several factors that decided the operating conditions for the water cooled model. The system needed to operate in way to keep the temperatures of certain materials below their maximum values. Aside from this, the system needed to operate safely based on previous and current operating water cooled systems.

Beryllium has a melting temperature of 1287°C [35]. This wasn't chosen as the maximum operating temperature because the material properties of Beryllium change, and it gets weaker with increasing temperature. It defines the maximum temperature for a Beryllium first wall to be 800°C [28]. This was the temperature limit for all of the models. The water cooled model operates well below this temperature because it is desired to keep the primary side water temperature below the saturation temperature to avoid nucleate boiling. However, it is common to have subcooled boiling occur in a PWR [36]. The primary side pressure in PWRs is

16 MPa [34]. It was chosen to operate the primary side of the water cooled system around this pressure. The average coolant velocity of the Sequoyah-1 PWR is  $4.82 \frac{m}{s}$  [37]. It was chosen to have the coolant velocity in the water cooled model be around, or below this value. These stated PWR values served as a starting point for determining the water cooled model's final operating conditions. The operating parameters of the water cooled model are summarized in table 3.3.

**Table 3.3.** Water Cooled Model Primary Side Operating Conditions

$P$ (MPa)	$T_{in}$ (K)	$T_{out}$ (K)	$\dot{m}$ ( $\frac{kg}{s}$ ) single coolant loop
15.5	561.4	610.6	678

**Table 3.4.** Water Cooled Model Secondary Side Operating Conditions

$P$ (MPa)	$T_{in}$ (K)	$T_{out}$ (K)	$\dot{m}$ ( $\frac{kg}{s}$ )
6.8	503.15	557.3	336.4

### 3.7 Helium and Carbon Dioxide Cooled Models

The helium and carbon dioxide TRACE models are geometrically identical. The models differ with respect to the primary side coolant and operating conditions. This section describes the various components used in the gas cooled models, how they were modeled in TRACE, and the entire gas cooled TRACE models. The gas cooled models are similar to the water cooled model, but had unique features compared to the water cooled model like a helical coil steam generator and no pressurizer.



### 3.7.1 Helical Coil Steam Generator

The helical coil steam generator used in the helium and carbon dioxide models is based on a generic helical coil model [38]. The model was designed for a heat load of 612 MWth. The steam generator secondary side consists of 5025 pipes with an inner diameter of 1.8 cm. The secondary pipe wall thickness is 1 mm. The average length of each secondary side pipe is 42.9 m. The inner coil diameter is 0.49 m and the outer coil diameter is 4.6 m. The coils have a height of 9.86 m. The secondary side pressure is 5 MPa.

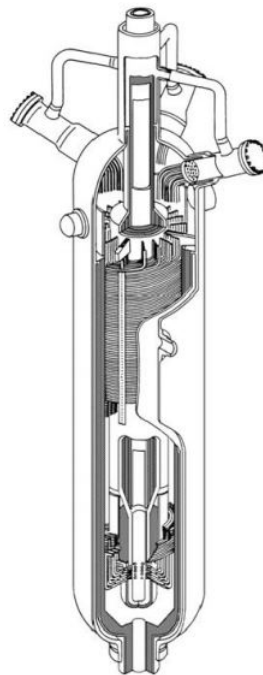


**Figure 3.17.** Cutaway of a Helical Coil Steam Generator [38]

Using the dimensions described in the previous paragraph, a TRACE model was built to represent the helical coil steam generator selected. The helical coil steam generator was modeled in TRACE with two pipes, a fill, and a break. Pipe 1050 represents the helical coil steam generator housing and pipe 1010 represents the 5025 helical coil pipes of the secondary side. Fill 20 and break 30 set the flow and boundary conditions for the entrance and exit of the helical coil pipes respectively.

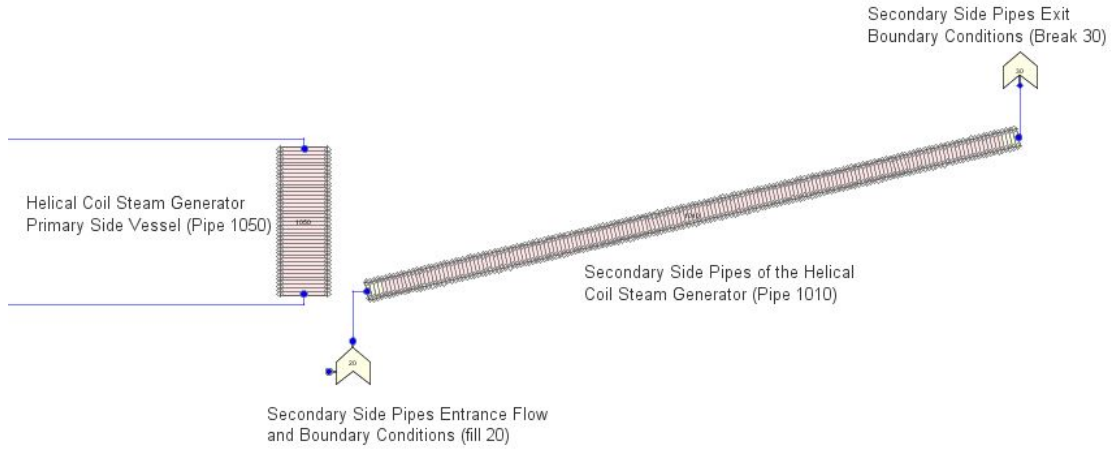


**Figure 3.18.** TRACE Helical Coil Steam Generator Model

The helical coil pipes are modeled with a curved pipe component in TRACE. There are 168 cells in total for the helical coil pipes with 160 cells representing the 42.9 m of average pipe length of the helical coil pipes inside the steam generator. The cell averaged flow area and cell edge flow area for each cell was calculated by finding the flow area of one secondary side pipe and multiplying by the number of pipes making up the secondary side. This process is shown in equations 3.12 and 3.13.

$$\text{single helical coil pipe flow area} = \pi \times \frac{D_i^2}{4} = 2.54469 \times 10^{-4} \text{ m}^2 \quad (3.12)$$

*Total flow area of helical coil pipes =*

$$\text{single pipe flow area} \times \text{number of pipes} = \quad (3.13)$$

$$\frac{2.54469 \times 10^{-4} \text{ m}^2}{\text{single pipe}} \times 5025 \text{ pipes} = 1.278707 \text{ m}^2$$

The total flow area of the helical coil pipes was determined to be  $1.278707 \text{ m}^2$  and the hydraulic diameter is 3 cm, the inner diameter of a single secondary side pipe. Together, the flow area and hydraulic diameter of the helical coil pipes let it represent 5025 circular cross section pipes each with an inner diameter of 3 cm.

Next, the average diameter of the coils was calculated and used to set the average coil diameter of the helical coil pipes. This was done by averaging the inner and outer coil radius. This average coil diameter is 2.545 m.

$$\begin{aligned} \text{average coil diameter} &= \\ \frac{\text{inner coild diameter} + \text{outer coil diameter}}{2} &= \quad (3.14) \\ \frac{0.49 \text{ m} + 4.6 \text{ m}}{2} &= 2.545 \text{ m} \end{aligned}$$

In TRACE, pipe 1010's "Tube Diameter Ratio" defines the ratio of the inside tube diameter vs the diameter of the coil [1]. Using the average coil diameter and given tube inner diameter, the "Tube Diameter Ratio" is  $7.465619 \times 10^{-3}$ . The average inclination angle of the secondary side pipes was found by taking the sin inverse of the coil height divided by the average pipe length.

$$\theta = \sin^{-1}\left(\frac{\text{coil height}}{\text{tube length}}\right) = \sin^{-1}\left(\frac{9.86 \text{ m}}{42.9 \text{ m}}\right) = 0.232 \text{ rad} \quad (3.15)$$

The calculated angle from equation 3.15 is used as the inclination angle of the helical coil pipes. With the helical coil pipes' flow area, hydraulic diameter, average coil diameter, tube diameter ratio, and inclination angle set to the values stated previously in this section, the helical coil pipes represent 5025 pipes, each with an inner diameter of 1.8 cm and an average coil diameter of 2.545 m, with an average inclination angle of 0.232 rad. The total heat transfer area is  $13,540 \text{ m}^2$ . The coil height for each of the 5025 pipes is 9.86 m.

Heat structure 1040 models the pipe walls of the helical coil pipes. Heat structure 1040 is a cylindrical inconel 600 tube with an inner diameter of 1.8 cm and a wall thickness of 1 mm, corresponding to the geometry of a single helical coil pipe. Heat structure 1040 is 42.9 m long. The surface multiplier for heat structure 1040 is set to 5025. This allows it to represent the 5025 pipe walls of the helical coil pipes. There are 160 cells for heat structure 1040. The inner surfaces of heat structure 1040 are connected to the helical coil pipes for the cells that represent the section of these pipes that are inside the steam generator housing. The outer surfaces of heat structure 1040 are connected to the fluid volumes of the helical coil steam generator housing, cells 1 through 40. This allows the primary side coolant to transfer its energy to the secondary side fluid through heat structure 1040.

#### **3.7.1.1 Helical Coil Steam Generator Mesh Size Error Analysis**

Richardson Extrapolation was used to quantify the error associated with the mesh size of the helical coil pipes. The process for performing this analysis was the same as for the u-tube steam generator of the water cooled model (section 3.6.1.1), but are stated here to avoid any confusion because the steam generators are different models. First, the components of the helical coil steam generator was isolated from the rest of the system, but a fill and break component were used to represent the boundary conditions of the helical coil steam generator housing. The fill and break component used the steady state conditions from the helium cooled model for the fluid volume before and after the helical coil steam generator housing respectively. The three mesh sizes used in this analysis were 1.0725 m, 0.53625 m, and 0.268125 m. The parameter chosen for the analysis was the gas velocity at 42.9 m from the first cell edge of the helical coil pipes at 3009 seconds of simulation time. This was plenty of time for the model to reach steady state conditions.

After confirming the model had reached steady state, the gas velocity in pipe 1010 42.9 m from the first cell edge of pipe 1010 at 1980 seconds of simulation time for all three mesh sizes was used to determine the error associated with the finest mesh. For equations 3.16, 3.17, and 3.18, the subscript numbers correspond to ranking of the mesh size from smallest to largest.

**Table 3.5.** Helical Coil Steam Generator Richardson Extrapolation Results and Values Used

h (mesh length in m)	r	p	$f_{computed} \frac{m}{s}$	$f_{exact} \frac{m}{s}$	error finest mesh $\frac{m}{s}$
0.268125	2	1.406502	11.840917	11.846	-0.005083
0.53625	2		11.832526		
1.0725			11.810282		

$$r = \frac{h_3}{h_2} = \frac{h_2}{h_1} = 2 \quad (3.16)$$

$$p = \frac{\ln(\frac{f_3 - f_2}{f_2 - f_1})}{\ln(r)} = 1.406502 \quad (3.17)$$

$$\epsilon_1 = f_1 - f_{exact} = \frac{f_2 - f_1}{r^p - 1} = -0.005083 \frac{m}{s} \quad (3.18)$$

### 3.7.2 Complete Helium and Carbon Dioxide Models

The helium and carbon dioxide cooled models are geometrically identical, but vary with respect to the coolant used and the operating conditions. This section provides the complete TRACE model for the helium and carbon dioxide cooled systems, followed by the operating conditions for each model.

This model includes the various components described in the preceding sections. The helium and carbon dioxide cooled models follow a very similar pattern to that of the water cooled model, but with an additional 2 pipes between the primary side exit of the steam generator and the diverging tee. The primary side coolant (helium or carbon dioxide) is pumped via pumps 70, 170, and 270 through coolant loops 1, 2, and 3 respectively. After passing through the coolant loops, the primary side

coolant from each coolant loop will converge in the converging tee before passing through the helical coil steam generator where its energy will be transferred to the secondary side water through the helical coil pipe walls to create a superheated steam that will enter and spin the turbine. After passing through the steam generator primary side shell, the primary side coolant passes through pipes 80 and 1060 before entering the diverging tee where the mass flow rate is split evenly between pipes 40, 50, and 60. After passing through pipes 40, 50, and 60, the coolant enters pumps 70, 170, and 270 respectively to be pumped back through the three coolant loops. This cycle is constantly repeated. The complete helium and carbon dioxide cooled TRACE model is shown in figure 3.19.

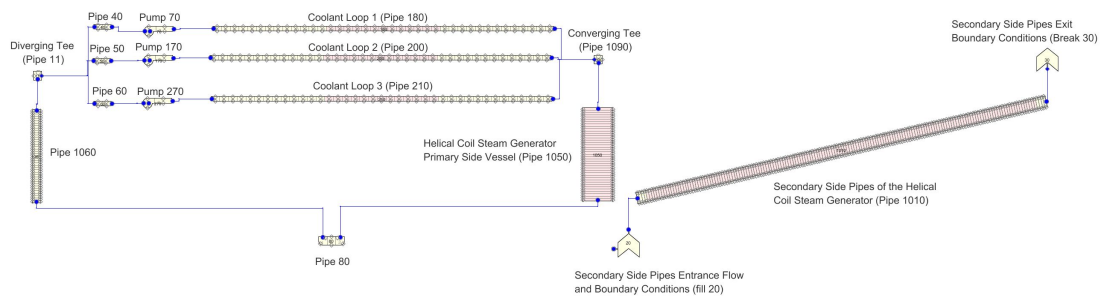


**Figure 3.19.** TRACE Helium and Carbon Dioxide Cooled Model

### 3.7.3 Helium Cooled Model Operating Conditions

This section provides the operating parameters for the helium cooled system and why these parameters were chosen. The process for deciding the operating conditions for the helium cooled system was the same as the water cooled system.

As stated in section 3.6.4, the maximum beryllium temperature for all models is 800°C [28]. The helium cooled system was designed to not exceed this temperature. Analysis has been performed to quantify the coolant velocity for a helium cooled first wall for Iiter. It is stated that the helium coolant velocity is 81 m/s [39]. It was chosen to have the coolant velocity in the helium cooled model operate around or below this velocity. Helium gas cooled fast reactors are set to operate at 9.1 MPa [10]. It was chosen to have the primary side pressure of the coolant be around this value. These conditions served as the starting point for the final parameters

chosen for the helium cooled model. The operating parameters of the helium cooled model are summarized in tables 3.6 and 3.7.

**Table 3.6.** Helium Cooled Model Primary Side Operating Conditions

$P$ (MPa)	$T_{in}$ (K)	$T_{out}$ (K)	$\dot{m}$ ( $\frac{kg}{s}$ ) single coolant loop
8.9	526.83	933.16	94.13

**Table 3.7.** Helium Cooled Model Secondary Side Operating Conditions

$P$ (MPa)	$T_{in}$ (K)	$T_{out}$ (K)	$\dot{m}$ ( $\frac{kg}{s}$ )
5	500	745.66	250

### 3.7.4 Carbon Dioxide Cooled Model Operating Parameters

This section provides the operating parameters for the carbon dioxide cooled system and why these parameters were chosen. The process for deciding the operating conditions for the carbon dioxide cooled system was the same as for the water and helium cooled systems.

As stated in section 3.6.4, the max beryllium temperature for all models is 800°C [28]. The mean coolant velocity in the carbon dioxide cooled Calder Hall AGR is 22.55 m/s in the hot ducts and 15 m/s in the cold ducts [4]. The carbon dioxide cooled model for this study was chosen to operate around the same coolant velocities. Multiple carbon dioxide cooled power systems are being analyzed to operate at pressures greater than 20 MPa [40]. This was chosen as the pressure limit for the carbon dioxide cooled model. The operating parameters of the carbon dioxide cooled model are summarized in tables 3.8 and 3.9.

**Table 3.8.** Carbon Dioxide Cooled Model Primary Side Operating Conditions

$P$ (MPa)	$T_{in}$ (K)	$T_{out}$ (K)	$\dot{m}$ ( $\frac{kg}{s}$ ) single coolant loop
12	586.51	923.36	491.78

**Table 3.9.** Carbon Dioxide Cooled Model Secondary Side Operating Conditions

$P$ (MPa)	$T_{in}$ (K)	$T_{out}$ (K)	$\dot{m}$ ( $\frac{kg}{s}$ )
5	500	746.96	250

### 3.8 Summary of Operating Conditions

The operating conditions were unique for each model analyzed in this study. The water cooled model operated at similar conditions to those of a PWR. The helium and carbon dioxide cooled models operated at conditions based on AGRs, GFRs, and other similar gas cooled systems. Tables 3.10 and 3.11 provides a summary of the operating conditions for all of the systems of this study.

**Table 3.10.** Primary Side Operating Conditions

Coolant	$P$ (MPa)	$T_{in}$ (K)	$T_{out}$ (K)	$\dot{m}$ ( $\frac{kg}{s}$ )
water	15.5	561.4	610.6	678
helium	8.9	526.83	933.16	94.13
carbon dioxide	12	586.51	923.36	491.78

**Table 3.11.** Secondary Side Operating Conditions

Coolant	$P$ (MPa)	$T_{in}$ (K)	$T_{out}$ (K)	$\dot{m}$ ( $\frac{kg}{s}$ )
water	6.8	503.15	557.3	336.4
helium	5	500	745.66	250
carbon dioxide	5	500	746.96	250



# Chapter 4 | Verification of Helium and Carbon Dioxide in TRACE

## 4.1 Introduction

TRACE is only verified and validated with light water as the working fluid in simulation. There have been some verification and validation tests performed with helium as the working fluid in TRACE, but not enough to define helium as verified and validated for TRACE [24]. This chapter goes over how helium and carbon dioxide were verified for the range of conditions used in this research by using the method of manufactured solutions. The fluid properties of helium were taken from TRACE's built in equations of state for helium and the carbon dioxide properties were provided to TRACE by an XPTB. Test cases were simulated in TRACE with operating conditions similar to the final set of conditions used in the helium and carbon dioxide cooled models. TRACE predicted results for various parameters were compared to hand calculated results for the same problems. The geometry for all test cases was the same geometry a single coolant channel in the vessel for a given coolant loop in the models of this study (13 m long 3 cm inner diameter pipe). There were four test cases ran for both helium and carbon dioxide, two for horizontal flow for each fluid, and two for vertical upward flow for each fluid. For the test cases in each direction (vertical upward and horizontal), there was a test case ran for adiabatic flow and a test case ran with a wall power of 557 kW, the same power as the power deposited into a single 13 m long coolant channel pipe wall for the models of this study. Each test case had identical geometry. For

both the adiabatic and non-adiabatic cases, the TRACE predicted pressure and coolant velocity vs axial position were compared to hand calculated results for these same parameters. Additionally, for the non-adiabatic cases, the TRACE predicted coolant temperature vs axial position was compared to hand calculated results for the same parameter. Physical parameters used by TRACE were compared to physical parameters from the NIST database.

Also, using an XPTB for carbon dioxide properties needed to be verified to determine if the values of the XPTB are reliable and if TRACE reads the correct values. The process for creating the XPTB for carbon dioxide is explained in chapter 2. The carbon dioxide XPTB verification is presented in section 4.4.2.5. The analysis performed this section verify using helium and carbon dioxide in TRACE simulations for the conditions used in the full TRACE models.

## 4.2 TRACE Model

The TRACE vertical and horizontal models for these verification cases are shown in figures 4.1 and 4.2 respectively. The component numbers are identical for the horizontal and vertical test cases. Fill 10's pressure and temperature are used to determine the fluid conditions entering pipe 20. Break 30's pressure is used to set the pressure for the preceding cells of pipe 20 because a pressure difference is needed to drive the flow. Tables 4.1 and 4.2 provides the fill and break boundary conditions for the helium and carbon dioxide verification cases respectively. The boundary conditions were the same for all of the models of a given coolant (i.e. one set of boundary conditions used for all helium verification cases and one set of boundary conditions used for all carbon dioxide verification cases). The fill conditions were chosen to match the steady state conditions of the coolants based on the fluid properties in the last cell of the cold leg of coolant loop 1 for each coolant's respective complete model. Similarly, the break conditions were chosen to match the steady state conditions of the coolants based on the conditions in the first cell of the hot leg if coolant loop 1 for each coolant's respective complete model. The mass flow rate was divided by 359 to account for the mass flow rate of coolant through a single coolant channel. Pipe 20 is a 13 m long pipe component with 13 cells, each 1 m long. This is the same cell length and number of cells as the coolant channels in the vessel for a single coolant loop. Heat structure 40 is used

to model the coolant channel pipe wall and also model the 557 kW of power that is deposited into a single coolant channel pipe wall for the non-adiabatic verification cases.



**Figure 4.1.** Horizontal Verification TRACE model

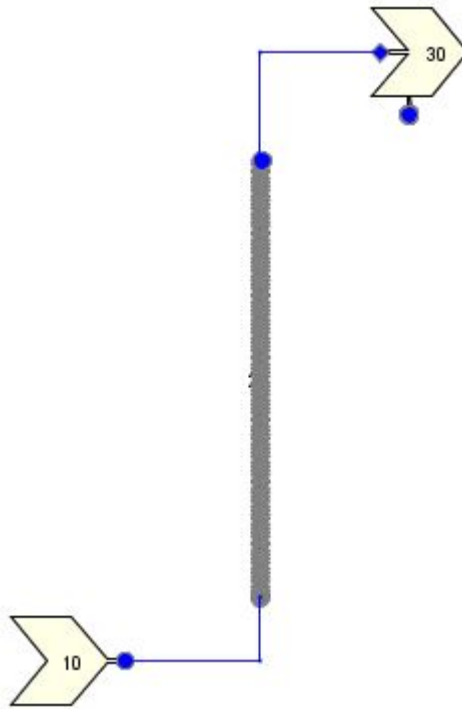


**Figure 4.2.** Vertical Verification TRACE model

**Table 4.1.** Helium Verification Model Boundary Conditions

	$P$ (MPa)	$\dot{m}$ ( $\frac{kg}{s}$ )	$T$ (K)
Fill 10	8.988	0.262	527.008
Break 30	8.897	N/A	932.685

**Table 4.2.** Carbon Dioxide Verification Model Boundary Conditions

	$P$ (MPa)	$\dot{m}$ ( $\frac{kg}{s}$ )	$T$ (K)
Fill 10	12.15	1.467	586.364
Break 30	12.02	N/A	923.261

## 4.3 Hand Calculations

This section reviews the procedure and equations used for calculating the results of the verification cases by hand. First, the fluid properties used by TRACE were compared to fluid properties from the NIST Chemistry webBook, SRD 69 [41] for identical conditions. The fluid properties were determined reliable. After this, the fluid properties used by TRACE were used in hand calculations for the fluid velocity, pressure drop, and fluid temperature vs axial position in the pipe.

The hand calculated values were calculated at the same axial positions as they were calculated in TRACE. TRACE calculates the coolant velocity at cell edges. The coolant temperature and pressure are cell averaged values and located at the center of a given cell in TRACE.

The hand calculated fluid velocity was found by equation 4.1.

$$V_{i\pm 1/2} = \frac{\dot{m}}{\rho_{i\pm 1/2} A} \quad (4.1)$$

The hand calculated coolant temperature at a given axial location was found by equation 4.2. The specific heat of helium and carbon dioxide will change with a change in temperature or pressure. The specific heat is not a built in plotting parameter for pipe components in TRACE. However, there is a signal variable in

TRACE that can plot the specific heat for a single cell of most fluid components, including pipes. This signal variable was used to obtain the specific heat for the axial midpoint of the pipe used in the verification test cases. This corresponded to cell 7 of pipe 20. The change in specific heat for helium and carbon dioxide cases is small and will have a very small impact on the coolant temperature. This is proven in the temperature vs axial position plots, figures 4.5,

$$T_i = T_{in} + \frac{q_{L_i}^{z_i}}{\dot{m}c_p} \quad (4.2)$$

The hand calculated pressure at a given axial location was found by equation 4.3. The hand calculated pressure was calculated at the same axial positions as in the TRACE verification models.

$$P_i = P_{i-1} - \frac{f_i \rho_i u_i^2 \Delta z}{2D} \quad (4.3)$$

Frictional pressure loss was the only hand calculated pressure loss accounted for in the horizontal flow tests. For vertical the flow verification tests, an additional hand calculated gravitational loss was accounted for. The overall hand calculated pressure loss for vertical flow verification tests was calculated using equation 4.4.

$$P_i = P_{i-1} - \frac{f_i \rho_i u_i^2 \Delta x}{2D_i} - \rho_i g z_i \quad (4.4)$$

## 4.4 Results

The TRACE simulations ran for 500 seconds of simulation time. This was plenty of runtime to ensure steady state results had been reached. To prove steady state results had been reached, various time dependent parameters vs time were plotted to show that the results were no longer changing with time. The results are presented for the helium verification cases in section 4.4.1, and the results for the carbon dioxide verification cases are provided in section 4.4.2

### 4.4.1 Helium Verification Test Results

This section provides the plots of TRACE predicted results vs hand calculated results for the four test cases described in section 4.1. The results from each test case are presented in their own subsections to avoid confusion.

#### 4.4.1.1 Horizontal Adiabatic Verification Case Results

Figures 4.3 and 4.4 show that the hand calculated velocity and pressure agree well for all axial positions of pipe 20 for the horizontal adiabatic test case. For both velocity and pressure, the difference between TRACE predicted results and hand calculated results is less than 1% for every data point.

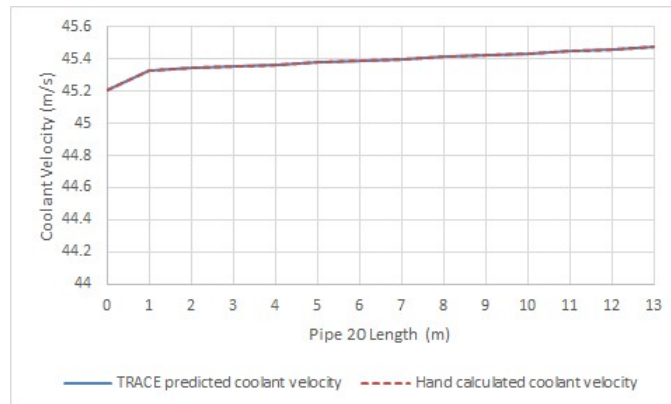


**Figure 4.3.** Helium Velocity Horizontal Adiabatic Verification Test Case

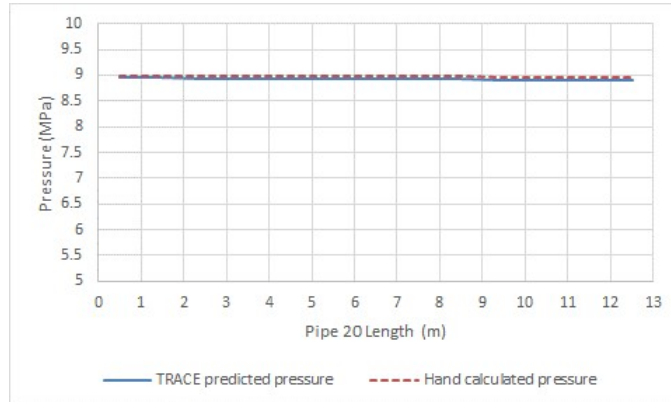


**Figure 4.4.** Helium Pressure Horizontal Adiabatic Verification Test Case

#### 4.4.1.2 Horizontal Non-Adiabatic Verification Case Results

Figures 4.5, 4.6, and 4.7 show that the TRACE predicted results for the temperature, velocity, and pressure vs axial position for the non-adiabatic horizontal test case agree well with the hand calculated results for these same parameters at every axial position. The difference between the TRACE predicted results and hand calculated results is less than 1% for every data point tested in the helium horizontal non-adiabatic test case.

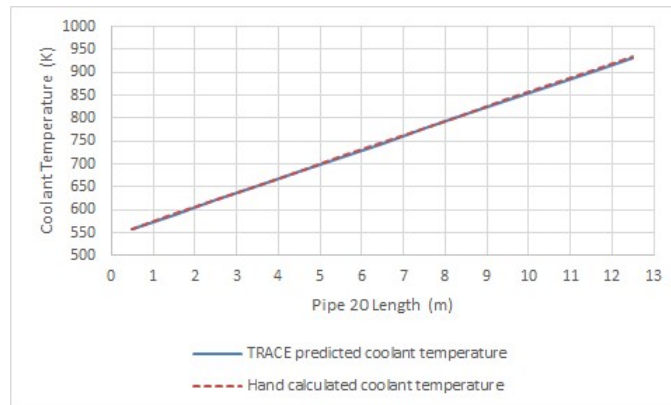


**Figure 4.5.** Helium Temperature Horizontal Non-Adiabatic Verification Test Case

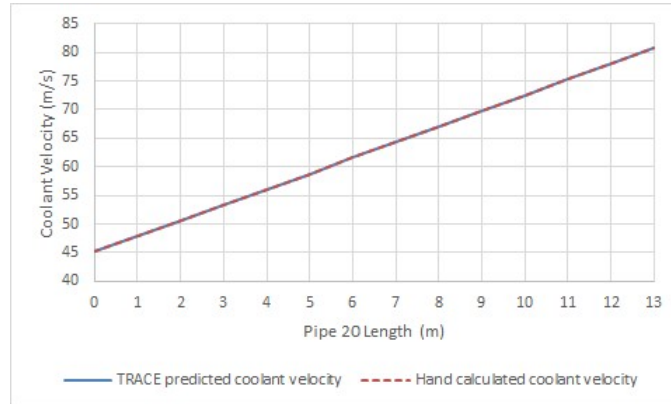


**Figure 4.6.** Helium Velocity Horizontal Non-Adiabatic Verification Test Case

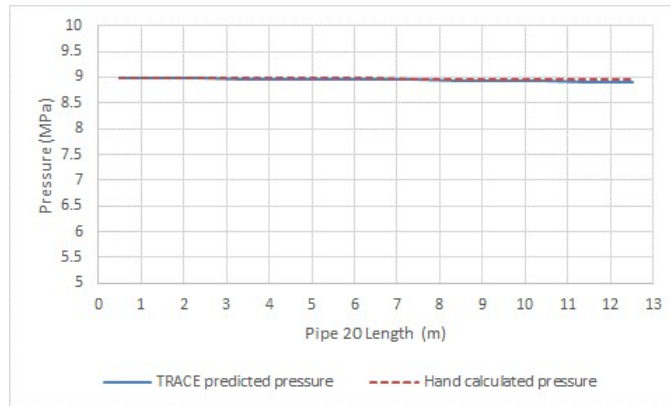


**Figure 4.7.** Helium Pressure Horizontal Non-Adiabatic Verification Test Case

#### 4.4.1.3 Vertical Adiabatic Verification Case Results

Figures 4.8 and 4.9 show that the hand calculated velocity and pressure agree well with the TRACE predicted velocity and pressure for all axial positions of pipe 20 for the helium vertical adiabatic test case. For both velocity and pressure, the difference between TRACE predicted results and hand calculated results is less than 1% for every data point.



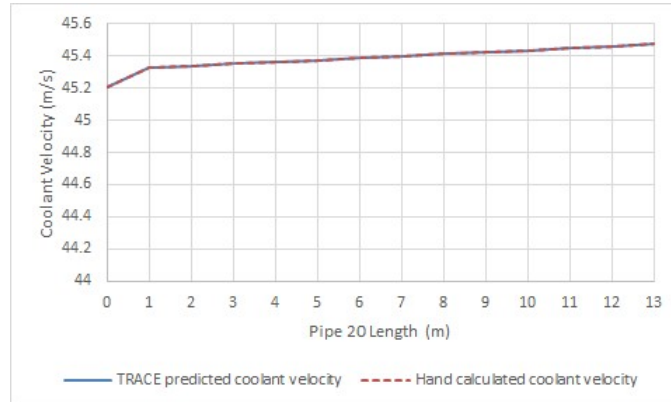


**Figure 4.8.** Helium Velocity Vertical Adiabatic Verification Test Case

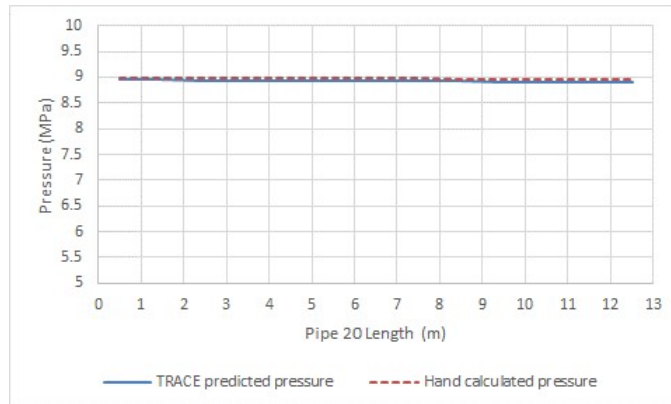


**Figure 4.9.** Helium Pressure Vertical Adiabatic Verification Test Case

#### 4.4.1.4 Vertical Non-Adiabatic Verification Case Results

Figures 4.10, 4.11, and 4.12 show that the TRACE predicted results for the temperature, velocity, and pressure vs axial position for the vertical non-adiabatic test case agree well with the hand calculated results for these same parameters at every axial position. The difference between the TRACE predicted results and hand calculated results is less than 1% for every data point tested in the helium horizontal non-adiabatic test case.

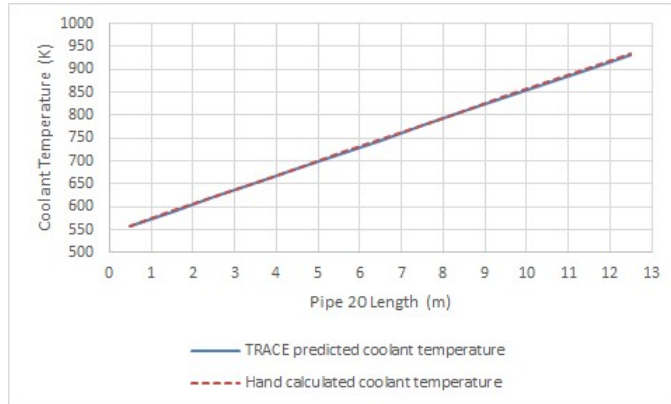


**Figure 4.10.** Helium Temperature Vertical Non-Adiabatic Verification Test Case

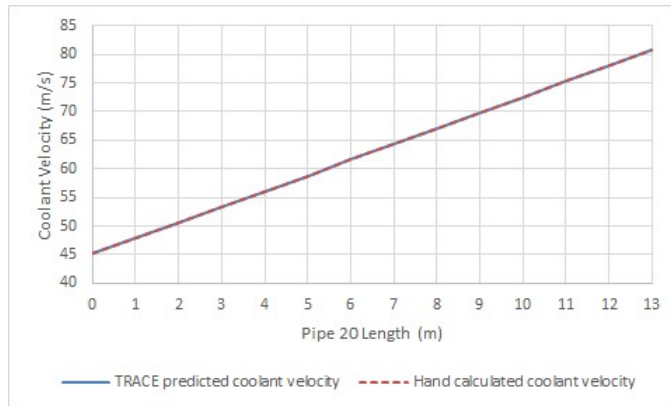


**Figure 4.11.** Helium Velocity Vertical Non-Adiabatic Verification Test Case

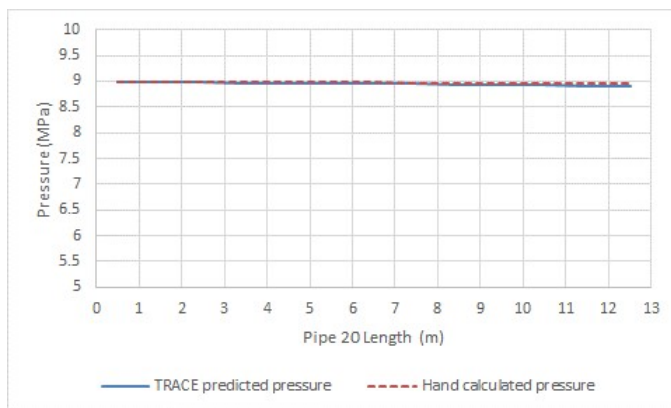


**Figure 4.12.** Helium Pressure Vertical Non-Adiabatic Verification Test Case

## 4.4.2 Carbon Dioxide Verification Test Results

This section follows the same format as the section that presented the helium verification test results, section 4.4.1. Section 4.4.2.5 is an additional section that includes the verification of the values of the carbon dioxide XPTB.

### 4.4.2.1 Horizontal Adiabatic Verification Case Results

Figures 4.13 and 4.14 show that the hand calculated velocity and pressure agree well for all axial positions of pipe 20 for the carbon dioxide horizontal adiabatic test case. For both velocity and pressure, the difference between TRACE predicted results and hand calculated results is less than 1% for every data point.

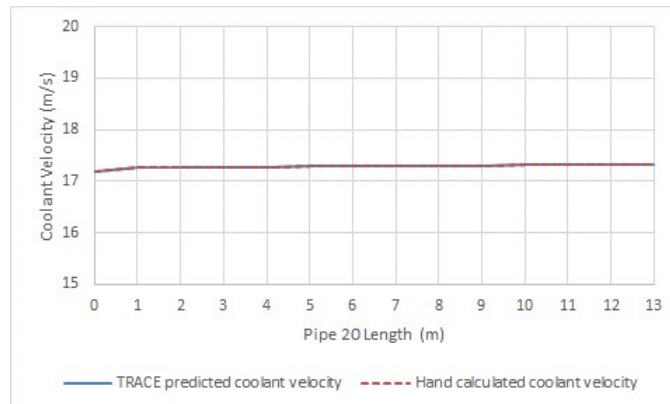


**Figure 4.13.** Carbon Dioxide Velocity Horizontal Adiabatic Verification Test Case

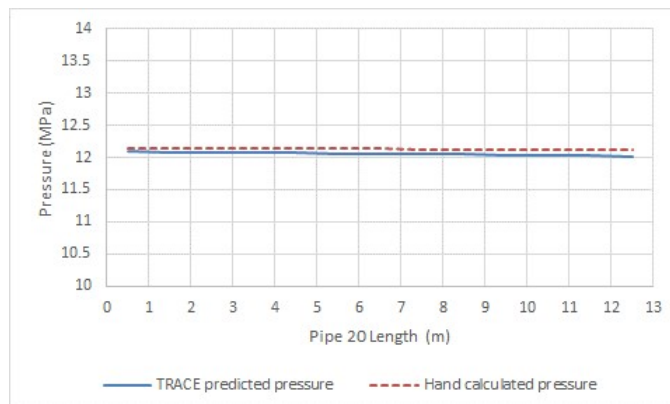


**Figure 4.14.** Carbon Dioxide Pressure Horizontal Adiabatic Verification Test Case

#### 4.4.2.2 Horizontal Non-Adiabatic Verification Case Results

Figures 4.15, 4.16, and 4.17 show that the TRACE predicted results for the coolant temperature, velocity, and pressure vs axial position for the non-adiabatic horizontal test case agree well with the hand calculated results for these same parameters at throughout the length of the pipe. The difference between the TRACE predicted results and hand calculated results is less than 1% for every axial position tested in the carbon dioxide horizontal non-adiabatic test case.

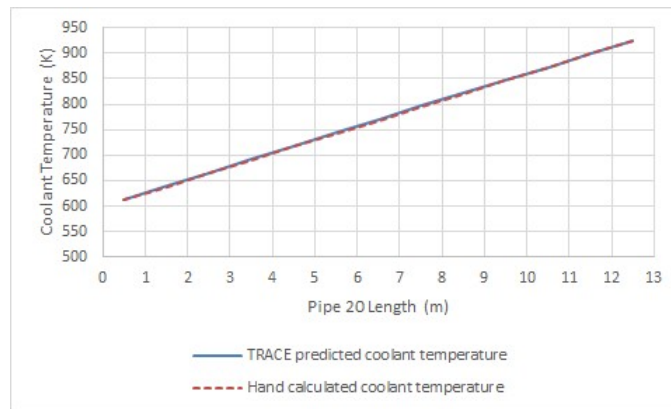


**Figure 4.15.** Carbon Dioxide Temperature Horizontal Non-Adiabatic Verification Test Case

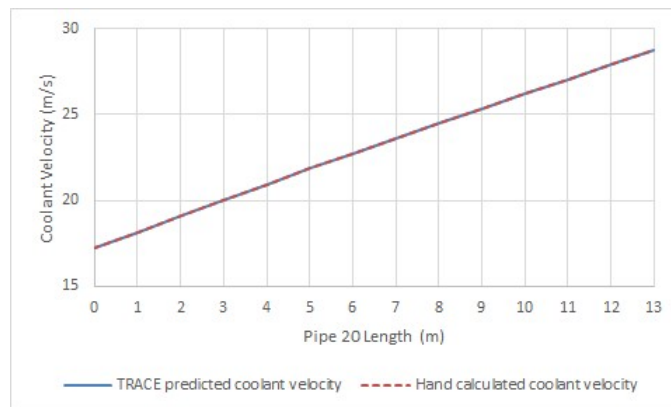


**Figure 4.16.** Carbon Dioxide Velocity Horizontal Non-Adiabatic Verification Test Case

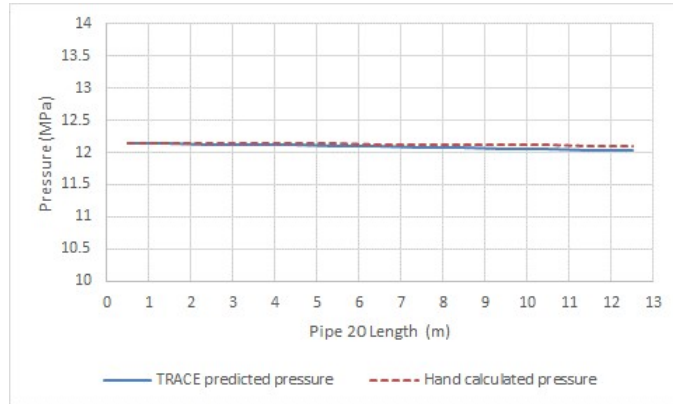


**Figure 4.17.** Carbon Dioxide Pressure Horizontal Non-Adiabatic Verification Test Case

#### 4.4.2.3 Vertical Adiabatic Verification Case Results

Figures 4.18 and 4.19 show that the TRACE predicted velocity and pressure agree well with the hand calculated velocity and pressure for every axial position of pipe 20 for the vertical adiabatic test case for carbon dioxide. For both velocity and pressure, the difference between TRACE predicted results and hand calculated results is less than 1% for every data point.

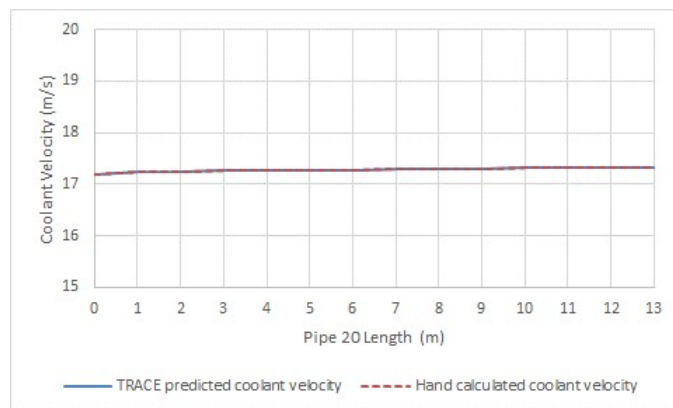


**Figure 4.18.** Carbon Dioxide Velocity Vertical Adiabatic Verification Test Case

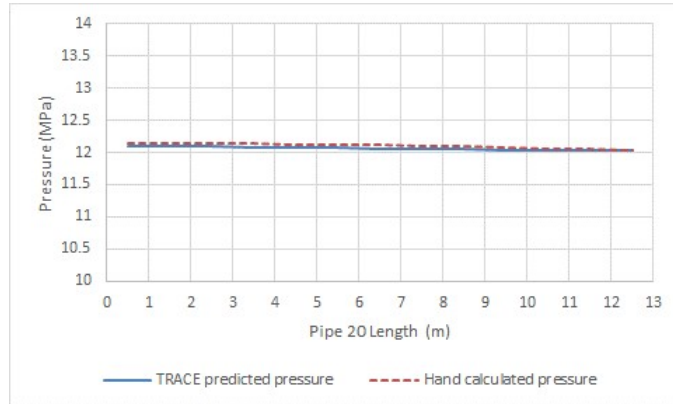


**Figure 4.19.** Carbon Dioxide Pressure Vertical Adiabatic Verification Test Case

#### 4.4.2.4 Vertical Non-Adiabatic Verification Case Results

Figures 4.20, 4.21, and 4.22 show that the TRACE predicted results for the carbon dioxide temperature, velocity, and pressure vs axial position for the non-adiabatic vertical test case agree well with the hand calculated results for these same parameters at every axial position. The difference between the TRACE predicted results and hand calculated results is less than 1% for every data point tested in the horizontal non-adiabatic test case.

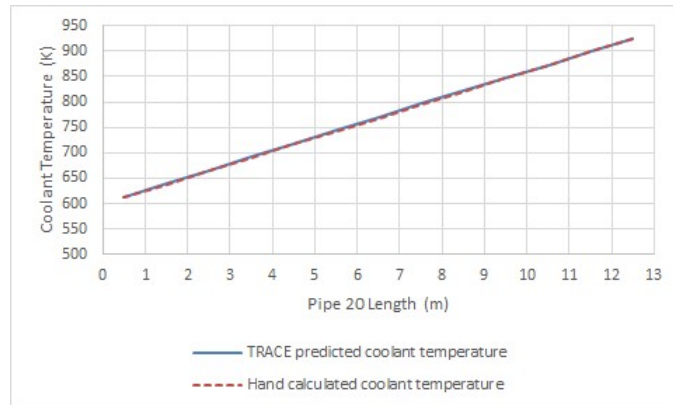


**Figure 4.20.** Carbon Dioxide Temperature Vertical Non-Adiabatic Verification Test Case

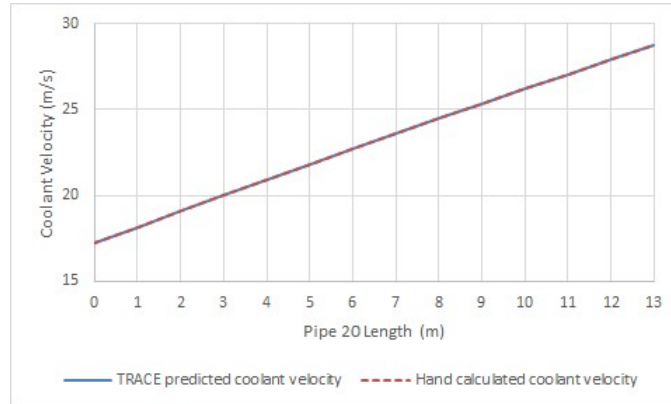


**Figure 4.21.** Carbon Dioxide Velocity Vertical Non-Adiabatic Verification Test Case

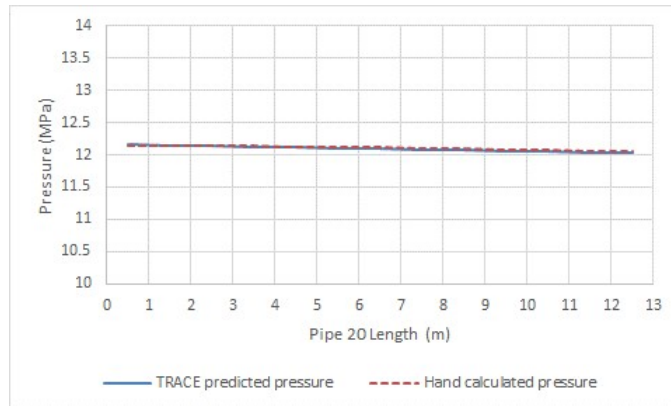


**Figure 4.22.** Carbon Dioxide Pressure Vertical Non-Adiabatic Verification Test Case

#### 4.4.2.5 Carbon Dioxide XPTB Verifiaction

This section presents the process for verifying the values of the carbon dioxide XPTB, and to verify that TRACE read the correct properties for the simulations performed in this research. To complete these verifications, the carbon dioxide fluid properties used by TRACE from cells 5 and 10 of the pipe in the horizontal non-adiabatic test case were compared to properties from the NIST Chemistry webBook, SRD 69 [41] for identical pressures and temperatures. The purpose of this was to compare the properties for two different sets of conditions. The properties compared were the carbon dioxide density, viscosity, internal energy, specific heat, enthalpy, and thermal conductivity. Tables 4.3 and 4.4 provide the properties used

by TRACE and the properties from the NIST Chemistry webBook, SRD 69 [41] for cell 5 and cell 10 respectively. Tables 4.3 and 4.4 also includes the percent difference between these two values.

**Table 4.3.** Carbon Dioxide Cell 5 XPTB Verification Test

Fluid Property	TRACE value	NIST webBook [41] value	% difference
Density $\left(\frac{kg}{m^3}\right)$	94.923485	94.922	$1.564 \times 10^{-3}$
Viscosity $\left(\frac{kg}{ms}\right)$	$3.408458 \times 10^{-5}$	$3.408 \times 10^{-5}$	$1.371 \times 10^{-3}$
Internal Energy $\left(\frac{J}{kg}\right)$	778683.19	778680	$4.0967 \times 10^{-4}$
Specific Heat $\left(\frac{J}{kgK}\right)$	1196.6256	1196.6	$2.139 \times 10^{-3}$
Enthalpy $\left(\frac{J}{kg}\right)$	915718.56	915720	$1.573 \times 10^{-4}$
Thermal Conductivity $\left(\frac{W}{mK}\right)$	0.053838	0.053838	$7.671 \times 10^{-4}$

**Table 4.4.** Carbon Dioxide Cell 10 XPTB Verification Test

Fluid Property	TRACE value	NIST webBook [41] value	% difference
Density $\left(\frac{kg}{m^3}\right)$	79.978394	79.978	$4.926 \times 10^{-4}$
Viscosity $\left(\frac{kg}{ms}\right)$	$3.717321 \times 10^{-5}$	$3.7173 \times 10^{-5}$	$5.542 \times 10^{-4}$
Internal Energy $\left(\frac{J}{kg}\right)$	899154.81	899150	$5.349 \times 10^{-4}$
Specific Heat $\left(\frac{J}{kgK}\right)$	1224.1157	1224.1	$1.283 \times 10^{-3}$
Enthalpy $\left(\frac{J}{kg}\right)$	1061154.6	1061200	$4.278 \times 10^{-3}$
Thermal Conductivity $\left(\frac{W}{mK}\right)$	0.06205734	0.062057	$5.463 \times 10^{-4}$

The small percent differences for the values in tables 4.3 and 4.4 can be attributed to the way TRACE reads the XPTB, and rounding values to different decimal places between TRACE and the NIST Chemistry webBook, SRD 69. As explained in chapter 2, TRACE interpolates linearly between points of the XPTB to obtain values used in calculations [24]. Although the change of some fluid properties is not linear, this is a good estimation because the temperature and pressure increments



for the carbon dioxide XPTB are relatively small. Regardless, this can attribute to a small difference between actual values and values used by TRACE. Also, the values from TRACE have a higher precision than the values from the NIST Chemistry webBook, SRD 69 [41]. This difference in precision will cause there to be a percentage difference between values, even if the same number is used because it can be rounded differently.

This section validates the properties of the carbon dioxide XPTB and the ability of TRACE to properly read and use these properties for the range of conditions used in the full carbon dioxide cooled model. Tables 4.3 and 4.4 show that there is less than one-hundredth of one percent difference between any given value read from the XPTB for TRACE and the corresponding value from the NIST Chemistry webBook, SRD 69 [41]. This small percentage difference is explained in the previous paragraph.

## 4.5 Chapter Conclusion

The method of manufactured solutions was used to verify the use of helium and carbon dioxide in TRACE. The test cases had identical geometry to that of a single coolant channel in the vessel of the complete system models. The flow conditions and power were the same between the verification test cases and for a single coolant channel of the complete models. The results from this verification analysis show that using helium and carbon dioxide in TRACE is verified for the final sets of conditions used in the complete helium and carbon dioxide cooled models. For every data point tested for all test cases, there was less than a 1% difference between the TRACE predicted results and the hand calculated results. Also, the properties of the carbon dioxide XPTB, the ability for TRACE to read the correct values of the carbon dioxide XPTB, and the ability for TRACE to use these values correctly in its equations was verified through the results of test cases ran and by the agreement between physical properties used by TRACE to those from the NIST Chemistry webBook, SRD 69 [41] for identical conditions. This means that the results from the simulations of the helium and carbon dioxide cooled models are reliable.

# Chapter 5 | Results

## 5.1 Introduction

This chapter provides the results and analysis for the different coolants analyzed in this study. The results are all taken at a point where the models have reached steady state. For each model, the simulation ran for 5000 seconds of simulation time. For axial profile results, the data is taken at the last time-step available for plotting. First, plots and charts of specific parameters are provided with a brief explanation of what physically causes the phenomena observed. Next, section 5.2 provides analysis of the results presented and suggests future work. Some figures presented in this chapter do not properly display the behavior discussed due to the results from all three coolants being plotted on the same plot. Appendix D provides the data corresponding to the plots provided in this chapter.

### 5.1.1 Coolant Pressure Drop in Vessel

Figures 5.1, 5.2, and 5.3 provide the axial pressure profile results at steady state for all models of this study through coolant loops 1, 2, and 3 respectively. For these figures, the first 13 m of a given coolant loop represents that coolant loop's cold leg, the next 13 m represent the 13 m long section of coolant channels that flow through the vessel for that coolant loop, and the last 13 m represent the hot leg for that coolant loop. As explained in chapter 3, for all coolant loops, cells 1 through 13 represent the cold leg, cells 14 through 26 represent the 13 m long section of coolant channels that flow through the vessel, and cells 27 through 39 represent the hot leg.

Although difficult to see from figures 5.1, 5.2, and 5.3, there is an much larger pressure drop gradient across the coolant channels in the vessel compared to across the cold or hot legs. This behavior is expected because there is a larger frictional pressure drop due to there being much more surface area in contact with the coolants through the coolant channels than in the cold or hot leg. The flow area is constant throughout the axial length of each coolant loop, but the cold and hot legs for a given coolant loop each represent a single  $5.684 \times 10^{-1}m$  inner diameter circular cross section pipe while the coolant channels for a given coolant loop represent 359 geometrically identical circular cross section pipes with an inner diameter of 3 cm.

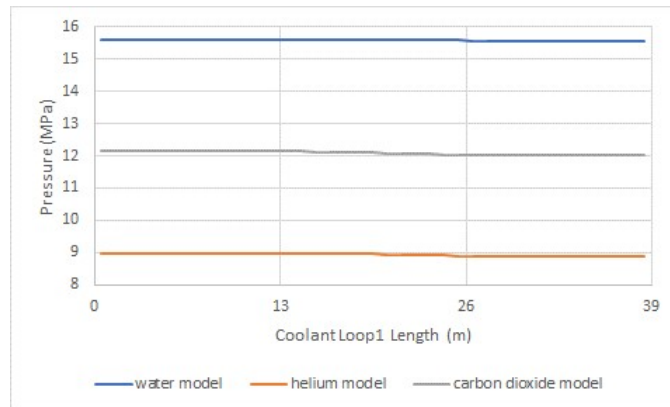


**Figure 5.1.** Coolant Loop 1 Axial Pressure Profile at Steady State

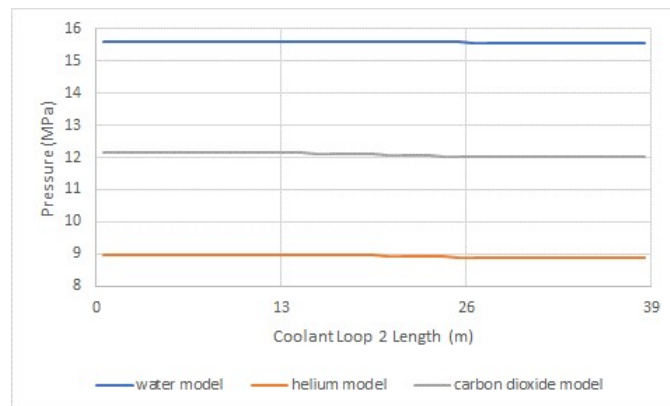


**Figure 5.2.** Coolant Loop 2 Axial Pressure Profile at Steady State

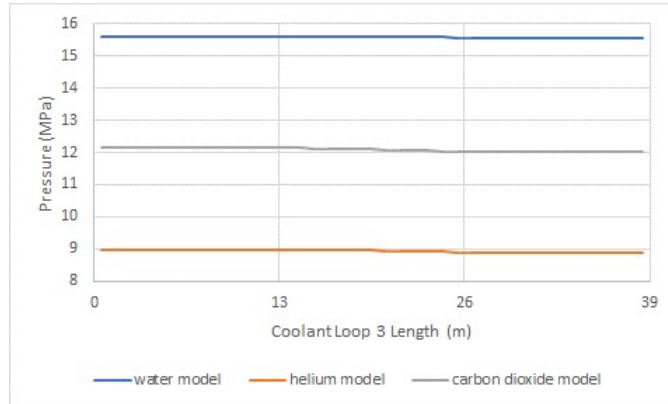


**Figure 5.3.** Coolant Loop 3 Axial Pressure Profile at Steady State

### 5.1.2 Coolant Axial Density Profile in Vessel

Figures 5.4, 5.5, and 5.6 show the steady state axial coolant density profiles for all models of this study through coolant loops 1, 2, and 3 respectively. These figures show that the density decreases for each coolant analyzed in this study as they flow through a given coolant loop. This is because the density for all of the coolants will decrease with decreasing pressure and with increasing temperature. Figures 5.1, 5.2, and 5.3 show that the pressure decreases for each coolant as it flows through any given coolant loop. The following section, section 5.1.3, provides the data for the coolant axial temperature profile for each model of this study. The coolant axial temperature profiles for the different coolants in each coolant loop are provided in figures 5.7, 5.8, and 5.9 and show that the coolant temperature increases for each coolant analyzed in this study. The coolant density has an effect on the coolant axial temperature rise in a given coolant loop. This phenomenon is explained in section 5.1.3.

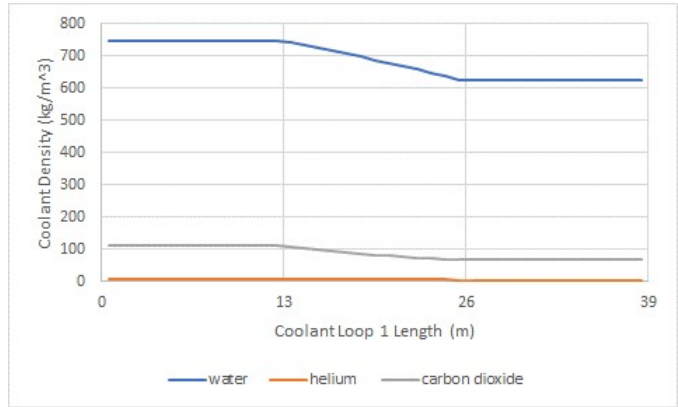


**Figure 5.4.** Coolant Loop 1 Axial Density Profile at Steady State

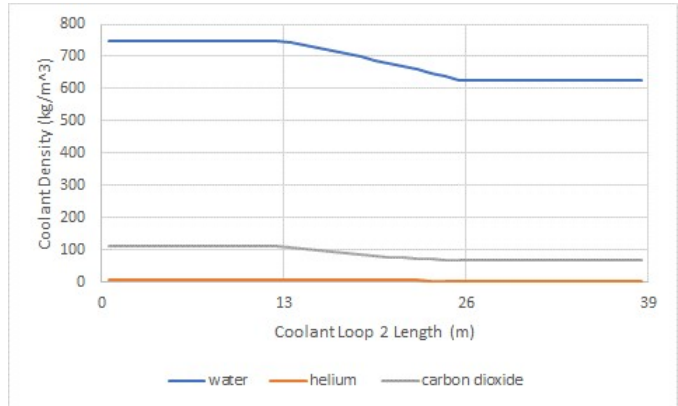


**Figure 5.5.** Coolant Loop 2 Axial Density Profile at Steady State

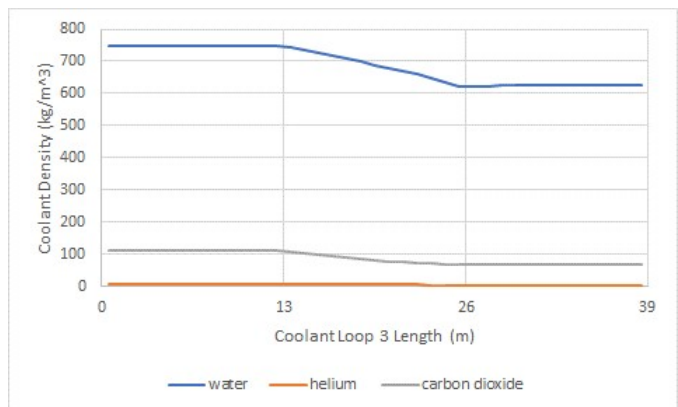


**Figure 5.6.** Coolant Loop 3 Axial Density Profile at Steady State

### 5.1.3 Coolant Axial Temperature Profile in Vessel

This section includes the coolant axial temperature profile results and other results that effect the axial temperature profile that aren't included in other section. The additional results included in this section besides the coolant axial temperature profile include the coolant mass flow rate for each coolant loop in the various models (table 5.1) and the specific heat at various locations for the coolant loops in each model (tables 5.2, 5.3, and 5.4).

Figures 5.7, 5.8, and 5.9 show the steady state axial coolant temperature profiles for all models of this study through coolant loops 1, 2, and 3 repectively. For these plots, the axial length sections of the cold leg, coolant channels, and hot leg for each coolant loop are the same as for the axial pressure profile plots. These can be reviewed in chapter 3 or section 5.1.1 of this chapter. Figures 5.7, 5.8, and 5.9 show that the temperature of the coolant increases for each coolant analyzed in this study as it flows through the coolant channels in the vessel. This is expected because it is assumed the power source deposits its energy into the coolant channel walls and this energy will be deposited into the coolant as it flows through the vessel. This assumption is explained in chapter 3.

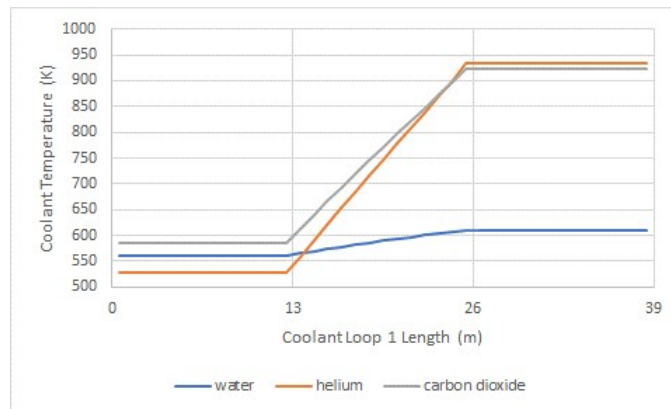


**Figure 5.7.** Coolant Loop 1 Coolant Axial Temperature Profile at Steady State

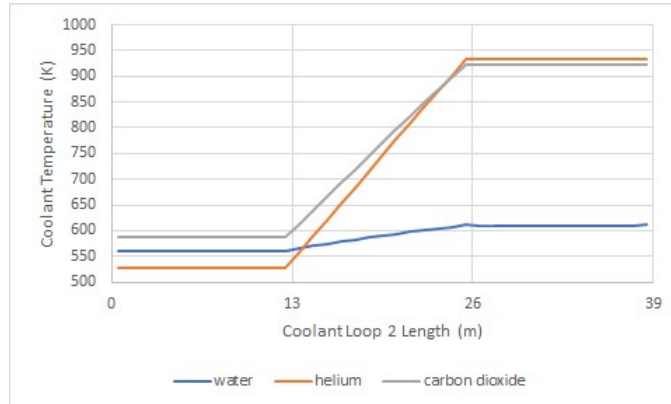


**Figure 5.8.** Coolant Loop 2 Coolant Axial Temperature Profile at Steady State

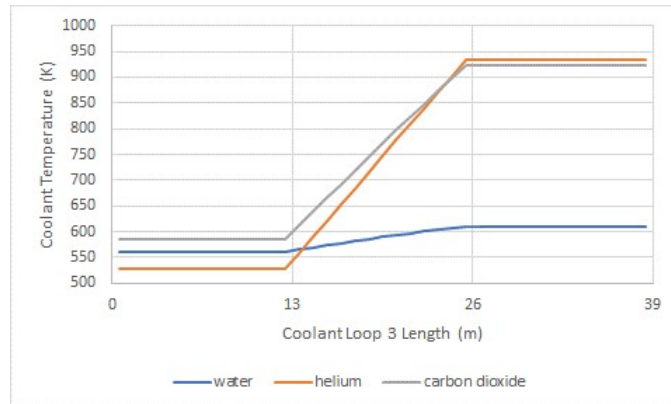


**Figure 5.9.** Coolant Loop 3 Coolant Axial Temperature Profile at Steady State

Because the power source is assumed uniform and constant for the system of this study, for a given coolant, the axial rise in coolant temperature will primarily depend on the mass flow rate and specific heat of said coolant. This relation show in equation 5.1. Table 5.1 provide the steady state mass flow rate for each coolant loop in each model of this study. TRACE doesn't have the built in capability to plot the specific heat for fluid cells of pipe components. However, there is a signal variable in TRACE that can plot the specific heat for a single cell of most fluid components, including pipes. Tables 5.2, 5.3, and 5.4 includes the specific heat from the last cell of the cold leg (cell 13), the middle cell of the coolant channels(cell 20), and the first cell of the hot leg (cell 27) for coolant loops 1, 2, and 3 respectively.

$$\Delta T = \frac{q}{\dot{m}c_p} \quad (5.1)$$

**Table 5.1.** Mass Flow Rates for a Single Coolant Loop TRACE Models

Coolant	$\dot{m} \left( \frac{kg}{s} \right)$
water	678
helium	94.13
carbon dioxide	491.78

**Table 5.2.** Specific Heat Coolant Loop 1

Coolant	$c_p \left( \frac{kJ}{kg-K} \right)$ cell 13	$c_p \left( \frac{kJ}{kg-K} \right)$ cell 20	$c_p \left( \frac{kJ}{kg-K} \right)$ cell 27
water	5.20986	5.99333	7.49022
helium	5.19403	5.19479	5.19543
carbon dioxide	1.17341	1.20456	1.24129

**Table 5.3.** Specific Heat Coolant Loop 2

Coolant	$c_p \left( \frac{kJ}{kg-K} \right)$ cell 13	$c_p \left( \frac{kJ}{kg-K} \right)$ cell 20	$c_p \left( \frac{kJ}{kg-K} \right)$ cell 27
water	5.20986	5.99284	7.48798
helium	5.19403	5.19479	5.19543
carbon dioxide	1.17341	1.20456	1.24129

**Table 5.4.** Specific Heat Coolant Loop 3

Coolant	$c_p \left( \frac{kJ}{kg-K} \right)$ cell 13	$c_p \left( \frac{kJ}{kg-K} \right)$ cell 20	$c_p \left( \frac{kJ}{kg-K} \right)$ cell 27
water	5.20986	5.99285	7.48904
helium	5.19403	5.19479	5.19543
carbon dioxide	1.17341	1.20456	1.24130



Tables 5.2, 5.3, and 5.4 show that there is less than a 0.1% increase in the specific heat for helium as it flows through the coolant channels. This explains why its temperature vs axial position is the most linear amongst the coolants analyzed in this study because there is a constant coolant mass flow rate for any system. As equation 5.1 shows, this means that there will be less than a 0.1% decrease in the change of helium temperature with respect to axial position in the coolant channel, or the derivative of the temperature with respect to axial position in the coolant channels.

In contrast to the specific heat of helium, the specific heat of water increases by over 43% over the length of the coolant channels in each coolant loop. This means that as the water flows through the coolant channels more and more energy is needed to increase its temperature because it has a constant mass flow rate. Hence, the rate of the rise in water temperature vs axial position will decrease as water flows through the coolant channels and its temperature profile vs axial position will not be nearly as linear as helium's temperature profile vs axial position. Figures 5.7, 5.8, and 5.9 show that there is a noticeable decrease in the slope of the water temperature vs axial position towards the ends of the coolant channels in each coolant loop. This is caused by a few factors. There is a small increase in the specific heat of water as it loses pressure through the coolant channels, but for our system water's specific heat is much more affected by the increase in its temperature through the coolant channels. The change in specific heat vs temperature is not linear for water. There is a greater increase in the specific heat vs temperature for water as its temperature gets closer to its saturation temperature. For the water cooled model in this study, the saturation temperature will decrease as the coolant flows through the coolant channels and loses pressure. Hence, the lowest saturation temperature in the coolant channels will be near the exit of a given coolant loop. The minimum saturation temperature for the water cooled model is 618.3 K for each coolant loop. So, for the water cooled system the saturation temperature of the water decreases as it flows through the coolant channels and its temperature increases as it flows through the coolant channels. This will cause a larger increase in the specific of water towards the ends of the coolant channels where the water temperature is about 7°C below the saturation temperature.

For the carbon dioxide cooled system, the change in specific heat over the length of the coolant channels in a given loop is about 5.8%. For the conditions

through the vessel, carbon dioxides change in specific heat vs axial position is nearly constant. Overall the carbon dioxide temperature vs axial position is nearly linear.

As can be seen in figures 5.7, 5.8, and 5.9, helium has the largest temperature rise through the coolant loops for the coolants analyzed in this research, followed by carbon dioxide, then water. This is largely due to the mass flow rate difference between the coolants as a result of the different coolant densities. Figures 5.4, 5.5, and 5.6 show that under the operating conditions for the models of this study, water has the highest density, followed by carbon dioxide, then helium. So, water is able to achieve a much higher mass flow rate for the same coolant velocity. The mass flow rate can be increased by increasing the coolant velocity, but this is not desired for the models in this study for various reasons. This is explained further in section 5.2. Tables 5.2, 5.3, and 5.4 show that for the operating conditions of the models in this study, water has the highest specific heat, followed by helium, then carbon dioxide. The product of the specific heat and mass flow rate for the models in this study is highest for water, followed by carbon dioxide, then helium. This explains why the temperature rise for these coolants is highest for helium, followed by carbon dioxide, then water. Analysis on the modifications that can be made to the system to change the parameters effecting the axial coolant temperature profile and the resulting other effects on the system are described and analyzed in section 5.2.

#### **5.1.4 Axial Coolant Velocity Profiles in Vessel**

Figures 5.10, 5.11, and 5.12 provide the axial coolant velocities for coolant loops 1, 2, and 3 respectively. These figures show that the largest increase in velocity is for helium, followed by carbon dioxide, then water. The mass flow rate is constant in our system for any given fluid due to conservation of mass. The increase in the coolants velocities is a direct result of the density decrease of the coolants as they flow through the coolant loops. This relation is shown in equation 5.2.

$$V = \frac{\dot{m}}{\rho A} \quad (5.2)$$

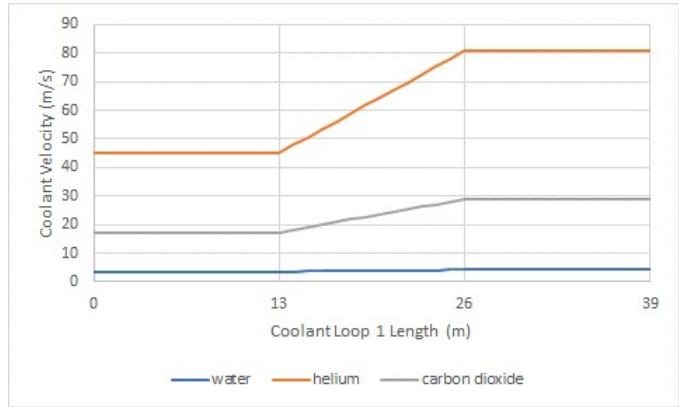


**Figure 5.10.** Coolant Loop 1 Axial Velocity Profile at Steady State

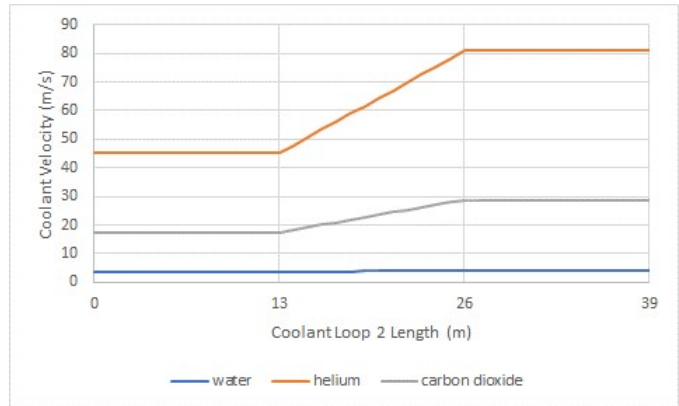


**Figure 5.11.** Coolant Loop 2 Axial Velocity Profile at Steady State

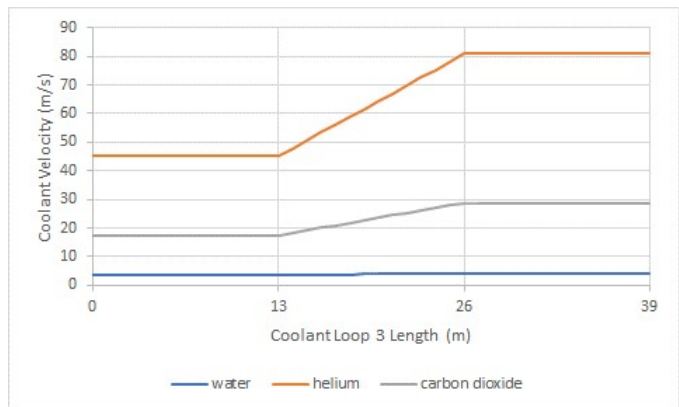


**Figure 5.12.** Coolant Loop 3 Axial Velocity Profile at Steady State

As explained in section 5.1.1, there is an increase in pressure drop through the coolant channels in any given coolant loop for all of the fluids. Section 5.1.2 explains that the coolant density is a function of pressure. So, as the pressure decreases, the coolant density decrease. Therefore, the coolant velocity will increase to keep a constant mass flow rate. The % density decrease across the coolant channels is largest for helium, followed by carbon dioxide, then water. Hence, the % increase in the coolant velocity is largest for helium, followed by carbon dioxide, then water. The affects on the other parameters of the system as a result of an increased coolant velocity are detailed in section 5.2.

### **5.1.5 Heat Transfer Coefficient in Coolant Channels**

As can be seen in figure 5.13, Water has the highest heat transfer coefficient, followed by helium, then carbon dioxide. Figure 5.13 also shows that the heat transfer coefficient increases for all of the fluids analyzed in this study as they flows through the coolant channels in the vessel. As a result of the pressure drop of the coolants through each coolant loop, there is an increase in the coolant velocity throughout these pipes to keep a constant mass flow rate. Additionally, the increase in the coolant velocity increases the pressure drop gradient. The increase in velocity will increase the heat transfer coefficient for all coolants of this study. For the water cooled model, an increase in the water temperature decreases the viscosity of the water. A decrease in the viscosity of the water will also increase the heat transfer coefficient by increasing the turbulence of the flow and decreasing the laminar sublayer. For the helium and carbon dioxide models, the viscosity increases with an increase in coolant temperature. A decrease in Pressure will decrease the viscosity for all of the coolants in this study. For the helium and carbon dioxide models, there is a small net increase in the coolant viscosity as the coolants flow through the coolant channels. The increasing coolant viscosity has a much smaller impact on the heat transfer coefficient than the increasing coolant velocity does. So, the heat transfer coefficient increases for the helium and carbon dioxide models as the coolant flows through the coolant channels. Overall, the heat transfer coefficient will increase for each coolant as it flows through the vessel.

Also, figure 5.13 shows there is a sharp increase in the heat transfer coefficient in the water cooled model towards the exits of the coolant channel loops in the vessel.

This is because there is a small amount of subcooled boiling towards the ends of the coolant channels in the vessel. This behavior is common in PWRs and increases the heat transfer coefficient where this phenomenon occurs [36]. The saturation temperature of the water decreases as it flows through the coolant channels as a result of the pressure decrease that occurs as it flows through the coolant channels. The minimum saturation temperature for each coolant loop in the water cooled model is 618.3 K. As can be seen in figures 5.7, 5.8, and 5.9, the maximum bulk coolant temperature for each coolant loop of the water cooled model stays below the saturation temperature. The coolant temperature for the water cooled model is below the saturation temperature of the coolant by about 7 °C.

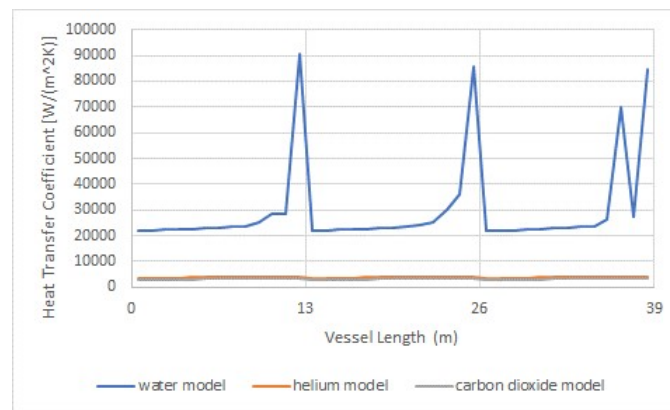


**Figure 5.13.** Heat Transfer Coefficients Axial Profile in Vessel at Steady State

### 5.1.6 Beryllium Axial Temperature Profile in Vessel

As stated in chapter 3, the limiting temperature for this study was 800°C for the beryllium armor layer, as determined by ITER [28]. Also, because it was assumed that all of the source energy gets deposited into the inconel 600 coolant channel walls and none of the source gammas interact with the beryllium armor layer, the max armor layer temperature was assumed to be equal to the outer surface temperature of the inconel 600 coolant channel walls because the beryllium armor layer will be in contact with this surface. The inconel 600 coolant channel walls are represented by heat structure 90. The axial temperature profiles at steady state

for the outer surface of the coolant channel walls for the coolants analyzed in this study are shown in figure 5.14.

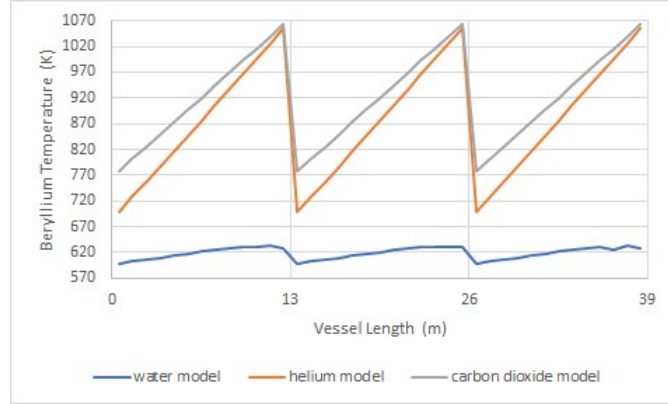


**Figure 5.14.** Beryllium Axial Temperature Profile in Vessel at Steady State

Figure 5.14 shows that the highest beryllium armor layer temperature occurs for every axial location in the vessel for the carbon dioxide cooled model, followed by the helium cooled model, then the water cooled model. Although helium has the largest coolant temperature rise and reaches the highest temperature overall of any of the coolants in this study, the beryllium armor layer temperature is still higher at every axial location in the vessel for the carbon dioxide cooled model. This is a direct result of the heat transfer coefficient,  $h$ , and the bulk coolant temperature through the coolant channels for each model of this study. The temperature at the inner surface of the coolant channels is directly related to the heat transfer coefficient,  $h$ , and the bulk fluid temperature,  $T_b$ . This relation is shown in equation 5.3. Assuming only the heat transfer coefficient changes, equation 5.3 shows that the temperature at the inner surface of the coolant channels will decrease if the heat transfer coefficient increases, and increase if the heat transfer coefficient decreases. Assuming only the bulk fluid temperature changes, equation 5.3 shows that the temperature at the inner surface of the coolant channels changes proportionally to the change in bulk fluid temperature. A higher temperature at the inner surface coolant channel walls results in a higher temperature at the outer surface of the coolant channel walls, and therefore a higher beryllium armor layer temperature.

$$T_w = \frac{q}{hA} + T_b \quad (5.3)$$

Figure 5.14 also shows that there is a noticeable decrease in the rate of the rise in beryllium temperature vs axial position towards the ends of the coolant channels in each coolant loop. As explained in the previous paragraph, a higher heat transfer coefficient decreases the difference in temperature between the coolant and the coolant channel pipe walls. So, the large increase in the water's heat transfer coefficient where sub-cooled boiling occurs corresponds to a decrease in the temperature difference between the water and the coolant channel pipe walls, which is directly related to the temperature of the beryllium. Also, as explained in section 5.1.3, the bulk coolant temperature of the water increases at a slower rate vs axial position as its specific heat increases towards the ends of the coolant channels in each coolant loop. This will also contribute to the decreased rate of temperature increase of the beryllium temperature vs axial position in the vessel for a given coolant loop.

### 5.1.7 Overall Efficiency

The overall efficiency of the models analyzed in this study were calculated by subtracting the pumping power of the system from the power produced by the turbine. This was explained in detail in chapter 3. For the water cooled model, the power for the pressurizer was neglected because at steady state this value oscillates around 0  $W$  and the maximum/minimum oscillations are negligible compared to the pumping power and turbine output power.

The overall efficiency of the system with the different coolants analyzed in this study has a degree of uncertainty. First, the turbine efficiencies used in this model are based on similar systems with the same coolants. The true turbine efficiencies need to be determined by measurement to be considered reliable. The pumps used in all of the models for this study were all identical and assumed 85% pumping efficiency. Most likely, specific pumps would need to be considered for each system based on the coolant used. The pumps for each unique system would have their own efficiencies associated with them. Also, as with any simulation tool that uses

PDEs to discretize equations, there will be numerical uncertainty associated with the results. Based on the system of this study and the assumptions made in this study, carbon dioxide serves as the best coolant with respect to the overall efficiency of the system. The turbine efficiency for the water cooled model was 34%, the overall efficiency of most PWR systems [5]. The turbine efficiency used for the helium and carbon dioxide cooled models was 40%, the overall efficiency of most AGR systems. Table 5.5 provides the overall efficiencies of the different models of this study with the assumptions previously stated.

**Table 5.5.** Overall System Efficiencies

Coolant in Model	Efficiency (%)
water	33.96
helium	39.28
carbon dioxide	39.66

## 5.2 Analysis

This section provides analysis based on the results presented in the previous sections of this chapter. The analysis also includes potential areas of future work related to this study.

The maximum beryllium temperature limits the temperature of the coolants for the helium and carbon dioxide cooled models. This limits the efficiency of these systems and limits the systems capabilities. The efficiency is limited because the temperature for the secondary side vapor is limited. Also, at high enough temperatures, helium and carbon dioxide can be used in chemical processes, such as hydrogen production. Water-splitting efficiencies for hydrogen production are very temperature dependent. As temperature increases from 900 to 1000 °C, hydrogen production efficiency increases from about 50 to 60 percent [42]. Using beryllium as the armor layer material in this study limits the efficiencies and applications of the helium and carbon dioxide cooled systems. Research can be done to analyze different materials for the armor layer of a fusion reactor and the effects on the system.



There are several modifications that can be made to the helium and carbon dioxide cooled systems to change how these systems operate and to increase the safety margin with respect to the maximum beryllium armor layer temperature. These modifications include increasing the coolant velocity, introducing heat transfer enhancing techniques, changing the operating conditions of the steam generator, increasing the pressure of the system, and operating these systems as brayton cycles instead of rankine cycles. The next few paragraphs describe how these changes will affect the various parameters of the helium and carbon dioxide cooled systems.

The first change that could be made to the helium and carbon dioxide cooled models to make the system perform differently would be to increase the coolant velocity. Although, assuming the same operating conditions besides coolant velocity, an increase in the coolant velocity will increase the heat transfer coefficient, there are other negatives of doing this. An increase in the coolant velocity will increase the pressure drop gradient. An increased pressure drop will increase the required pumping power for a given system. This will decrease the overall efficiency of the system. Increasing the coolant velocity will also put more of a physical strain on the system, and materials may degrade faster. For example, at high enough coolant velocities, flow induced vibrations can occur. Flow induced vibrations can cause a range of issues from reduced process efficiency and unplanned shutdowns to decreased equipment life or even loss of containment [43]. Also, there can be a large amount of environmental and occupational noise resulting from flow induced vibrations [44]. It is worth noting that the highest velocity may not cause the worst vibrations [44]. The system in this study may need to be modified to properly account for the affects from an increase in the coolant velocity. Future work could be done to analyze the affects of high coolant velocities, including flow induced vibrations, for the system in this study and other power plant systems. Also, techniques for reducing flow induced vibrations can be further researched.

There are heat transfer enhancing mechanisms that can be considered for the helium and carbon dioxide cooled models to decrease the required coolant velocity to keep the beryllium armor layer temperature below its maximum value. A number of heat transfer enhancement techniques in connection with the ITER design have been examined. The heat transfer enhancement techniques examined included microfins [45], porous media [46], jet impingement [47], particulate addition [48],

swirl tape [49], two dimensional roughness [50], three dimensional roughness [50], swirl rod insert [51], and swirl rod insert with two dimensional roughness [51]. There are positives and negatives to consider for any heat transfer enhancing mechanism. Heat transfer enhancing mechanisms have the benefit of increasing the heat transfer coefficient for a given fluid. As explained in section 5.1.5, for the system in this study an increase in the heat transfer coefficient for a given coolant will decrease the difference between the temperature at the inner surface of the coolant channels and the coolant bulk fluid temperature, and therefore decrease the beryllium armor layer temperature. This will also increase the maximum coolant temperatures allowed for the system in this study. As stated earlier in this section, An increase coolant temperature can increase the power produced by the turbine by increasing the temperature of the secondary side fluid. Also, a higher temperature coolant can allow the system to be used efficiently for other applications, including chemical processes. Increasing the heat transfer coefficient will also benefit the system by decreasing the required mass flow rate to achieve desired temperatures. This can affect the system in many ways. The decreased mass flow rate could potentially result in a decrease in pressure drop. Therefore, the net power of the system has the potential to be increased. The coolant can also experience an increase in pressure drop with heat transfer enhancing mechanisms due to some of these techniques requiring additional surface in contact with the coolant, increased roughness of the surfaces in contact with the coolant, complex flow configurations, etc. This has the potential to be a negative on the net power of the system. The pumping power required could increase or decrease based on many factors. A decrease in required mass flow rate could result in a lower required pump impeller rotational speed. The pump could also need to overcome a higher pressure difference due to the increased pressure drop resulting from the addition of heat transfer enhancing mechanisms. Some heat transfer enhancing mechanisms do not have an extensive research history and can be looked into further before being determined reliable. Analyzing any heat transfer enhancing mechanism for the system of this study and other power systems can be looked into further. Other first wall armor materials should be considered to not limit the system and to allow the system to perform better.

The steam generator for the helium and carbon dioxide cooled models could operate differently to decrease the coolant temperature entering the coolant channels.

A decrease in the temperature of the coolant entering the coolant channels would allow more flexibility of the primary side operating conditions to keep the beryllium temperature below its maximum value. This can be done by decreasing the temperature at which the coolant exits the stem generator. Assuming the primary side operating conditions stay the same, this can be achieved by decreasing the temperature at the outer surface of the helical coil pipe walls.

There is only a small change in the specific heat of helium and carbon dioxide with a decrease in temperature. The specific heat of helium will slightly increase and the specific heat of carbon dioxide will slightly decrease with a decrease in temperature. So, the total change in temperature of the coolant through the steam generator will be nearly the same with a change in temperature. This phenomenon was explained in more detail for the rise in coolant temperature through the coolant channels of the vessel in section 5.1.3. The temperature of the coolant exiting the steam generator is more effected by the decrease in temperature of the helical coil pipe walls than the change in its specific heat. Equation 5.4 shows the relation between the primary side bulk coolant temperature,  $T_b$ , and the helical coil wall outer surface temperature,  $T_w$ .

$$T_b = \frac{q}{hA} + T_w \quad (5.4)$$

To decrease the temperature of the outer surface of the helical coil pipe walls throughout the steam generator, the temperature of the coolant entering the steam generator can be changed and/or the mass flow rate of the secondary side coolant entering the helical coil pipes can be changed. Assuming only the secondary side coolant temperature entering the steam generator changes, the secondary side coolant will be at a lower temperature throughout the length of the helical coil pipes, thus decreasing the temperature of the outer surface of the helical coil pipe walls. The turbine efficiency, and overall efficiency of the system would decrease as a result of this. Except turbine efficiency decreasing, the same affects will occur if only the mass flow rate of the secondary side coolant entering the helical coil pipes is increased. The turbine efficiency, and overall efficiency of the system might decrease as a result of an increased secondary side mass flow rate. Further research could

be done into different steam generators and/or different secondary side operating conditions for the steam generator in the helium and carbon dioxide cooled systems and the affects of these changes on the helium and carbon dioxide cooled systems.

Another change to make the system of this study perform differently with helium or carbon dioxide as the coolant would be to increase the pressure of the coolant. Increasing the pressure of the coolant will increase the density for both helium and carbon dioxide. An increase in the coolant density will decrease the required coolant velocity to achieve the same mass flow rate. The pressure drop is a function of the coolant velocity squared. The pressure drop is also a function of the coolant density. The coolant velocity decreasing has a larger impact on the pressure gradient than the coolant density increasing. Overall, an increase in the system pressure would result in a decrease in the pressure drop of the coolant through the system. Increasing the pressure of the coolant would potentially require a change in the design of the system. Increasing the pressure of helium or carbon dioxide increases the specific heat for each fluid. This will result in a lower axial temperature rise of these coolants in the system of this study assuming the same geometry, power, and mass flow rate. The change in specific heat vs pressure for helium and carbon dioxide are both very small in magnitude and will have a very small effect on the coolant axial temperature rise in the system of this study compared to other factors explained in previous sections. There is still more research that should be done into high pressure helium and high pressure carbon dioxide cooled systems.

Another change that could have been made to the helium and carbon dioxide cooled systems would be to make the cycles Brayton cycles. Brayton cycles have a few trade-offs compared to Rankine cycles. First, there could be an increase in the overall efficiency of the system. For a Brayton cycle helium cooled gas cooled fast reactor (GFR), efficiencies are predicted to be around 48%. This predicted efficiency is for when the pressure of the helium is at 9.1 *MPa* and the exit temperature of the coolant from the vessel is 850°C [10]. Studies would need to be done to determine the efficiency of the system of this study because the coolant temperature can't be that high with beryllium as the armor layer material. This is another reason to consider a different armor layer material. For a carbon dioxide cooled GFR, efficiencies up to 50% are achievable. This efficiency was predicted for when the pressure of the carbon dioxide is at 20 *MPa* and the exit temperature of the coolant from the vessel is 650°C [52]. To operate the carbon dioxide cooled system

of this study at 20 *MPa*, several design changes may need to be made to account for this increase in pressure of the coolant. Further work would also need to be done to determine if this coolant temperature is sufficient to keep the beryllium temperature below its maximum temperature of 800 °C. Again, this is a reason to consider and research different armor layer materials. An advantage of a Brayton cycle carbon dioxide cooled system over a Brayton cycle helium cooled system is the ability to have better natural circulation flow through the system. Assuming the system operates at GFR conditions, the density change of carbon dioxide through the system would be greater than the density change of helium through the system. This would result in better natural circulation flow for decay heat removal from the vessel without the pumps/compressors working [52]. Another advantage of Brayton cycle for both a helium cooled and carbon dioxide cooled system compared to a Rankine cycle is there would be no steam generator. This could reduce the physical space needed for the entire system and would also result in potentially less sources of error if the steam generator is no longer a part of the system. More research could be done to analyze Brayton cycle systems with helium or carbon dioxide as the coolant.

Based on the results of this research, water performs as the best coolant for the system analyzed in this study. Water performs best as a coolant with respect to the maximum armor layer temperature. Also, there is uncertainty associated with the efficiencies used in this study. Therefore, the importance of overall efficiency is less than the other parameters when used for determining the best coolant for the system of this study. The helium and carbon dioxide cooled systems can be modified to perform better with respect to maximum beryllium temperature, but will suffer with respect to other parameters. There is also uncertainty with some modifications that can be made to the helium and carbon dioxide cooled models. Further research could be performed to analyze the changes that could be made to the helium and carbon dioxide cooled systems. The maximum beryllium temperature limits the efficiency and uses of the helium and carbon dioxide cooled systems. Further research could be done to analyze different materials with a higher melting temperature than beryllium to replace beryllium in the armor layer.

# Chapter 6 |

## Conclusions and Future Work

This study analyzed the use of water, helium, and carbon dioxide as coolant for a fusion FRC machine. These are among the top coolants being considered for Generation IV nuclear reactors and fusion reactors. SNAP was used to build TRACE models for each coolant analyzed in this study for the same power source and vessel coolant channel design. The common components across all models were the power source, coolant channels geometry, and pump geometry. The models were all Rankine cycle models with water as the secondary side coolant. The water cooled model used a u-tube steam generator, while the helium and carbon dioxide cooled models used a helical coil steam generator. The operating conditions were unique for each system, but based on systems for each coolant that are in use or being researched.

After building the TRACE models and finalizing the operating conditions for each model, simulations were performed to gather results for each unique system. TRACE is only verified and validated for use with water in simulation. So, the method of manufactured solutions was used to verify the use of helium and carbon dioxide in TRACE for the range of conditions in the models for each respective coolant. After verifying using helium and carbon dioxide for TRACE simulations with the range of conditions used in this research, the results were determined reliable for the purpose of this study and analysis was performed to determine the best coolant for the system analyzed in this thesis.

Based on this study, it was determined that water performed as the best coolant for the system analyzed. For the operating conditions used in this research, water is able to keep the beryllium temperature below the maximum beryllium temperature much easier than the helium and carbon dioxide cooled systems. Also, there is

uncertainty associated with the turbine efficiencies used in this study. So, the overall efficiency is not as important of a parameter in determining the best coolant for the system in this study as other parameters. Theoretically, the helium and carbon dioxide cooled systems should have a higher efficiency than the water cooled model. Currently, beryllium is amongst the top materials in consideration for the armor layer in a fusion reactor. It has a relatively low melting point for power applications. A low  $z$  material is desired for a fusion reactor because source gammas are much less likely to interact with the armor layer. At the operating conditions used in this study, water is able to keep the beryllium temperature much lower than the maximum beryllium temperature. The maximum beryllium temperature limits the efficiency and capabilities of the helium and carbon dioxide cooled systems.

There are several areas that can be looked into further related to this study including changes to the helium and carbon dioxide cooled models, different material selections for the system used in this study, and further verification and validation of helium and carbon dioxide for TRACE. There are several modification and additions that can be made to the helium and carbon dioxide cooled systems to change the performance of the system. The degree of uncertainty varies with each potential modification and/or addition to the system in this study. Heat transfer enhancing mechanisms, operating at a higher pressure, and/or operating as a Brayton cycle are among the various options to modify the helium and carbon dioxide cooled systems that can be looked into further. Further research could be done to analyze different materials with a higher melting temperature than beryllium to replace beryllium in the armor layer. Aside from modifications and additions to the systems, further work can be done to verify and validate using helium and carbon dioxide as a fluid in TRACE models and simulations. Other fluids, such as molten salts and liquid metals, can be further verified and validated for use in TRACE too.

# Appendix A | Input File For TRACE Water Cooled Model

## A.1 Introduction

The TRACE input file for the water cooled model is provided in this appendix. The input file is presented in two columns due to the length of the input file. The file reads from the top left to bottom left to top right to bottom right of each page.

## A.2 TRACE Water Cooled Model Input File

```

free format
*m: SNAP:Symbolic Nuclear Analysis Package, Version 2.5.7, July 14, 2017
*m: PLUGIN:TRACE Version 3.8.4
*m: CODE:TRACE V 5.0 Patch 5
*m: DATE:3/20/18
*
*
*****
* main data *
*****
*
*      numtcr      ieos      inopt      nmat      id2o
*      1          0          1          2          0
*
*
*****
* namelist data *
*****
*
&inopts
dtstrt=-1.0,
graphlevel="full",
ikfac=1,
usesjc=3,
numgentbl=1,
npower=1,
nhtstr=5,
mixednumerics=2
&end
*
*****
* Model Flags *
*****
*
*      dstep      timet
*      0          0.0
*
*      stdyst      trans1      ncomp      njun      ipak
*      0          1          29          25          1
*
*      epso      epsi
*      1.0E-4    1.0E-4
*
*      oitmax      sitmax      isolut      ncontr      nccfl
*      10          10          0          0          0
*
*      ntsv      ntcbl      ntcf      ntrp      ntcp
*      46        44        18        0          0
*
*****
* component-number data *
*****
*
* Component input order (IORDER)
*--- type --- num ----- name ----- + jun1 jun2 jun3
* PIPE * 11 s * + 0 1464
* PIPE * 40 s * + 1524 1554
* PIPE * 46 s * $41$ int-loop c-leg vssl c6 + 575 1644
* PIPE * 50 s * + 1534 1564
* PIPE * 60 s * + 1544 1574
* PUMP * 70 s * RCP + 1554 1154
* VALVE * 110 s * PZR SRV + 884 714
* BREAK * 140 s * + 714
* PUMP * 170 s * RCP + 1564 10
* PIPE * 180 s * + 1154 1654
* PIPE * 200 s * + 10 1624
* PIPE * 210 s * + 1204 1614
* PUMP * 270 s * RCP + 1574 1204
* PIPE * 311 s * Primary Side SG Tube bundle + 1464 564
* PIPE * 320 s * Primary Side SG Tube bundle + 1634 564
* FILL * 350 s * SG Feedwater BC + 604
* PIPE * 351 s * SG Feedwater Nozzle + 604 554
* PIPE * 352 s * SG Downcomer + 624 544

```



```

* PIPE * 353 s * SG Boiler and Steam Separator + 0 614 * idsv isvn ilcn icn1 icn2
* PIPE * 354 s * SG Transition Cone + 574 624 * 320 21 611 1 0
* BREAK * 355 s * SG Steam Line Pressure BC + 614 * * idsv isvn ilcn icn1 icn2
* PRIZER * 611 s * pressurizer + 884 575 * 323 32 70 2 0
* PIPE * 1090 s * * * * *
* HTSTR * 20 s * * * *
* HTSTR * 30 s * * * *
* POWER * 80 s * * * *
* HTSTR * 90 s * * * *
* HTSTR * 381 s * SG Tube bundle Walls + * idsv isvn ilcn icn1 icn2
* HTSTR * 390 s * SG Tube bundle Walls + * 325 21 311 1 0
*****
* Mixed Numerics Time Integration/Spatial Difference Methods *
*****
* - Time Integration Method defaults to SETS *
* - Spatial Difference Method defaults to First-order upwind *
*
* --type-- num time int method space diff method
* PRIZER * 611 *SETS*1 *First-order upwind*ie
*
*****
* material properties *
*****
* matb* 50 51 e * idsv isvn ilcn icn1 icn2
* ptbln* -3 -2 e * 425 21 311 1 0
* User Defined Material : 50 * idsv isvn ilcn icn1 icn2
* 426 21 200 7 0
*n: beryllium *
* rhonum sphtnum condnum emisnum * idsv isvn ilcn icn1 icn2
* 0 1 1 0 * 427 75 311 1 0
* prptb temp rho emis * idsv isvn ilcn icn1 icn2
* prptb* 300.0 1850.0 0.18s * 523 32 270 2 0
* prptb* 800.0 1850.0 0.18s * *
* prptb* 1500.0 1850.0 0.18e * idsv isvn ilcn icn1 icn2
* 524 75 311 1 0
* specific heat fit *
* toffset tlower tupper a0 a1 * idsv isvn ilcn icn1 icn2
* 0.0 300.0 1500.0 606.91 5.3382 * 525 21 311 1 0
* a2 a3 a4 a5 *
* -4.1726E-3 1.2723E-6 0.0 0.0 * idsv isvn ilcn icn1 icn2
* 526 21 210 1 0
* thermal conductivity functional fit *
* toffset tlower tupper a0 a1 * idsv isvn ilcn icn1 icn2
* 0.0 300.0 1500.0 430.35 -1.1674 * 527 75 311 1 0
* a2 a3 a4 a5 *
* 1.6044E-3 -1.0097E-6 2.3642E-10 0.0 * idsv isvn ilcn icn1 icn2
* User Defined Material : 51 * 528 32 70 3 0
*n: tungsten *
* rhonum sphtnum condnum emisnum * idsv isvn ilcn icn1 icn2
* 0 1 1 0 * 529 75 70 2 0
* prptb temp rho emis * idsv isvn ilcn icn1 icn2
* prptb* 253.0 1.93E4 0.04s * 530 21 40 2 0
* prptb* 2500.0 1.93E4 0.04e * *
* specific heat fit *
* toffset tlower tupper a0 a1 * idsv isvn ilcn icn1 icn2
* 0.0 293.0 2500.0 116.37 0.071119 * 531 21 180 1 0
* a2 a3 a4 a5 *
* -6.5828E-5 3.2396E-8 -5.4523E-12 0.0 * idsv isvn ilcn icn1 icn2
* 532 32 170 1 0
* thermal conductivity functional fit *
* toffset tlower tupper a0 a1 * idsv isvn ilcn icn1 icn2
* 0.0 293.0 2500.0 240.51 -0.2899 * 533 75 170 2 0
* a2 a3 a4 a5 *
* 2.5403E-4 -1.0263E-7 1.5238E-11 0.0 * idsv isvn ilcn icn1 icn2
* 534 21 50 2 0
*
* idsv isvn ilcn icn1 icn2 *
* 535 21 200 1 0
*****
* Starting Signal Variable Section of Model *
*****
* idsv isvn ilcn icn1 icn2 *
* 1 0 0 0 0 * idsv isvn ilcn icn1 icn2
* 537 75 270 2 0
* idsv isvn ilcn icn1 icn2 *
* 5 27 311 1 0 * idsv isvn ilcn icn1 icn2
* 538 21 60 2 0
* idsv isvn ilcn icn1 icn2 *
* 105 28 353 11 0 * idsv isvn ilcn icn1 icn2
* 539 21 210 1 0
* idsv isvn ilcn icn1 icn2 *
* 106 105 353 10 0 * idsv isvn ilcn icn1 icn2
* 540 86 180 13 0
* idsv isvn ilcn icn1 icn2 *
* 109 105 350 1 0 * idsv isvn ilcn icn1 icn2
* 541 86 180 20 0
* idsv isvn ilcn icn1 icn2 *
* 218 23 311 1 0 * idsv isvn ilcn icn1 icn2
* 542 86 180 27 0
* idsv isvn ilcn icn1 icn2 *
* 301 0 0 0 0 * idsv isvn ilcn icn1 icn2
* 550 86 200 13 0
* idsv isvn ilcn icn1 icn2 *
* 316 69 353 11 0 * idsv isvn ilcn icn1 icn2
* 551 86 200 20 0
* idsv isvn ilcn icn1 icn2 *
* 317 29 311 1 0 * idsv isvn ilcn icn1 icn2
* 552 86 200 27 0

```

```

*
*          idsv      isvn      ilcn      icn1      icn2      *n: delta P
*          560        86        210        13         0
*
*          idsv      isvn      ilcn      icn1      icn2      *
*          561        86        210        20         0
*
*          idsv      isvn      ilcn      icn1      icn2      *
*          562        86        210        27         0
*
*****
* Finished Signal Variable Section of Model *
*****
*
*
*****
* Starting Control System Section of Model *
*****
*
***** Control Blocks *****
*n: coolant inlet temperature
*
*          idcb      icbn      icb1      icb2      icb3
*          -4         9         0         0         0
*
*          cbgain    cbxmin    cbmax    cbcon1    cbcon2
*          1.0       -1.0E20    1.0E20    563.15    0.0
*
*n: coolant exit temperature BC
*
*          idcb      icbn      icb1      icb2      icb3
*          -7         9         0         0         0
*
*          cbgain    cbxmin    cbmax    cbcon1    cbcon2
*          1.0       -1.0E20    1.0E20    563.15    0.0
*
*n: net power
*
*          idcb      icbn      icb1      icb2      icb3
*          -8         54        -141      -17        0
*
*          cbgain    cbxmin    cbmax    cbcon1    cbcon2
*          1.0       -1.0E20    1.0E20    0.0       0.0
*
*          idcb      icbn      icb1      icb2      icb3
*          -9         14         323      324        0
*
*          cbgain    cbxmin    cbmax    cbcon1    cbcon2
*          1.0       -1.0E20    1.0E20    0.0       0.0
*
*n: pumping power loop 1
*
*          idcb      icbn      icb1      icb2      icb3
*          -10        14         -11       -13        0
*
*          cbgain    cbxmin    cbmax    cbcon1    cbcon2
*          1.0       -1.0E20    1.0E20    0.0       0.0
*
*          idcb      icbn      icb1      icb2      icb3
*          -11        104         3         0         0
*
*          cbgain    cbxmin    cbmax    cbcon1    cbcon2
*          1.0       -1.0E20    1.0E20    0.0       0.0
*
*          ids *      -12      -9      -15e
*
*n: delta P
*
*          idcb      icbn      icb1      icb2      icb3
*          -12        54         326      325        0
*
*          cbgain    cbxmin    cbmax    cbcon1    cbcon2
*          1.0       -1.0E20    1.0E20    0.0       0.0
*
*          idcb      icbn      icb1      icb2      icb3
*          -13        39         327      -14        0
*
*          cbgain    cbxmin    cbmax    cbcon1    cbcon2
*          1.0       -1.0E20    1.0E20    0.0       0.0
*
*          idcb      icbn      icb1      icb2      icb3
*          -14        9         0         0         0
*
*          cbgain    cbxmin    cbmax    cbcon1    cbcon2
*          1.0       -1.0E20    1.0E20    9.81      0.0
*
*          idcb      icbn      icb1      icb2      icb3
*          -15        9         0         0         0
*
*          cbgain    cbxmin    cbmax    cbcon1    cbcon2
*          1.0       -1.0E20    1.0E20    9810.0    0.0
*
*n: total pumping power
*
*          idcb      icbn      icb1      icb2      icb3
*          -16        57        -10      -110      -210
*
*          cbgain    cbxmin    cbmax    cbcon1    cbcon2
*          1.0       -1.0E20    1.0E20    0.0       0.0
*
*n: total pumping power
*
*          idcb      icbn      icb1      icb2      icb3
*          -17        57        -220     -122      -22
*
*          cbgain    cbxmin    cbmax    cbcon1    cbcon2
*          1.0       -1.0E20    1.0E20    0.0       0.0
*
*
*          idcb      icbn      icb1      icb2      icb3
*          -21        54         531      530         0
*
*          cbgain    cbxmin    cbmax    cbcon1    cbcon2
*          1.0       -1.0E20    1.0E20    0.0       0.0
*
*
*          idcb      icbn      icb1      icb2      icb3
*          -22        39        -21      -24         0
*
*          cbgain    cbxmin    cbmax    cbcon1    cbcon2
*          1.0       -1.0E20    1.0E20    0.0       0.0
*
*
*          idcb      icbn      icb1      icb2      icb3
*          -24        14         528      529         0
*
*          cbgain    cbxmin    cbmax    cbcon1    cbcon2
*          1.0       -1.0E20    1.0E20    0.0       0.0
*
*
*          idcb      icbn      icb1      icb2      icb3
*          -109       14         423      424         0
*
*          cbgain    cbxmin    cbmax    cbcon1    cbcon2
*          1.0       -1.0E20    1.0E20    0.0       0.0
*
*n: pumping power loop 2
*
*          idcb      icbn      icb1      icb2      icb3
*          -110       14        -111     -113        0
*
*          cbgain    cbxmin    cbmax    cbcon1    cbcon2
*          1.0       -1.0E20    1.0E20    0.0       0.0
*
*          idcb      icbn      icb1      icb2      icb3
*          -111       104         3         0         0
*
*          cbgain    cbxmin    cbmax    cbcon1    cbcon2
*          1.0       -1.0E20    1.0E20    0.0       0.0
*
*          ids *      -112      -109     -115e
*
*n: delta P
*
*          idcb      icbn      icb1      icb2      icb3
*          -112       54         426      425         0
*
*          cbgain    cbxmin    cbmax    cbcon1    cbcon2
*          1.0       -1.0E20    1.0E20    0.0       0.0
*
*          idcb      icbn      icb1      icb2      icb3
*          -113       39         427      -114        0
*
*          cbgain    cbxmin    cbmax    cbcon1    cbcon2
*          1.0       -1.0E20    1.0E20    0.0       0.0
*
*          idcb      icbn      icb1      icb2      icb3
*          -114         9         0         0         0
*
*          cbgain    cbxmin    cbmax    cbcon1    cbcon2
*          1.0       -1.0E20    1.0E20    9.81      0.0
*
*          idcb      icbn      icb1      icb2      icb3
*          -115         9         0         0         0
*
*          cbgain    cbxmin    cbmax    cbcon1    cbcon2
*          1.0       -1.0E20    1.0E20    9810.0    0.0
*
*
*          idcb      icbn      icb1      icb2      icb3
*          -116       56         -130     0         0
*
*          cbgain    cbxmin    cbmax    cbcon1    cbcon2
*          1.0       -1.0E20    1.0E20    0.0       0.0
*
*
*          idcb      icbn      icb1      icb2      icb3
*          -120       54         106      109         0
*
*          cbgain    cbxmin    cbmax    cbcon1    cbcon2
*          1.0       -1.0E20    1.0E20    0.0       0.0
*
*n: delta P
*
*          idcb      icbn      icb1      icb2      icb3
*          -121       54         535      534         0
*
*          cbgain    cbxmin    cbmax    cbcon1    cbcon2
*          1.0       -1.0E20    1.0E20    0.0       0.0
*
*          idcb      icbn      icb1      icb2      icb3
*          -122       39        -121     -124         0
*
*          cbgain    cbxmin    cbmax    cbcon1    cbcon2
*          1.0       -1.0E20    1.0E20    0.0       0.0
*
*          idcb      icbn      icb1      icb2      icb3
*          -124        14         532      533         0
*
*          cbgain    cbxmin    cbmax    cbcon1    cbcon2
*          1.0       -1.0E20    1.0E20    0.0       0.0
*
*          idcb      icbn      icb1      icb2      icb3
*          -130       39        -120     105         0
*
*          cbgain    cbxmin    cbmax    cbcon1    cbcon2
*          1.0       -1.0E20    1.0E20    0.0       0.0

```

```

*n: Turbine Power
*
*   idcb      icbn      icb1      icb2      icb3
*   -141      39        -150      -116      0
*   cbgain    cbxmin    cbmax    cbcon1    cbcon2
*   1.0       -1.0E20    1.0E20    0.0       0.0
*
*
*   idcb      icbn      icb1      icb2      icb3
*   -150      9         0         0         0
*   cbgain    cbxmin    cbmax    cbcon1    cbcon2
*   1.0       -1.0E20    1.0E20    0.34      0.0
*
*
*   idcb      icbn      icb1      icb2      icb3
*   -209      14        523       524       0
*   cbgain    cbxmin    cbmax    cbcon1    cbcon2
*   1.0       -1.0E20    1.0E20    0.0       0.0
*
*n: pumping power loop 3
*
*   idcb      icbn      icb1      icb2      icb3
*   -210      14        -211      -213      0
*   cbgain    cbxmin    cbmax    cbcon1    cbcon2
*   1.0       -1.0E20    1.0E20    0.0       0.0
*
*
*   idcb      icbn      icb1      icb2      icb3
*   -211      104       3         0         0
*   cbgain    cbxmin    cbmax    cbcon1    cbcon2
*   1.0       -1.0E20    1.0E20    0.0       0.0
*
*   ids      *        -212      -209      -215e
*
*n: delta P
*
*   idcb      icbn      icb1      icb2      icb3
*   -212      54        526       525       0
*   cbgain    cbxmin    cbmax    cbcon1    cbcon2
*   1.0       -1.0E20    1.0E20    0.0       0.0
*
*
*   idcb      icbn      icb1      icb2      icb3
*   -213      39        527       -214      0
*   cbgain    cbxmin    cbmax    cbcon1    cbcon2
*   1.0       -1.0E20    1.0E20    0.0       0.0
*
*
*   idcb      icbn      icb1      icb2      icb3
*   -214      9         0         0         0
*   cbgain    cbxmin    cbmax    cbcon1    cbcon2
*   1.0       -1.0E20    1.0E20    9.81      0.0
*
*
*   idcb      icbn      icb1      icb2      icb3
*   -215      9         0         0         0
*   cbgain    cbxmin    cbmax    cbcon1    cbcon2
*   1.0       -1.0E20    1.0E20    9810.0    0.0
*
*n: delta P
*
*   idcb      icbn      icb1      icb2      icb3
*   -219      54        539       538       0
*   cbgain    cbxmin    cbmax    cbcon1    cbcon2
*   1.0       -1.0E20    1.0E20    0.0       0.0
*
*
*   idcb      icbn      icb1      icb2      icb3
*   -220      39        -219      -222      0
*   cbgain    cbxmin    cbmax    cbcon1    cbcon2
*   1.0       -1.0E20    1.0E20    0.0       0.0
*
*
*   idcb      icbn      icb1      icb2      icb3
*   -222      14        536       537       0
*   cbgain    cbxmin    cbmax    cbcon1    cbcon2
*   1.0       -1.0E20    1.0E20    0.0       0.0
*
*n: SG feedwater controller
*
*   idcb      icbn      icb1      icb2      icb3
*   -305      22        316       -306      -307
*   cbgain    cbxmin    cbmax    cbcon1    cbcon2
*   1.0       -1.0E20    1.0E20    0.0       0.0
*
*
*   idcb      icbn      icb1      icb2      icb3
*   -306      9         0         0         0
*   cbgain    cbxmin    cbmax    cbcon1    cbcon2
*   1.0       -1.0E20    1.0E20    100.0     0.0
*
*
*   idcb      icbn      icb1      icb2      icb3
*   -307      20        301       -308      0
*   cbgain    cbxmin    cbmax    cbcon1    cbcon2
*   1.0       -1.0E20    1.0E20    0.0       0.0
*
*
*   idcb      icbn      icb1      icb2      icb3
*   -308      9         0         0         0
*   cbgain    cbxmin    cbmax    cbcon1    cbcon2
*   1.0       -1.0E20    1.0E20    30.0      0.0

```

```

*
*****
* Finished Control System Section of Model *
*****
*
*
*****
* Starting General Table Section of Model *
*****
* gtblnm*      1e
*n: heat flux vs. time
*
*
* tablenumber
* 1
* npts      tabletype      xcbsvid      tripid      outbounds
* 8         2              1           0           0
*
* Time(s)      Heatfx(W/m^2)
* tableid *    0.0          0.0a
* tableid * 1000.0       0.0a
* tableid * 1050.0       0.0a
* tableid * 2000.0       0.0a
* tableid * 1.0E4        0.0a
* tableid * 1.000001E4   0.0a
* tableid * 1.000101E4   0.0a
* tableid * 1.0002E4     0.0e
*****
* Finished General Table Section of Model *
*****
*
*
***** type      num      userid      component name
pipe           11       0            unnamed
* ncells      nodes      jun1      jun2      epsw
* 1           0         0         1464     0.0
* nsides
* 3
* nclk        junlk      ncmpto      nclkto      nlevto
* 1           1524       0          0          0
* theta       ientrn
* 90.0        0
* nclk        junlk      ncmpto      nclkto      nlevto
* 1           1534       0          0          0
* theta       ientrn
* 90.0        0
* nclk        junlk      ncmpto      nclkto      nlevto
* 1           1544       0          0          0
* theta       ientrn
* 90.0        0
* ichf        iconc      pipetype     ipow      npipes
* 1           0         0          0          1
* radin       th      houtv      toutl
* 0.0         0.0      0.0        0.0
* toutv       pwin      pwoff      rpwm      pwscl
* 0.0         0.0      0.0        0.0        0.0
* dx *        1.0e
* vol * 0.76128644e
* fa * 0.76128644 0.76128644e
* kfacs * 0.0 0.0 0.0e
* grav * 0.0 0.0 0.0e
* hd * 0.98453035 0.98453035e
* nff * 1 -1e
* alp * 0.0e
* vl * 0.0 10.0e
* vv * 0.0 0.0e
* tl * 615.305e
* tv * 615.305e
* p * 1.5E7e
* pa * 0.0e
***** type      num      userid      component name
pipe           40       0            unnamed
* ncells      nodes      jun1      jun2      epsw
* 2           0         1524     1554     0.0
* nsides
* 0
* ichf        iconc      pipetype     ipow      npipes
* 1           0         0          0          1
* radin       th      houtv      toutl
* 0.0         0.0      0.0        0.0
* toutv       pwin      pwoff      rpwm      pwscl
* 0.0         0.0      0.0        0.0        0.0
* dx *        1.0 1.0e
* vol * 0.25376215 0.25376215e
* fa * 0.25376215 0.25376215 0.25376215e
* kfacs * 0.0 0.0 0.0e
* grav * 0.0 0.0 0.0e
* hd * 0.56841886 0.56841886 0.56841886e
* nff * 1 1 1e
* alp * 0.0 0.0e
* vl * 0.0 0.0 0.0e
* vv * 0.0 0.0 0.0e
* tl * 615.305 615.305e
* tv * 615.305 615.305e
* p * 1.5E7 1.5E7e
* pa * 0.0 0.0e
*

```

```

*
***** type          num      userid      component name
pipe          46          0      $41$ int-loop c-leg vssl c6
* ncells      2          0          jun1      epsw      1644      0.0
* nsides      0
* ichf        iconc      pipetype      ipow      npipes
* 1           0          0          0          1
* radin       th          houtl      houtv      toutl
* 0.0         0.0         0.0         0.0         0.0
* toutv       pwin      pwoff      rpwm      pwscl
* 0.0         0.0         0.0         0.0         0.0
* dx          1.4733      1.4733e
* vol         0.58123    0.58123e
* fa          0.36316811 0.10744247 0.10744247e
* kf          0.0         0.0         0.0
* grav        -1.0        -0.99999998 -0.99999998e
* hd          2.43       0.36986484 0.36986484e
* nff         -100       1          -1e
* alp         0.0         0.0         0.0
* vl          0.0         0.0         0.0e
* vv          0.0         0.0         0.0e
* tl          550.0      550.0e
* tv          550.0      550.0e
* p           1.0E7     1.0E7e
* pa          0.0         0.0e
*
***** type          num      userid      component name
pipe          50          0          unnamed
* ncells      2          0          jun1      epsw      1564      0.0
* nsides      0
* ichf        iconc      pipetype      ipow      npipes
* 1           0          0          0          1
* radin       th          houtl      houtv      toutl
* 0.0         0.0         0.0         0.0         0.0
* toutv       pwin      pwoff      rpwm      pwscl
* 0.0         0.0         0.0         0.0         0.0
* dx          1.0         1.0e
* vol         0.25376215 0.25376215e
* fa          0.25376215 0.25376215e
* kf          0.0         0.0         0.0e
* grav        0.0         0.0         0.0e
* hd          0.56841886 0.56841886e
* nff         1           1          1e
* alp         0.0         0.0         0.0e
* vl          0.0         0.0         0.0e
* vv          0.0         0.0         0.0e
* tl          615.305    615.305e
* tv          615.305    615.305e
* p           1.5E7     1.5E7e
* pa          0.0         0.0e
*
***** type          num      userid      component name
pipe          60          0          unnamed
* ncells      2          0          jun1      epsw      1574      0.0
* nsides      0
* ichf        iconc      pipetype      ipow      npipes
* 1           0          0          0          1
* radin       th          houtl      houtv      toutl
* 0.0         0.0         0.0         0.0         0.0
* toutv       pwin      pwoff      rpwm      pwscl
* 0.0         0.0         0.0         0.0         0.0
* dx          1.0         1.0e
* vol         0.25376215 0.25376215e
* fa          0.25376215 0.25376215e
* kf          0.0         0.0         0.0e
* grav        0.0         0.0         0.0e
* hd          0.56841886 0.56841886e
* nff         1           1          1e
* alp         0.0         0.0         0.0e
* vl          0.0         0.0         0.0e
* vv          0.0         0.0         0.0e
* tl          615.305    615.305e
* tv          615.305    615.305e
* p           1.5E7     1.5E7e
* pa          0.0         0.0e
*
***** type          num      userid      component name
pump          70          0          RCP
* ncells      2          0          jun1      epsw      1154      0.0
* nsides      0
* ichf        iconc      ipmpty      irp      ipm
* 1           0          1          1          1
* ipmtr       ipmsv      npmptb      npmsv      npmprf
* 0           1          8          0          0
* radin       th          houtl      houtv      toutl
* 0.0         0.0         0.0         0.0         0.0
* toutv       effmi      eta
* 0.0         3455.0     85.0
* tfr0        tfr1      tfr2      tfr3      tfrb
* 0.0         0.0         0.0         0.0         0.0
*
***** type          num      userid      component name
pipe          110         0          PZR SRV
* ncells      0          0          jun1      epsw      884      714      0.0
* ichf        iconc      ivty      ivps      nvb2
* 1           0          1          1          0
* ivtr        ivsv      nvb1      nvsv      nvrf
* 0           320       2          0          0
* ivtrov      ivtyov   ivtrlo    intlossoff nkopen
* 0           0          0          0          0
* rvmx        rvov      fminov    fmaxov
* 1.0E20     10.0      1.0        0.0
* radin       th          houtl      houtv      toutl
* 0.0         0.0         0.0         0.0         0.0
* toutv       avlve     hvlve     favlve    xpos
* 0.0         7.854E-5 0.01      0.0         0.0
* dx          f          0.0000e+00e
* vol         f          0.0000e+00e
* fa          f          1.9635E-3e
* kf          f          0.0e
* grav        f          1.0e
* hd          f          0.05e
* nff         f          1e
* alp         f          0.0000e+00e
* vl          f          0.0e
* vv          f          0.0e
* tl          f          0.0000e+00e
* tv          f          0.0000e+00e
* p           f          0.0000e+00e
* pa          f          0.0000e+00e
* vtbl       1.6E7     0.0s
* vtbl       1.7E7     1.0e
*
***** type          num      userid      component name
break         140         0          unnamed
* jun1       ibty      isat      ioff      adjpress
* 714        0          0          0          0
* dxin       volin    alpin     tin      pin
* 2.7233333 12.629997 1.0        300.0    1.01385E5
* pain       concin   rbmx      poff     belv
* 0.0        0.0         1.0E20    0.0         0.0
*
***** type          num      userid      component name
pump          170         0          RCP
* ncells      2          0          jun1      epsw      1564      10      0.0
* nsides      0
* ichf        iconc      ipmpty      irp      ipm
* 1           0          1          1          1
* ipmtr       ipmsv      npmptb      npmsv      npmprf
* 0           1          9          0          0
* radin       th          houtl      houtv      toutl
* 0.0         0.0         0.0         0.0         0.0
* toutv       effmi      eta
* 0.0         3455.0     85.0
* tfr0        tfr1      tfr2      tfr3      tfrb
* 0.0         0.0         0.0         0.0         0.0
* rhead       rtork    rflow     rrho     romega
* 831.0      3.5949E4 5.651     745.0    124.5
* omegan      omgoff   romgm      omgscl   npmpsd
* 40.0       0.0         200.0     1.0        0
* option      4
* dx          2.0         2.0e
* vol         0.5075243 0.5075243e
* fa          0.25376215 0.25376215e
* kf          0.0         0.0         0.0e
* grav        0.0         0.0         0.0e

```







```

* pa * 0.0e
*
***** type num userid component name
fill 350 0 SG Feedwater BC
* jun1 ifty ioff
* 604 10 0
* iftr ifsv nftb nfv nfrf
* 0 0 0 0 0
* twtold rfmx concin felv
* 0.0 0.0 0.0 0.0
* dxin volin alpin vlin tlin
* 1.0 0.5 0.0 0.8603 503.15
* pin pain flowin vvin tvin
* 6.825809E6 0.0 750.0 0.0 503.15
* ifmlsv ifmvsv iftlsv iftvsv ifasv
* -305 0 0 0 0
* ifpsv ifpasv ifcnsv
* 0 0 0
*
***** type num userid component name
pipe 351 0 SG Feedwater Nozzle
* ncells nodes jun1 jun2 epsw
* 1 0 604 554 0.0
* nsides
* 0
* ichf iconc pipetype ipow npipes
* 1 0 0 0 1
* radin th houtl houtv toutl
* 0.0 0.0 0.0 0.0 0.0
* toutv pwin pwoff rpwmx pswcl
* 0.0 0.0 0.0 0.0 0.0
* dx * 1.0e
* vol * 0.5e
* fa * 0.5 0.5e
* kfac * 1.0E-10 0.0e
* grav * 0.0 0.0e
* hd * 0.1 0.1e
* nff * 1 1e
* alp * 0.0e
* vl * 0.0 0.0e
* vv * 0.0 0.0e
* tl * 440.0e
* tv * 440.0e
* p * 4.85E6e
* pa * 0.0e
*
***** type num userid component name
pipe 352 0 SG Downcomer
* ncells nodes jun1 jun2 epsw
* 6 0 624 544 0.0
* nclnk junkl ncmpto nclkto nlevto
* 2 554 0 0 0
* theta ientrn
* 90.0 0
* ichf iconc pipetype ipow npipes
* 1 0 0 0 1
* radin th houtl houtv toutl
* 0.0 0.0 0.0 0.0 0.0
* toutv pwin pwoff rpwmx pswcl
* 0.0 0.0 0.0 0.0 0.0
* dx * 1.0 1.175 0.7113307 0.7113307s
* dx * 0.7113307 0.1e
* vol * 1.1 1.175 2.175 2.175s
* vol * 2.175 0.1092e
* fa * 0.53724987 0.53724987 0.53724987 0.53724987s
* fa * 0.53724987 0.53724987 0.53724987e
* kfac * 3.0E-3 0.0 0.0 0.0s
* kfac * 0.0 0.0 0.0 0.2e
* grav * -1.0 -1.0 -1.0 -1.0s
* grav * -1.0 -1.0 -1.0e
* hd * 6.0 6.0 6.0 6.0s
* hd * 6.0 6.0 6.0 6.0e
* nff * 1 1 1 1s
* nff * 1 1 1e
* alp * 1.0 0.0 0.0 0.0s
* alp * 0.0 0.0e
* vl * 0.0 0.0 0.0 0.0s
* vl * 0.0 0.0 0.0e
* vv * 0.0 0.0 0.0 0.0s
* vv * 0.0 0.0 0.0e
* tl * 535.14 535.14 535.14 535.14s
* tl * 535.14 535.14e
* tv * 535.14 535.14 535.14 535.14s
* tv * 535.14 535.14e
* p * 4.85E6 4.85E6 4.85E6 4.85E6s
* p * 4.85E6 4.85E6e
* pa * 0.0 0.0 0.0 0.0s
* pa * 0.0 0.0e
*
***** type num userid component name
pipe 353 0 SG Boiler and Steam Separator
* ncells nodes jun1 jun2 epsw
* 10 0 0 614 0.0
* nsides
* 2
*
***** type num userid component name
pipe 354 0 SG Transition Cone
* ncells nodes jun1 jun2 epsw
* 1 0 574 624 0.0
* nsides
* 0
* ichf iconc pipetype ipow npipes
* 1 0 0 0 1
* radin th houtl houtv toutl
* 0.0 0.0 0.0 0.0 0.0
* toutv pwin pwoff rpwmx pswcl
* 0.0 0.0 0.0 0.0 0.0
* dx * 0.97278219e
* vol * 12.09954e
* fa * 9.0 0.53724987e
* kfac * 1.0E-10 3.0E-3e
* grav * -1.0 -1.0e
* hd * 0.1 6.0e
* nff * 1 1e
* alp * 1.0e
* vl * 0.0 0.0e
* vv * 0.0 0.0e
* tl * 535.14e
* tv * 535.14e
* p * 4.85E6e
* pa * 0.0e
*
***** type num userid component name
break 355 0 SG Steam Line Pressure BC
* jun1 ibty isat ioff adjpress
* 614 0 0 0 0
* dxin volin alpin tin pin
* 4.35 24.8 1.0 535.14 6.825809E6
* pain concin rbmx poff belv
* 0.0 0.0 1.0E20 0.0 0.0
*
*
* Mixednumerics Time Integration Method set to SETS
* Space Difference Method set to First-order upwind
***** type num userid component name
prizer 611 0 pressurizer
* ncells nodes jun1 jun2

```











```

0          1          1          0          0
* ipwrad   ipwdep   promheat  decaheat  wtbypass  * zpwbtbi* 1.0 1.0 1.0 1.0 1.0s
0          0          0.0        0.0        0.0      * zpwbtbi* 1.0 1.0 1.0 1.0
* nzpzw    nzpwi    nfbpwt    nrpwr    nrpwi     *****
0          0          0          1          0      * Finished Power Components *
* react    tneut     rpwoff    rrpwmx    rpsacl    *****
0.0        0.0        0.0        1.0E20    1.0      *
* rpowri   zpwin    zpwoff    rzpwmx    *
6.0E8     0.0        0.0        0.0      *
* extsou   pldr      pdrat     fucrac    end
0.0        0.0        1.0        1.0      *
* rdpwr * 1.0 1.0 1.0 1.0 1.0s * Timestep Data *
* rdpwr * 1.0 1.0 1.0 1.0 1.0s * *****
* cpwr * 1.0e *
* zpwbtbi* 0.0s * dtmin dtmax tend rtwfp
* zpwbtbi* 1.0 1.0 1.0 1.0 1.0s * 1.0E-10 1.0 5000.0 10.0
* zpwbtbi* 1.0 1.0 1.0 1.0 1.0s * edint gfint dmpint sedint
* zpwbtbi* 1.0 1.0 1.0 1.0 1.0s * 100.0 1.0 100.0 1.0
* zpwbtbi* 1.0 1.0 1.0 1.0 1.0s *
* zpwbtbi* 1.0 1.0 1.0 1.0 1.0s * endflag
* zpwbtbi* 1.0 1.0 1.0 1.0 1.0s * -1.0

```

# Appendix B | Input File For TRACE Helium Cooled Model

## B.1 Introduction

The TRACE input file for the helium cooled model is provided in this appendix. The input file is presented in two columns due to the length of the input file. The file reads from the top left to bottom left to top right to bottom right of each page.

## B.2 TRACE Helium Cooled Model Input File

```

free format
*m: SNAP:Symbolic Nuclear Analysis Package, Version 2.5.7, July 14, 2017
*m: PLUGIN:TRACE Version 3.8.4
*m: CODE:TRACE V 5.0 Patch 5
*m: DATE:3/20/18
*
*
* main data *
*
*      numtcr      ieos      inopt      nmat      id2o
*      1          0          1          2          0
*
*
* namelist data *
*
* &inopts
dtstrt=-1.0,
graphlevel="full",
ikfac=1,
noair=0,
usesjc=3,
npower=1,
nhtstr=3,
igas=3
&end
*
* Model Flags *
*
*      dstep      timet
*      0          0.0
*      stdyst      trans1      ncomp      njun      ipak
*      1          0          21          18          1
*      epso      eps
*      1.0E-4      1.0E-4
*      oitmax      sitmax      isolut      ncontr      nccfl
*      10          10          0          0          0
*      ntsv      ntcb      ntcf      ntrp      ntcp
*      40          45          18          0          0
*
* component-number data *
*
* Component input order (IORDER)
*--- type --- num ----- name ----- + jun1 jun2 jun3
* PIPE * 11 s * + 1634 0
* FILL * 20 s * + 10
* BREAK * 30 s * + 20
* PIPE * 40 s * + 1524 1644
* PIPE * 50 s * + 1534 1664
* PIPE * 60 s * + 1544 1694
* PUMP * 70 s * RCP + 1644 1654
* PIPE * 80 s * + 1624 1614
* PUMP * 170 s * RCP + 1664 1674
* PIPE * 180 s * + 1654 11
* PIPE * 200 s * + 1674 50
* PIPE * 210 s * + 1684 60
* PUMP * 270 s * RCP + 1694 1684
* PIPE * 1010 s * + 10 20
* PIPE * 1050 s * + 1614 70
* PIPE * 1060 s * + 1624 1634
* PIPE * 1090 s * + 0 70
* POWER * 10 s * +

```

```

* HTSTR * 90 s * +
* HTSTR * 100 s * +
* HTSTR * 1040 e * +
*
*****
* material properties *
*****
*
* matb* 50 51 e
* ptbln* -3 -2 e
* User Defined Material : 50
*
*n: beryllium
*
* rhonum sphtnum condnum emisnum
* 0 1 1 0
*
* prptb temp rho emis
* prptb* 300.0 1850.0 0.18s
* prptb* 800.0 1850.0 0.18s
* prptb* 1500.0 1850.0 0.18e
*
* specific heat fit
* toffset tlower tupper a0 a1
* 0.0 300.0 1500.0 606.91 5.3382
* a2 a3 a4 a5
* -4.1726E-3 1.2723E-6 0.0 0.0
* thermal conductivity functional fit
* toffset tlower tupper a0 a1
* 0.0 300.0 1500.0 430.35 -1.1674
* a2 a3 a4 a5
* 1.6044E-3 -1.0097E-6 2.3642E-10 0.0
* User Defined Material : 51
*
*n: tungsten
*
* rhonum sphtnum condnum emisnum
* 0 1 1 0
*
* prptb temp rho emis
* prptb* 253.0 1.93E4 0.04s
* prptb* 2500.0 1.93E4 0.04e
*
* specific heat fit
* toffset tlower tupper a0 a1
* 0.0 293.0 2500.0 116.37 0.071119
* a2 a3 a4 a5
* -6.5828E-5 3.2396E-8 -5.4523E-12 0.0
* thermal conductivity functional fit
* toffset tlower tupper a0 a1
* 0.0 293.0 2500.0 240.51 -0.2899
* a2 a3 a4 a5
* 2.5403E-4 -1.0263E-7 1.5238E-11 0.0
*
*****
* Starting Signal Variable Section of Model *
*****
*
* idsv isvsn ilcn icn1 icn2
* 1 0 0 0 0
*
* idsv isvsn ilcn icn1 icn2
* 105 69 1010 169 0
*
* idsv isvsn ilcn icn1 icn2
* 106 105 1010 167 0
*
* idsv isvsn ilcn icn1 icn2
* 109 105 20 1 0
*
* idsv isvsn ilcn icn1 icn2
* 323 29 70 1 0
*
* idsv isvsn ilcn icn1 icn2
* 324 74 80 2 0
*
* idsv isvsn ilcn icn1 icn2
* 325 21 80 2 0
*
* idsv isvsn ilcn icn1 icn2
* 326 21 180 1 0
*
* idsv isvsn ilcn icn1 icn2
* 327 74 80 2 0
*
* idsv isvsn ilcn icn1 icn2
* 423 29 170 1 0
*
* idsv isvsn ilcn icn1 icn2
* 424 74 80 2 0
*
* idsv isvsn ilcn icn1 icn2
* 425 21 80 2 0
*
* idsv isvsn ilcn icn1 icn2
* 426 21 200 7 0
*
* idsv isvsn ilcn icn1 icn2
* 427 74 80 2 0
*
* idsv isvsn ilcn icn1 icn2
* 523 29 270 1 0
*
* idsv isvsn ilcn icn1 icn2
* 524 74 80 2 0
*
* idsv isvsn ilcn icn1 icn2
* 525 21 80 2 0
*
* idsv isvsn ilcn icn1 icn2
* 526 21 210 1 0
*
* idsv isvsn ilcn icn1 icn2
* 527 74 80 2 0
*
* idsv isvsn ilcn icn1 icn2
* 528 29 70 3 0
*
* idsv isvsn ilcn icn1 icn2
* 529 74 70 2 0
*
* idsv isvsn ilcn icn1 icn2
* 530 21 40 2 0
*
* idsv isvsn ilcn icn1 icn2
* 531 21 180 1 0
*
* idsv isvsn ilcn icn1 icn2
* 532 29 170 3 0
*
* idsv isvsn ilcn icn1 icn2
* 533 74 170 2 0
*
* idsv isvsn ilcn icn1 icn2
* 534 21 50 2 0
*
* idsv isvsn ilcn icn1 icn2
* 535 21 200 1 0
*
* idsv isvsn ilcn icn1 icn2
* 536 29 270 3 0
*
* idsv isvsn ilcn icn1 icn2
* 537 74 270 2 0
*
* idsv isvsn ilcn icn1 icn2
* 538 21 60 2 0
*
* idsv isvsn ilcn icn1 icn2
* 539 21 210 1 0
*
* idsv isvsn ilcn icn1 icn2
* 540 85 180 13 0
*
* idsv isvsn ilcn icn1 icn2
* 541 85 180 20 0
*
* idsv isvsn ilcn icn1 icn2
* 542 85 180 27 0
*
* idsv isvsn ilcn icn1 icn2
* 550 85 200 13 0
*
* idsv isvsn ilcn icn1 icn2
* 551 85 200 20 0
*
* idsv isvsn ilcn icn1 icn2
* 552 85 200 27 0
*
* idsv isvsn ilcn icn1 icn2
* 560 85 210 13 0
*
* idsv isvsn ilcn icn1 icn2
* 561 85 210 20 0
*
* idsv isvsn ilcn icn1 icn2
* 562 85 210 27 0
*
*****
* Finished Signal Variable Section of Model *
*****
*
*
*
* Starting Control System Section of Model *
*****
*
* Control Blocks
*
* Gas volume fraction BC
*
* idcb icbn icb1 icb2 icb3
* -1 9 0 0 0
* cbgain cbxmin cbmax cbcon1 cbcon2
* 1.0 -1.0E20 1.0E20 1.0 0.0
*
*n: Entrance vapor mass flow controller
*
* idcb icbn icb1 icb2 icb3
* -2 9 0 0 0
* cbgain cbxmin cbmax cbcon1 cbcon2
* 1.0 -1.0E20 1.0E20 90.0 0.0

```

```

*n: NCG PP BC
*
* idcb icbn icb1 icb2 icb3
* -3 9 0 0 0
* cbgain cbxmin cbmax cbcon1 cbcon2
* 1.0 -1.0E20 1.0E20 1.5E7 0.0
*
*n: Pressure BC
*
* idcb icbn icb1 icb2 icb3
* -4 9 0 0 0
* cbgain cbxmin cbmax cbcon1 cbcon2
* 1.0 -1.0E20 1.0E20 1.5E7 0.0
*
*n: Entrance temperature BC
*
* idcb icbn icb1 icb2 icb3
* -5 9 0 0 0
* cbgain cbxmin cbmax cbcon1 cbcon2
* 1.0 -1.0E20 1.0E20 600.0 0.0
*
*n: Exit Temperature BC
*
* idcb icbn icb1 icb2 icb3
* -6 9 0 0 0
* cbgain cbxmin cbmax cbcon1 cbcon2
* 1.0 -1.0E20 1.0E20 800.0 0.0
*
*n: secondary mass flow
*
* idcb icbn icb1 icb2 icb3
* -7 9 0 0 0
* cbgain cbxmin cbmax cbcon1 cbcon2
* 1.0 -1.0E20 1.0E20 250.0 0.0
*
*n: net power
*
* idcb icbn icb1 icb2 icb3
* -8 54 -141 -17 0
* cbgain cbxmin cbmax cbcon1 cbcon2
* 1.0 -1.0E20 1.0E20 0.0 0.0
*
* idcb icbn icb1 icb2 icb3
* -9 14 323 324 0
* cbgain cbxmin cbmax cbcon1 cbcon2
* 1.0 -1.0E20 1.0E20 0.0 0.0
*
*n: pumping power loop 1
*
* idcb icbn icb1 icb2 icb3
* -10 14 -11 -13 0
* cbgain cbxmin cbmax cbcon1 cbcon2
* 1.0 -1.0E20 1.0E20 0.0 0.0
*
* idcb icbn icb1 icb2 icb3
* -11 104 3 0 0
* cbgain cbxmin cbmax cbcon1 cbcon2
* 1.0 -1.0E20 1.0E20 0.0 0.0
*
* ids * -12 -9 -15e
*
*n: delta P
*
* idcb icbn icb1 icb2 icb3
* -12 54 326 325 0
* cbgain cbxmin cbmax cbcon1 cbcon2
* 1.0 -1.0E20 1.0E20 0.0 0.0
*
* idcb icbn icb1 icb2 icb3
* -13 39 327 -14 0
* cbgain cbxmin cbmax cbcon1 cbcon2
* 1.0 -1.0E20 1.0E20 0.0 0.0
*
* idcb icbn icb1 icb2 icb3
* -14 9 0 0 0
* cbgain cbxmin cbmax cbcon1 cbcon2
* 1.0 -1.0E20 1.0E20 9.81 0.0
*
* idcb icbn icb1 icb2 icb3
* -15 9 0 0 0
* cbgain cbxmin cbmax cbcon1 cbcon2
* 1.0 -1.0E20 1.0E20 9810.0 0.0
*
*n: total pumping power
*
* idcb icbn icb1 icb2 icb3
* -16 57 -10 -110 -210
* cbgain cbxmin cbmax cbcon1 cbcon2
* 1.0 -1.0E20 1.0E20 0.0 0.0
*
*n: total pumping power
*
* idcb icbn icb1 icb2 icb3
* -17 57 -220 -122 -22
* cbgain cbxmin cbmax cbcon1 cbcon2
* 1.0 -1.0E20 1.0E20 0.0 0.0
*
*n: delta P
*
* idcb icbn icb1 icb2 icb3
* -21 54 531 530 0
* cbgain cbxmin cbmax cbcon1 cbcon2
* 1.0 -1.0E20 1.0E20 0.0 0.0
*
* idcb icbn icb1 icb2 icb3
* -22 39 -21 -24 0
* cbgain cbxmin cbmax cbcon1 cbcon2
* 1.0 -1.0E20 1.0E20 0.0 0.0
*
* idcb icbn icb1 icb2 icb3
* -24 14 528 529 0
* cbgain cbxmin cbmax cbcon1 cbcon2
* 1.0 -1.0E20 1.0E20 0.0 0.0
*
* idcb icbn icb1 icb2 icb3
* -109 14 423 424 0
* cbgain cbxmin cbmax cbcon1 cbcon2
* 1.0 -1.0E20 1.0E20 0.0 0.0
*
*n: pumping power loop 2
*
* idcb icbn icb1 icb2 icb3
* -110 14 -111 -113 0
* cbgain cbxmin cbmax cbcon1 cbcon2
* 1.0 -1.0E20 1.0E20 0.0 0.0
*
* idcb icbn icb1 icb2 icb3
* -111 104 3 0 0
* cbgain cbxmin cbmax cbcon1 cbcon2
* 1.0 -1.0E20 1.0E20 0.0 0.0
*
* ids * -112 -109 -115e
*
*n: delta P
*
* idcb icbn icb1 icb2 icb3
* -112 54 426 425 0
* cbgain cbxmin cbmax cbcon1 cbcon2
* 1.0 -1.0E20 1.0E20 0.0 0.0
*
* idcb icbn icb1 icb2 icb3
* -113 39 427 -114 0
* cbgain cbxmin cbmax cbcon1 cbcon2
* 1.0 -1.0E20 1.0E20 0.0 0.0
*
* idcb icbn icb1 icb2 icb3
* -114 9 0 0 0
* cbgain cbxmin cbmax cbcon1 cbcon2
* 1.0 -1.0E20 1.0E20 9.81 0.0
*
* idcb icbn icb1 icb2 icb3
* -115 9 0 0 0
* cbgain cbxmin cbmax cbcon1 cbcon2
* 1.0 -1.0E20 1.0E20 9810.0 0.0
*
* idcb icbn icb1 icb2 icb3
* -116 56 -130 0 0
* cbgain cbxmin cbmax cbcon1 cbcon2
* 1.0 -1.0E20 1.0E20 0.0 0.0
*
* idcb icbn icb1 icb2 icb3
* -120 54 106 109 0
* cbgain cbxmin cbmax cbcon1 cbcon2
* 1.0 -1.0E20 1.0E20 0.0 0.0
*
*n: delta P
*
* idcb icbn icb1 icb2 icb3
* -121 54 535 534 0
* cbgain cbxmin cbmax cbcon1 cbcon2
* 1.0 -1.0E20 1.0E20 0.0 0.0
*
* idcb icbn icb1 icb2 icb3
* -122 39 -121 -124 0
* cbgain cbxmin cbmax cbcon1 cbcon2
* 1.0 -1.0E20 1.0E20 0.0 0.0
*
* idcb icbn icb1 icb2 icb3
* -124 14 532 533 0
* cbgain cbxmin cbmax cbcon1 cbcon2
* 1.0 -1.0E20 1.0E20 0.0 0.0
*
* idcb icbn icb1 icb2 icb3
* -130 39 -120 105 0
* cbgain cbxmin cbmax cbcon1 cbcon2
* 1.0 -1.0E20 1.0E20 0.0 0.0

```



```

*n: Turbine Power
*
*      idcb      icbn      icb1      icb2      icb3
*      -141      39      -150      -116      0
*      cbgain      cbxmin      cbmax      cbcon1      cbcon2
*      1.0      -1.0E20      1.0E20      0.0      0.0
*
*
*      idcb      icbn      icb1      icb2      icb3
*      -150      9      0      0      0
*      cbgain      cbxmin      cbmax      cbcon1      cbcon2
*      1.0      -1.0E20      1.0E20      0.4      0.0
*
*
*      idcb      icbn      icb1      icb2      icb3
*      -209      14      523      524      0
*      cbgain      cbxmin      cbmax      cbcon1      cbcon2
*      1.0      -1.0E20      1.0E20      0.0      0.0
*
*n: pumping power loop 3
*
*      idcb      icbn      icb1      icb2      icb3
*      -210      14      -211      -213      0
*      cbgain      cbxmin      cbmax      cbcon1      cbcon2
*      1.0      -1.0E20      1.0E20      0.0      0.0
*
*
*      idcb      icbn      icb1      icb2      icb3
*      -211      104      3      0      0
*      cbgain      cbxmin      cbmax      cbcon1      cbcon2
*      1.0      -1.0E20      1.0E20      0.0      0.0
*
*      ids      -212      -209      -215e
*
*n: delta P
*
*      idcb      icbn      icb1      icb2      icb3
*      -212      54      526      525      0
*      cbgain      cbxmin      cbmax      cbcon1      cbcon2
*      1.0      -1.0E20      1.0E20      0.0      0.0
*
*
*      idcb      icbn      icb1      icb2      icb3
*      -213      39      527      -214      0
*      cbgain      cbxmin      cbmax      cbcon1      cbcon2
*      1.0      -1.0E20      1.0E20      0.0      0.0
*
*
*      idcb      icbn      icb1      icb2      icb3
*      -214      9      0      0      0
*      cbgain      cbxmin      cbmax      cbcon1      cbcon2
*      1.0      -1.0E20      1.0E20      9.81      0.0
*
*
*      idcb      icbn      icb1      icb2      icb3
*      -215      9      0      0      0
*      cbgain      cbxmin      cbmax      cbcon1      cbcon2
*      1.0      -1.0E20      1.0E20      9810.0      0.0
*
*n: delta P
*
*      idcb      icbn      icb1      icb2      icb3
*      -219      54      539      538      0
*      cbgain      cbxmin      cbmax      cbcon1      cbcon2
*      1.0      -1.0E20      1.0E20      0.0      0.0
*
*
*      idcb      icbn      icb1      icb2      icb3
*      -220      39      -219      -222      0
*      cbgain      cbxmin      cbmax      cbcon1      cbcon2
*      1.0      -1.0E20      1.0E20      0.0      0.0
*
*
*      idcb      icbn      icb1      icb2      icb3
*      -222      14      536      537      0
*      cbgain      cbxmin      cbmax      cbcon1      cbcon2
*      1.0      -1.0E20      1.0E20      0.0      0.0
*
*****
* Finished Control System Section of Model *
*****
***** type      num      userid      component name
pipe      11      0      unnamed
*      ncells      nodes      jun1      jun2      epsw
*      1      0      1634      0      0.0
*      nsides      3
*      nclk      junlk      ncмпто      nclkto      nlevto
*      1      1524      0      0      0
*      theta      ientrn
*      90.0      0
*      nclk      junlk      ncмпто      nclkto      nlevto
*      1      1534      0      0      0
*      theta      ientrn
*      90.0      0
*      nclk      junlk      ncмпто      nclkto      nlevto
*      1      1544      0      0      0
*      theta      ientrn
*****
*      dx      1.0
*      vol      0.25376215 0.25376215e 0.25376215e
*      fa      0.25376215 0.25376215 0.25376215e
*      kfacc      0.0 0.0 0.0 0.0e
*      grav      0.0 0.0 0.0 0.0e
*      hd      0.56841886 0.56841886 0.56841886e
*      nff      1 1 1e
*      alp      1.0 1.0e
*      vl      0.0 0.0 0.0e
*      vv      0.0 0.0 0.0e
*      tl      615.305 615.305e
*      tv      615.305 615.305e
*      p      1.0E7 1.0E7e
*      pa      1.0E7 1.0E7e
*****
***** type      num      userid      component name
pipe      50      0      unnamed
*      ncells      nodes      jun1      jun2      epsw
*      2      0      1534      1664      0.0
*      nsides      0
*      ichf      iconc      pipetype      ipow      npipes
*      1      0      0      0      1
*      radin      th      houtl      houtv      toutl
*      0.0 0.0 0.0 0.0 0.0
*      toutv      pwin      pwoff      rpwm      pwscl
*      0.0 0.0 0.0 0.0 0.0
*      dx      1.0 1.0e
*      vol      0.25376215 0.25376215e 0.25376215e
*      fa      0.25376215 0.25376215 0.25376215e
*      kfacc      0.0 0.0 0.0 0.0e
*      grav      0.0 0.0 0.0 0.0e
*      hd      0.56841886 0.56841886 0.56841886e
*      nff      1 1 1e
*      alp      1.0 1.0e
*      vl      0.0 0.0 0.0e
*      vv      0.0 0.0 0.0e
*      tl      615.305 615.305e
*      tv      615.305 615.305e
*      p      1.0E7 1.0E7e
*      pa      1.0E7 1.0E7e
*****

```

```

* tl * 615.305 615.305e
* tv * 615.305 615.305e
* p * 1.0E7 1.0E7e
* pa * 1.0E7 1.0E7e
*
***** type num userid component name
pipe 60 0 unnamed
* ncells 2 nodes jun1 jun2 epsw
* 2 0 1544 1694 0.0
* nsides 0
* ichf iconc pipetype ipow npipes
* 1 0 0 0 1
* radin th houtl houtv toutl
* 0.0 0.0 0.0 0.0 0.0
* toutv pwin pwoff rpwmw pwscl
* 0.0 0.0 0.0 0.0 0.0
* dx * 1.0 1.0e
* vol * 0.25376215 0.25376215e
* fa * 0.25376215 0.25376215 0.25376215e
* kfacc * 0.0 0.0 0.0e
* grav * 0.0 0.0 0.0e
* hd * 0.56841886 0.56841886 0.56841886e
* nff * 1 1 1e
* alp * 1.0 1.0e
* vl * 0.0 0.0 0.0e
* vv * 0.0 0.0 0.0e
* tl * 615.305 615.305e
* tv * 615.305 615.305e
* p * 1.0E7 1.0E7e
* pa * 1.0E7 1.0E7e
*
***** type num userid component name
pump 70 0 RCP
* ncells 2 nodes jun1 jun2 epsw
* 2 0 1644 1654 0.0
* nsides 0
* ichf iconc ipmpty irp ipm
* 1 0 1 1 1
* ipmtr ipmsv npmptb npmsv npmprf
* 0 1 8 0 0
* radin th houtl houtv toutl
* 0.0 0.0 0.0 0.0 0.0
* toutv effmi eta
* 0.0 3455.0 85.0
* tfr0 tfr1 tfr2 tfr3 tfrb
* 0.0 0.0 0.0 0.0 0.0
* tfr10 tfr11 tfr12 tfr13
* 0.0 0.0 0.0 0.0
* rhead rtork rflow rrho romega
* 831.0 3.5949E4 5.651 745.0 124.5
* omegan omgoff romgmx omgscl nmpspd
* 500.0 0.0 500.0 1.0 0
* option 4
* dx * 2.0 2.0e
* vol * 0.5075243 0.5075243e
* fa * 0.25376215 0.25376215 0.25376215e
* kfacc * 0.0 0.0 0.0e
* grav * 0.0 0.0 0.0e
* hd * 0.56841886 0.56841886 0.56841886e
* nff * 1 1 1e
* alp * 1.0 1.0e
* vl * 0.0 0.0 0.0e
* vv * 0.0 0.0 0.0e
* tl * 618.007 618.007e
* tv * 618.007 618.007e
* p * 1.0E7 1.0E7e
* pa * 1.0E7 1.0E7e
* pmptb * 0.0 446.0 1.005 446.0s
* pmptb * 1.0E4 446.0 1.00001E4 446.0s
* pmptb * 1.001E4 446.0 1.002E4 446.0s
* pmptb * 1.003E4 446.0 1.02E4 446.0s
*
***** type num userid component name
pipe 80 0 unnamed
* ncells 3 nodes jun1 jun2 epsw
* 3 0 1624 1614 0.0
* nsides 0
* ichf iconc pipetype ipow npipes
* 1 0 0 0 1
* radin th houtl houtv toutl
* 0.0 0.0 0.0 0.0 0.0
* toutv pwin pwoff rpwmw pwscl
* 0.0 0.0 0.0 0.0 0.0
* dx * 1.0 1.0 1.0e
* vol * 0.76128644 0.76128644 0.76128644e
* fa * 0.76128644 0.76128644 9.7036963e
* kfacc * 0.0 0.0 0.0e
* grav * -1.0 0.0 0.0
* hd * 0.98453035 0.98453035 0.98453035 0.041759401e
* nff * 1 1 1 -1e
* alp * 1.0 1.0 1.0e
* vl * 7.7 0.0 0.0 -7.7e
* vv * 7.7 0.0 0.0 -7.7e
* tl * 615.305 615.305 615.305e
* tv * 615.305 615.305 615.305e
* p * 1.0E7 1.0E7 1.0E7e
* pa * 1.0E7 1.0E7 1.0E7e
*
***** type num userid component name
pump 170 0 RCP
* ncells 2 nodes jun1 jun2 epsw
* 2 0 1664 1674 0.0
* nsides 0
* ichf iconc ipmpty irp ipm
* 1 0 1 1 1
* ipmtr ipmsv npmptb npmsv npmprf
* 0 1 8 0 0
* radin th houtl houtv toutl
* 0.0 0.0 0.0 0.0 0.0
* toutv effmi eta
* 0.0 3455.0 85.0
* tfr0 tfr1 tfr2 tfr3 tfrb
* 0.0 0.0 0.0 0.0 0.0
* tfr10 tfr11 tfr12 tfr13
* 0.0 0.0 0.0 0.0
* rhead rtork rflow rrho romega
* 831.0 3.5949E4 5.651 745.0 124.5
* omegan omgoff romgmx omgscl nmpspd
* 500.0 0.0 500.0 1.0 0
* option 4
* dx * 2.0 2.0e
* vol * 0.5075243 0.5075243e
* fa * 0.25376215 0.25376215 0.25376215e
* kfacc * 0.0 0.0 0.0e
* grav * 0.0 0.0 0.0e
* hd * 0.56841886 0.56841886 0.56841886e
* nff * 1 1 1e
* alp * 1.0 1.0e
* vl * 0.0 0.0 0.0e
* vv * 0.0 0.0 0.0e
* tl * 618.007 618.007e
* tv * 618.007 618.007e
* p * 1.0E7 1.0E7e
* pa * 1.0E7 1.0E7e
* pmptb * 0.0 446.0 1.005 446.0s
* pmptb * 1.0E4 446.0 1.00001E4 446.0s
* pmptb * 1.001E4 446.0 1.002E4 446.0s
* pmptb * 1.003E4 446.0 1.02E4 446.0s
*
***** type num userid component name
pipe 180 0 unnamed
* ncells 39 nodes jun1 jun2 epsw
* 39 0 1654 11 2.0E-7
* nsides 0
* ichf iconc pipetype ipow npipes
* 1 0 0 0 1
* radin th houtl houtv toutl
* 0.0 0.0 0.0 0.0 0.0
* toutv pwin pwoff rpwmw pwscl
* 0.0 0.0 0.0 0.0 0.0
* dx * 1.0 1.0 1.0 1.0s
* dx * 1.0 1.0 1.0 1.0s
* dx * 1.0 1.0 1.0 1.0s
* dx * 1.0 1.0 1.0 1.0s
* dx * 1.0 1.0 1.0 1.0s
* dx * 1.0 1.0 1.0 1.0s
* dx * 1.0 1.0 1.0 1.0s
* dx * 1.0 1.0 1.0 1.0s
* dx * 1.0 1.0 1.0 1.0s
* dx * 1.0 1.0 1.0 1.0s
* dx * 1.0 1.0 1.0 1.0s
* dx * 1.0 1.0 1.0 1.0s
* dx * 1.0 1.0 1.0e
* vol * 0.25376215 0.25376215 0.25376215 0.25376215s
* vol * 0.25376215 0.25376215 0.25376215 0.25376215s
* vol * 0.25376215 0.25376215 0.25376215 0.25376215s
* vol * 0.25376215 0.25376215 0.25376215 0.25376215s
* vol * 0.25376215 0.25376215 0.25376215 0.25376215s
* vol * 0.25376215 0.25376215 0.25376215 0.25376215s
* vol * 0.25376215 0.25376215 0.25376215 0.25376215s
* vol * 0.25376215 0.25376215 0.25376215 0.25376215s
* vol * 0.25376215 0.25376215 0.25376215 0.25376215s
* vol * 0.25376215 0.25376215 0.25376215 0.25376215s
* vol * 0.25376215 0.25376215 0.25376215 0.25376215s
* vol * 0.25376215 0.25376215 0.25376215 0.25376215s
* vol * 0.25376215 0.25376215 0.25376215 0.25376215s
* vol * 0.25376215 0.25376215 0.25376215 0.25376215s
* vol * 0.25376215 0.25376215 0.25376215 0.25376215s
* vol * 0.25376215 0.25376215 0.25376215 0.25376215s
* vol * 0.25376215 0.25376215 0.25376215 0.25376215s
* vol * 0.25376215 0.25376215 0.25376215 0.25376215s
* vol * 0.25376215 0.25376215 0.25376215 0.25376215s
* vol * 0.25376215 0.25376215 0.25376215 0.25376215s
* vol * 0.25376215 0.25376215 0.25376215 0.25376215s
* vol * 0.25376215 0.25376215 0.25376215 0.25376215s
* vol * 0.25376215 0.25376215 0.25376215 0.25376215s
* vol * 0.25376215 0.25376215 0.25376215 0.25376215s
* vol * 0.25376215 0.25376215 0.25376215 0.25376215s
* kfacc * 0.0 0.0 0.0 0.0s
* kfacc * 0.0 0.0 0.0 0.0s
* kfacc * 0.0 0.0 0.0 0.0s
* kfacc * 0.0 2.08914E-3 0.0 0.0s
* kfacc * 0.0 0.0 0.0 0.0s
* kfacc * 0.0 0.0 0.0 0.0s
* kfacc * 0.0 2.08914E-3 0.0 0.0s
* kfacc * 0.0 0.0 0.0 0.0s
* kfacc * 0.0 0.0 0.0 0.0s
* kfacc * 0.0 0.0 0.0 0.0s
* kfacc * 0.0 0.0 0.0 0.0s

```



































# Appendix C |

## Input File For TRACE Carbon Dioxide Cooled Model

### C.1 Introduction

The TRACE input file for the carbon dioxide cooled model is provided in this appendix. The input file is presented in two columns due to the length of the input file. The file reads from the top left to bottom left to top right to bottom right of each page.

### C.2 TRACE Carbon Dioxide Cooled Model Input File

```

free format
*m: SNAP:Symbolic Nuclear Analysis Package, Version 2.5.7, July 14, 2017
*m: PLUGIN:TRACE Version 3.8.4
*m: CODE:TRACE V 5.0 Patch 5
*m: DATE:3/20/18
*
*****
* main data *
*****
*          numtcr          ieos          inopt          nmat          id2o
*          1              0              1              2              0
*
*
*****
* namelist data *
*****
*
&inopts
dtstrt=-1.0,
graphlevel="full",
ikfac=1,
noair=0,
usesjce3,
npower=1,
nhtstr=2,
fluids='H2O','XPTB'
&end
*
*****

* Model Flags *
*****
*          dstep          timet
*          0              0.0
*          stdyst          transi          ncomp          njun          ipak
*          0              1              20              18              1
*          epso          epsa
*          1.0E-4          1.0E-4
*          oitmax          sitmax          isolut          ncontr          nccfl
*          10              10              0              0              0
*          ntsv          ntcb          ntcf          ntrp          ntcp
*          40              45              18              0              0
*
*****
* component-number data *
*****
*
* Component input order (IORDER)
*--- type ---- num ----- name -----+ jun1 jun2 jun3
* PIPE * 11 s * + 1634 0
* FILL * 20 s * + 10
* BREAK * 30 s * + 20
* PIPE * 40 s * + 1524 1644
* PIPE * 50 s * + 1534 1664
* PIPE * 60 s * + 1544 1694
* PUMP * 70 s * RCP + 1644 1654
* PIPE * 80 s * + 1624 1614
* PUMP * 170 s * RCP + 1664 1674
* PIPE * 180 s * + 1654 11
* PIPE * 200 s * + 1674 50
* PIPE * 210 s * + 1684 60

```

```

* PUMP * 270 s * RCP + 1694 1684 * idsv isvn ilcn icn1 icn2
* PIPE * 1010 s * + 10 20 * 427 74 80 2 0
* PIPE * 1050 s * + 1614 70 *
* PIPE * 1060 s * + 1624 1634 * idsv isvn ilcn icn1 icn2
* PIPE * 1090 s * + 0 70 * 523 29 270 1 0
* POWER * 10 s * + *
* HTSTR * 90 s * + * idsv isvn ilcn icn1 icn2
* HTSTR * 1040 e * + * 524 74 80 2 0
*
* material properties *
*
* math* 50 51 e *
* ptbln* -3 -2 e *
* User Defined Material : 50 *
*
*n: beryllium *
* rhonum sphtnum condnum emisnum *
* 0 1 1 0 *
* prptb temp rho emis *
* prptb* 300.0 1850.0 0.18s *
* prptb* 800.0 1850.0 0.18s *
* prptb* 1500.0 1850.0 0.18e *
*
* specific heat fit *
* toffset tlower tupper a0 a1 *
* 0.0 300.0 1500.0 606.91 5.3382 *
* a2 a3 a4 a5 *
* -4.1726E-3 1.2723E-6 0.0 0.0 *
* thermal conductivity functional fit *
* toffset tlower tupper a0 a1 *
* 0.0 300.0 1500.0 430.35 -1.1674 *
* a2 a3 a4 a5 *
* 1.6044E-3 -1.0097E-6 2.3642E-10 0.0 *
* User Defined Material : 51 *
*
*n: tungsten *
* rhonum sphtnum condnum emisnum *
* 0 1 1 0 *
* prptb temp rho emis *
* prptb* 253.0 1.93E4 0.04s *
* prptb* 2500.0 1.93E4 0.04e *
*
* specific heat fit *
* toffset tlower tupper a0 a1 *
* 0.0 293.0 2500.0 116.37 0.071119 *
* a2 a3 a4 a5 *
* -6.5828E-5 3.2396E-8 -5.4523E-12 0.0 *
* thermal conductivity functional fit *
* toffset tlower tupper a0 a1 *
* 0.0 293.0 2500.0 240.51 -0.2899 *
* a2 a3 a4 a5 *
* 2.5403E-4 -1.0263E-7 1.5238E-11 0.0 *
*
*
* Starting Signal Variable Section of Model *
*
* idsv isvn ilcn icn1 icn2 *
* 1 0 0 0 0 *
* idsv isvn ilcn icn1 icn2 *
* 105 69 1010 167 0 *
* idsv isvn ilcn icn1 icn2 *
* 106 105 1010 168 0 *
* idsv isvn ilcn icn1 icn2 *
* 109 105 20 1 0 *
* idsv isvn ilcn icn1 icn2 *
* 323 29 70 1 0 *
* idsv isvn ilcn icn1 icn2 *
* 324 74 80 2 0 *
* idsv isvn ilcn icn1 icn2 *
* 325 21 80 2 0 *
* idsv isvn ilcn icn1 icn2 *
* 326 21 180 1 0 *
* idsv isvn ilcn icn1 icn2 *
* 327 74 80 2 0 *
* idsv isvn ilcn icn1 icn2 *
* 423 29 170 1 0 *
* idsv isvn ilcn icn1 icn2 *
* 424 74 80 2 0 *
* idsv isvn ilcn icn1 icn2 *
* 425 21 80 2 0 *
* idsv isvn ilcn icn1 icn2 *
* 426 21 200 7 0
*
*****
* Finished Signal Variable Section of Model *
*****
*
***** Control Blocks *****
*n: Gas volume fraction BC
* idcb icbn icb1 icb2 icb3
* -1 9 0 0 0
* cbgain cbxmin cbmax cbcon1 cbcon2 cbcon3
* 1.0 -1.0E20 1.0E20 1.0 0.0
*
*n: Entrance vapor mass flow controller
*

```

```

*      idcb      icbn      icb1      icb2      icb3      *      idcb      icbn      icb1      icb2      icb3
*      -2        9        0        0        0      *      -17       57      -220     -122     -22
*      cbgain    cbxmin    cbmax    cbcon1    cbcon2    *      cbgain    cbxmin    cbmax    cbcon1    cbcon2
*      1.0      -1.0E20    1.0E20    600.0    0.0      *      1.0      -1.0E20    1.0E20    0.0      0.0
*
*n: NCG PP BC
*
*      idcb      icbn      icb1      icb2      icb3      *      idcb      icbn      icb1      icb2      icb3
*      -3        9        0        0        0      *      -21       54      531      530      0
*      cbgain    cbxmin    cbmax    cbcon1    cbcon2    *      cbgain    cbxmin    cbmax    cbcon1    cbcon2
*      1.0      -1.0E20    1.0E20    1.5E7    0.0      *      1.0      -1.0E20    1.0E20    0.0      0.0
*
*n: Pressure BC
*
*      idcb      icbn      icb1      icb2      icb3      *      idcb      icbn      icb1      icb2      icb3
*      -4        9        0        0        0      *      -22       39      -21      -24      0
*      cbgain    cbxmin    cbmax    cbcon1    cbcon2    *      cbgain    cbxmin    cbmax    cbcon1    cbcon2
*      1.0      -1.0E20    1.0E20    1.5E7    0.0      *      1.0      -1.0E20    1.0E20    0.0      0.0
*
*n: Entrance temperature BC
*
*      idcb      icbn      icb1      icb2      icb3      *      idcb      icbn      icb1      icb2      icb3
*      -5        9        0        0        0      *      -24       14      528      529      0
*      cbgain    cbxmin    cbmax    cbcon1    cbcon2    *      cbgain    cbxmin    cbmax    cbcon1    cbcon2
*      1.0      -1.0E20    1.0E20    600.0    0.0      *      1.0      -1.0E20    1.0E20    0.0      0.0
*
*n: Exit Temperature BC
*
*      idcb      icbn      icb1      icb2      icb3      *      idcb      icbn      icb1      icb2      icb3
*      -6        9        0        0        0      *      -109      14      423      424      0
*      cbgain    cbxmin    cbmax    cbcon1    cbcon2    *      cbgain    cbxmin    cbmax    cbcon1    cbcon2
*      1.0      -1.0E20    1.0E20    800.0    0.0      *      1.0      -1.0E20    1.0E20    0.0      0.0
*
*n: secondary mass flow
*
*      idcb      icbn      icb1      icb2      icb3      *      idcb      icbn      icb1      icb2      icb3
*      -7        9        0        0        0      *      -110      14      -111     -113     0
*      cbgain    cbxmin    cbmax    cbcon1    cbcon2    *      cbgain    cbxmin    cbmax    cbcon1    cbcon2
*      1.0      -1.0E20    1.0E20    250.0    0.0      *      1.0      -1.0E20    1.0E20    0.0      0.0
*
*n: net power
*
*      idcb      icbn      icb1      icb2      icb3      *      idcb      icbn      icb1      icb2      icb3
*      -8        54      -141     -17      0      *      -111      104      3        0        0
*      cbgain    cbxmin    cbmax    cbcon1    cbcon2    *      cbgain    cbxmin    cbmax    cbcon1    cbcon2
*      1.0      -1.0E20    1.0E20    0.0      0.0      *      1.0      -1.0E20    1.0E20    0.0      0.0
*
*      ids *      -112     -109     -115e
*
*n: delta P
*
*      idcb      icbn      icb1      icb2      icb3      *      idcb      icbn      icb1      icb2      icb3
*      -9        14      323      324      0      *      -112      54      426      425      0
*      cbgain    cbxmin    cbmax    cbcon1    cbcon2    *      cbgain    cbxmin    cbmax    cbcon1    cbcon2
*      1.0      -1.0E20    1.0E20    0.0      0.0      *      1.0      -1.0E20    1.0E20    0.0      0.0
*
*n: pumping power loop 1
*
*      idcb      icbn      icb1      icb2      icb3      *      idcb      icbn      icb1      icb2      icb3
*      -10       14      -11      -13      0      *      -113      39      427     -114     0
*      cbgain    cbxmin    cbmax    cbcon1    cbcon2    *      cbgain    cbxmin    cbmax    cbcon1    cbcon2
*      1.0      -1.0E20    1.0E20    0.0      0.0      *      1.0      -1.0E20    1.0E20    0.0      0.0
*
*      idcb      icbn      icb1      icb2      icb3      *      idcb      icbn      icb1      icb2      icb3
*      -11       104      3        0        0      *      -114      9        0        0        0
*      cbgain    cbxmin    cbmax    cbcon1    cbcon2    *      cbgain    cbxmin    cbmax    cbcon1    cbcon2
*      1.0      -1.0E20    1.0E20    0.0      0.0      *      1.0      -1.0E20    1.0E20    9.81     0.0
*
*      ids *      -12      -9      -15e
*
*n: delta P
*
*      idcb      icbn      icb1      icb2      icb3      *      idcb      icbn      icb1      icb2      icb3
*      -12       54      326      325      0      *      -115      9        0        0        0
*      cbgain    cbxmin    cbmax    cbcon1    cbcon2    *      cbgain    cbxmin    cbmax    cbcon1    cbcon2
*      1.0      -1.0E20    1.0E20    0.0      0.0      *      1.0      -1.0E20    1.0E20    9810.0   0.0
*
*      idcb      icbn      icb1      icb2      icb3      *      idcb      icbn      icb1      icb2      icb3
*      -13       39      327     -14      0      *      -116      56     -130      0        0
*      cbgain    cbxmin    cbmax    cbcon1    cbcon2    *      cbgain    cbxmin    cbmax    cbcon1    cbcon2
*      1.0      -1.0E20    1.0E20    0.0      0.0      *      1.0      -1.0E20    1.0E20    0.0      0.0
*
*n: delta P
*
*      idcb      icbn      icb1      icb2      icb3      *      idcb      icbn      icb1      icb2      icb3
*      -14        9        0        0        0      *      -120      54     106     109      0
*      cbgain    cbxmin    cbmax    cbcon1    cbcon2    *      cbgain    cbxmin    cbmax    cbcon1    cbcon2
*      1.0      -1.0E20    1.0E20    9.81     0.0      *      1.0      -1.0E20    1.0E20    0.0      0.0
*
*      idcb      icbn      icb1      icb2      icb3      *      idcb      icbn      icb1      icb2      icb3
*      -15        9        0        0        0      *      -121      54     535     534      0
*      cbgain    cbxmin    cbmax    cbcon1    cbcon2    *      cbgain    cbxmin    cbmax    cbcon1    cbcon2
*      1.0      -1.0E20    1.0E20    9810.0   0.0      *      1.0      -1.0E20    1.0E20    0.0      0.0
*
*n: total pumping power
*
*      idcb      icbn      icb1      icb2      icb3      *      idcb      icbn      icb1      icb2      icb3
*      -16        57     -10     -110     -210    *      -122      39     -121     -124      0
*      cbgain    cbxmin    cbmax    cbcon1    cbcon2    *      cbgain    cbxmin    cbmax    cbcon1    cbcon2
*      1.0      -1.0E20    1.0E20    0.0      0.0      *      1.0      -1.0E20    1.0E20    0.0      0.0
*
*n: total pumping power
*

```

```

*      idcb      icbn      icb1      icb2      icb3      *      nclk      junlk      ncмпто      nclkto      nlevto
*      -130      39        -120      105      0        *      1          1534      0          0          0
*      cbgain     cbxmin     cbmax     cbcon1     cbcon2     *      theta      ientrn
*      1.0       -1.0E20      1.0E20      0.0        0.0        *      90.0      0
*
*n: Turbine Power
*
*      idcb      icbn      icb1      icb2      icb3      *      nclk      junlk      ncмпто      nclkto      nlevto
*      -141      39        -150      -116      0        *      1          1544      0          0          0
*      cbgain     cbxmin     cbmax     cbcon1     cbcon2     *      theta      ientrn
*      1.0       -1.0E20      1.0E20      0.0        0.0        *      90.0      0
*
*      idcb      icbn      icb1      icb2      icb3      *      nclk      junlk      ncмпто      nclkto      nlevto
*      -150      9         0         0         0        *      1          1544      0          0          0
*      cbgain     cbxmin     cbmax     cbcon1     cbcon2     *      theta      ientrn
*      1.0       -1.0E20      1.0E20      0.0        0.0        *      90.0      0
*
*      idcb      icbn      icb1      icb2      icb3      *      nclk      junlk      ncмпто      nclkto      nlevto
*      -209      14        523      524      0        *      1          1544      0          0          0
*      cbgain     cbxmin     cbmax     cbcon1     cbcon2     *      theta      ientrn
*      1.0       -1.0E20      1.0E20      0.0        0.0        *      90.0      0
*
*      dx * 1.0e
*      vol * 0.76128644e
*      fa * 0.76128644 0.76128644e
*      kfacs * 0.0 0.0e
*      grav * 1.0 1.0e
*      hd * 0.98453035 0.98453035e
*      nff * 1 ie
*      alp * 1.0e
*      vl * -7.7 0.0e
*      vv * -7.7 0.0e
*      tl * 615.305e
*      tv * 615.305e
*      p * 1.3E7e
*      pa * 0.0e
*
***** type num userid component name
fill 20 0 unnamed
* eos phasechange
H20 true
* jun1 ifty ioff
10 10 0
* iftr ifsv nftb nfsv nfrf
0 0 0 0 0
* twtold rfmr concin felv
0.0 0.0 0.0
* dxin volin alpin tlin
0.32014925 0.40937701 0.0 500.0
* pain vrain tvin
5.0E6 0.0 500.0
* ifmlsv ifmvsv iftlsv iftvsv
-7 0 0 0
* ifpsv ifpasv ifcnsv
0 0 0
*
***** type num userid component name
break 30 0 unnamed
* eos phasechange
H20 true
* jun1 ibty isat ioff adjpres
20 0 0 0 0
* dxin volin alpin tin pin
0.32014925 0.40937701 1.0 884.8 5.0E6
* pain concin rbmr poff belv
0.0 0.0 1.0E20 0.0 0.0
*
***** type num userid component name
pipe 40 0 unnamed
* eos phasechange
XPTB true
* ncells nodes jun1 jun2 epsw
2 0 1524 1644 0.0
* nsides
0
* ichf iconc pipetype ipow npipes
1 0 0 0 1
* radin th houtv tout1
0.0 0.0 0.0 0.0
* toutv pwin pwoff rpwmr pwscl
0.0 0.0 0.0 0.0
*
* dx * 1.0 1.0e
* vol * 0.25376215 0.25376215e
* fa * 0.25376215 0.25376215 0.25376215e
* kfacs * 0.0 0.0 0.0e
* grav * 0.0 0.0 0.0e
* hd * 0.56841886 0.56841886 0.56841886e
* nff * 1 1 1e
* alp * 1.0 1.0e
* vl * 0.0 0.0 0.0e
* vv * 0.0 0.0 0.0e
* tl * 615.305 615.305e
* tv * 615.305 615.305e
* p * 1.3E7 1.3E7e
* pa * 0.0 0.0e
*
***** type num userid component name
pipe 11 0 unnamed
* eos phasechange
XPTB true
* ncells nodes jun1 jun2 epsw
1 0 1634 0 0.0
* nsides
3
* nclk junlk ncмпто nclkto nlevto
1 1524 0 0 0
* theta ientrn
90.0 0
*
***** type num userid component name
pipe 50 0 unnamed
* eos phasechange
XPTB true
* ncells nodes jun1 jun2 epsw
2 0 1534 1664 0.0
* nsides
0
* ichf iconc pipetype ipow npipes
0 0 0 0 0

```

```

*      1      0      0      0      1      *      ncells      nodes      jun1      jun2      epsw
*      radin      th      houtl      houtv      toutl      *      nsides
*      toutv      pwin      pwoff      rpwmx      pwscl
* dx *      1.0      1.0e
* vol *      0.25376215      0.25376215e
* fa *      0.25376215      0.25376215e      0.25376215e
* kfac *      0.0      0.0      0.0e
* grav *      0.0      0.0      0.0e
* hd *      0.56841886      0.56841886e      0.56841886e
* nff *      1      1      1e
* alp *      1.0      1.0e
* vl *      0.0      0.0      0.0e
* vv *      0.0      0.0      0.0e
* tl *      615.305      615.305e
* tv *      615.305      615.305e
* p *      1.3E7      1.3E7e
* pa *      0.0      0.0e
*
***** type      num      userid      component name
pipe      60      0      unnamed
*      eos      phasechange
*      XPTB      true
*      ncells      nodes      jun1      jun2      epsw
*      nsides
*      0
*      ichf      iconc      pipetype      ipow      npipes
*      1      0      0      0      1
*      radin      th      houtl      houtv      toutl
*      0.0      0.0      0.0      0.0      0.0
*      toutv      pwin      pwoff      rpwmx      pwscl
*      0.0      0.0      0.0      0.0      0.0
* dx *      1.0      1.0e
* vol *      0.25376215      0.25376215e
* fa *      0.25376215      0.25376215e      0.25376215e
* kfac *      0.0      0.0      0.0e
* grav *      0.0      0.0      0.0e
* hd *      0.56841886      0.56841886e      0.56841886e
* nff *      1      1      1e
* alp *      1.0      1.0e
* vl *      0.0      0.0      0.0e
* vv *      0.0      0.0      0.0e
* tl *      615.305      615.305e
* tv *      615.305      615.305e
* p *      1.3E7      1.3E7e
* pa *      0.0      0.0e
*
***** type      num      userid      component name
pump      70      0      RCP
*      eos      phasechange
*      XPTB      true
*      ncells      nodes      jun1      jun2      epsw
*      nsides
*      0
*      ichf      iconc      ipmpty      irp      ipm
*      1      0      1      1      1
*      imptr      impsv      npmptb      npmsv      npmprf
*      0      1      8      0      0
*      radin      th      houtl      houtv      toutl
*      0.0      0.0      0.0      0.0      0.0
*      toutv      effmi      eta
*      0.0      3455.0      85.0
*      tfr0      tfr1      tfr2      tfr3      tfrb
*      0.0      0.0      0.0      0.0      0.0
*      tfr10      tfr11      tfr12      tfr13
*      0.0      0.0      0.0      0.0
*      rhead      rtork      rflow      rrho      romega
*      831.0      3.5949E4      5.651      745.0      124.5
*      omegan      omgoff      romgm      omgscl      npmpsd
*      40.0      0.0      200.0      1.0      0
*      option
*      4
* dx *      2.0      2.0e
* vol *      0.5075243      0.5075243e
* fa *      0.25376215      0.25376215e      0.25376215e
* kfac *      0.0      0.0      0.0e
* grav *      0.0      0.0      0.0e
* hd *      0.56841886      0.56841886e      0.56841886e
* nff *      1      1      1e
* alp *      1.0      1.0e
* vl *      0.0      0.0      0.0e
* vv *      0.0      0.0      0.0e
* tl *      618.007      618.007e
* tv *      618.007      618.007e
* p *      1.3E7      1.3E7e
* pa *      0.0      0.0e
* pmptb *      0.0      150.0      1.005      150.0s
* pmptb *      1.0E4      150.0      1.00001E4      150.0s
* pmptb *      1.001E4      150.0      1.002E4      150.0s
* pmptb *      1.003E4      150.0      1.02E4      150.0s
*
***** type      num      userid      component name
pipe      80      0      unnamed
*      eos      phasechange
*      XPTB      true

```

















```

* pa * 0.0 0.0 0.0 0.0s * hcomon1 * 180 26 0 0e
* pa * 0.0 0.0 0.0 0.0s * hcomon1 * 200 14 0 0e
* pa * 0.0 0.0 0.0 0.0s * hcomon1 * 200 15 0 0e
* pa * 0.0 0.0 0.0 0.0s * hcomon1 * 200 16 0 0e
* pa * 0.0 0.0 0.0 0.0s * hcomon1 * 200 17 0 0e
* pa * 0.0 0.0 0.0 0.0s * hcomon1 * 200 18 0 0e
* pa * 0.0 0.0 0.0 0.0s * hcomon1 * 200 19 0 0e
* pa * 0.0 0.0 0.0 0.0e * hcomon1 * 200 20 0 0e
* * * hcomon1 * 200 21 0 0e
* * * hcomon1 * 200 22 0 0e
***** type num userid component name
pipe eos 1090 0 unnamed
* phasechange true
* XPTB true
* ncells nodes jun1 jun2 epsw * hcomon1 * 200 23 0 0e
* 1 0 0 70 0.0 * hcomon1 * 200 24 0 0e
* nsides 3 * hcomon1 * 200 25 0 0e
* nclk junk ncempt nclkto nlevo * hcomon1 * 200 26 0 0e
* 1 11 0 0 * hcomon1 * 200 27 0 0e
* theta ientrn * hcomon1 * 210 14 0 0e
* 90.0 0 * hcomon1 * 210 15 0 0e
* nclk junk ncempt nclkto nlevo * hcomon1 * 210 16 0 0e
* 1 50 0 0 * hcomon1 * 210 17 0 0e
* theta ientrn * hcomon1 * 210 18 0 0e
* 90.0 0 * hcomon1 * 210 19 0 0e
* nclk junk ncempt nclkto nlevo * hcomon1 * 210 20 0 0e
* 1 60 0 0 * hcomon1 * 210 21 0 0e
* theta ientrn * hcomon1 * 210 22 0 0e
* 90.0 0 * hcomon1 * 210 23 0 0e
* ichf iconc pipetype ipow npipes * hcomon1 * 210 24 0 0e
* 1 0 0 0 1 * hcomon1 * 210 25 0 0e
* radin th houtv toutl * hcomon1 * 210 26 0 0e
* 0.0 0.0 0.0 0.0 * qflxbco2 * 0.0e
* toutv pwin pwoff rpumx pwscl * qflxbco2 * 0.0e
* 0.0 0.0 0.0 0.0 * qflxbco2 * 0.0e
* dx * 1.0e * qflxbco2 * 0.0e
* vol * 0.76128644e * qflxbco2 * 0.0e
* fa * 0.76128644 9.7036963e * qflxbco2 * 0.0e
* kfacc * 0.0 0.0e * qflxbco2 * 0.0e
* grav * -1.0 -1.0e * qflxbco2 * 0.0e
* hd * 0.98453035 0.041759401e * qflxbco2 * 0.0e
* nff * 1 -1e * qflxbco2 * 0.0e
* alp * 1.0e * qflxbco2 * 0.0e
* vl * 0.0 7.7e * qflxbco2 * 0.0e
* vv * 0.0 7.7e * qflxbco2 * 0.0e
* tl * 615.305e * qflxbco2 * 0.0e
* tv * 615.305e * qflxbco2 * 0.0e
* p * 1.3E7e * qflxbco2 * 0.0e
* pa * 0.0e * qflxbco2 * 0.0e
* * * qflxbco2 * 0.0e
* * * qflxbco2 * 0.0e
* * * qflxbco2 * 0.0e
*****
* Starting Heat Structure Section of Model *
*****
***** type num userid component name
htstr 90 1 unnamed
* nzhstr grids hscyl ichf * qflxbco2 * 0.0e
* 39 0 1 1 * qflxbco2 * 0.0e
* nofuelrod plane liqlev iaxcmd * qflxbco2 * 0.0e
* 1 3 0 0 * qflxbco2 * 0.0e
* nmrx nfcil hdri hdro * qflxbco2 * 0.0e
* 0 0 1 0.0 0.0 * qflxbco2 * 0.0e
* nhot nodes fmon nzmax reflod * qflxbco2 * 0.0e
* 0 10 0 202 0 * qflxbco2 * 0.0e
* dtxht(1) dtxht(2) dzmht hgapo * dhtstrz * 1.0 1.0 1.0 1.0s
* 0.0 0.0 1.0E-3 6300.0 * dhtstrz * 1.0 1.0 1.0 1.0s
* * dhtstrz * 1.0 1.0 1.0 1.0s
* idbcin * 2 2 2 2s * dhtstrz * 1.0 1.0 1.0 1.0s
* idbcin * 2 2 2 2s * dhtstrz * 1.0 1.0 1.0 1.0s
* idbcin * 2 2 2 2s * dhtstrz * 1.0 1.0 1.0 1.0s
* idbcin * 2 2 2 2s * dhtstrz * 1.0 1.0 1.0 1.0s
* idbcin * 2 2 2 2s * dhtstrz * 1.0 1.0 1.0 1.0s
* idbcin * 2 2 2 2s * dhtstrz * 1.0 1.0 1.0 1.0s
* idbcin * 2 2 2 2s * dhtstrz * 1.0 1.0 1.0e
* idbcin * 2 2 2e * rdx * 359.0e
* idbcin * 2 2 2 * rard * 0.015 0.01511111 0.015222222 0.015333333 0.015444444s
* idbcin * 2 2 2 * rard * 0.015555556 0.015666667 0.015777778 0.015888889 0.016e
* idbcin * 0 0 0 0s * matr * 12 12 12 12 s
* idbcin * 0 0 0 0s * matr * 12 12 12 12 s
* idbcin * 0 0 0 0s * matr * 12 e
* idbcin * 0 0 0 0s * nfax * 1 1 1 1s
* idbcin * 0 0 0 0s * nfax * 1 1 1 1s
* idbcin * 0 0 0 0s * nfax * 1 1 1 1s
* idbcin * 0 0 0 0s * nfax * 1 1 1 1s
* idbcin * 0 0 0 0s * nfax * 1 1 1 1s
* idbcin * 0 0 0 0s * nfax * 1 1 1 1s
* idbcin * 0 0 0e * nfax * 1 1 1 1s
* hcomon1 * 180 14 0 0e * nfax * 1 1 1 1s
* hcomon1 * 180 15 0 0e * nfax * 1 1 1 1s
* hcomon1 * 180 16 0 0e * nfax * 1 1 1e
* hcomon1 * 180 17 0 0e * rftn * 500.0 500.0 500.0 500.0s
* hcomon1 * 180 18 0 0e * rftn * 500.0 500.0 500.0 500.0s
* hcomon1 * 180 19 0 0e * rftn * 500.0 500.0 500.0 500.0s
* hcomon1 * 180 20 0 0e * rftn * 500.0 500.0 500.0 500.0s
* hcomon1 * 180 21 0 0e * rftn * 500.0 500.0 500.0 500.0s
* hcomon1 * 180 22 0 0e * rftn * 500.0 500.0 500.0 500.0s
* hcomon1 * 180 23 0 0e * rftn * 500.0 500.0 500.0 500.0s
* hcomon1 * 180 24 0 0e * rftn * 500.0 500.0 500.0 500.0s
* hcomon1 * 180 25 0 0e * rftn * 500.0 500.0 500.0 500.0s

```













```

* rftn *      700.0      700.0      700.0      700.0s
* rftn *      700.0      700.0      700.0      700.0s
* rftn *      700.0      700.0      700.0      700.0s
* rftn *      700.0      700.0      700.0      700.0s
* rftn *      700.0      700.0      700.0      700.0s
* rftn *      700.0      700.0      700.0      700.0s
* rftn *      700.0      700.0      700.0      700.0s
* rftn *      700.0      700.0      700.0      700.0s
* rftn *      700.0      700.0      700.0      700.0s
* rftn *      700.0      700.0      700.0      700.0s
* rftn *      700.0      700.0      700.0      700.0s
* rftn *      700.0      700.0      700.0      700.0s
* rftn *      700.0      700.0      700.0      700.0s
* rftn *      700.0      700.0      700.0      700.0s
* rftn *      700.0      700.0      700.0      700.0s
* rftn *      700.0      700.0      700.0      700.0s
* rftn *      700.0      700.0      700.0      700.0s
* rftn *      700.0      700.0      700.0      700.0s
* rftn *      700.0      700.0      700.0      700.0e
*****
* Finished Heat Structure Section of Model *
*****
*
*
*
*****
* Starting Power Components *
*****
***** type      num      userid      component name
power      10
* numpwr      chanpow      0      unnamed
*
* htnum *      90 e
* irpwtly      ndgx      ndhx      nrts      nhist
6      0      0      100      0
* irpwttr      irpwsv      nrpwtb      nrpwsv      nrpwrif
0      1      4      0      0
* izpwttr      izpwsv      nzpwtb      nzpwsv      nzpwrif
0      1      1      0      0
* ipwrad      ipwdep      promheat      decaheat      wtbypass

0      0      0.0      0.0      0.0
* nzpwz      nzpwi      nfbpwt      nrpwr      nrpwi
0      0      0      1      0
* react      tneut      rpwoff      rrpwmx      rpwscl
0.0      0.0      0.0      1.0E20      1.0
* rpowri      zpwin      zpwoff      rzpwmx
0.0      0.0      0.0      0.0
* extsou      pldr      pdrat      fucrac
0.0      0.0      1.0      1.0
* rdpwr *      1.0      1.0      1.0      1.0      1.0s
* rdpwr *      1.0      1.0      1.0      1.0      1.0s
* cpowr *      1.0e
* zpwtbi*      0.0s
* zpwtbi*      1.0      1.0      1.0      1.0s
* zpwtbi*      1.0      1.0      1.0      1.0s
* zpwtbi*      1.0      1.0      1.0      1.0s
* zpwtbi*      1.0      1.0      1.0      1.0s
* zpwtbi*      1.0      1.0      1.0      1.0s
* zpwtbi*      1.0      1.0      1.0      1.0s
* zpwtbi*      1.0      1.0      1.0      1.0s
* zpwtbi*      1.0      1.0      1.0      1.0e
* rpwtbr*      0.0      0.0s
* rpwtbr*      20.0      0.0s
* rpwtbr*      21.0      6.0E6s
* rpwtbr*      1.0E4      6.0E6s
*****
* Finished Power Components *
*****
*
*
*
end
*
*****
* Timestep Data *
*****
* dtmin      dtmax      tend      rtwfp
1.0E-10      1.0      5000.0      10.0
* edint      gfint      dmpint      sedint
100.0      1.0      100.0      1.0
* endflag
-1.0

```

# Appendix D | Chapter 5 Plots Values

## D.1 Introduction

This appendix provides data points gathered for the plots presented in Chapter 5 of this document. The tables are presented in the order that their corresponding plots appear in chapter 5.

## D.2 Chapter 5 Plot Results

**Table D.1.** Coolant Loop 1 Axial Pressure Profile at Steady State

axial position (m)	$P$ (MPa) water cooled model	$P$ (MPa) helium cooled model	$P$ (MPa) carbon dioxide cooled model
0.5	15.600747	8.989802	12.153318
1.5	15.600685	8.989674	12.153117
2.5	15.600623	8.989546	12.152915
3.5	15.600561	8.989419	12.152712
4.5	15.600499	8.989293	12.152509
5.5	15.600437	8.989167	12.152306
6.5	15.600376	8.989041	12.152103
7.5	15.600314	8.988914	12.1519
8.5	15.600252	8.988788	12.151698
9.5	15.60019	8.988662	12.151495
10.5	15.600129	8.988536	12.151292
11.5	15.600067	8.98841	12.151089
12.5	15.600005	8.988284	12.150887
13.5	15.598084	8.984392	12.144966
14.5	15.596053	8.979279	12.136913
15.5	15.594	8.973901	12.128532
16.5	15.591924	8.968258	12.119828
17.5	15.589825	8.962348	12.110803
18.5	15.587701	8.956168	12.101457
19.5	15.58555	8.949719	12.091789
20.5	15.583371	8.942998	12.081801
21.5	15.58116	8.936004	12.071493
22.5	15.578918	8.928734	12.060865
23.5	15.576639	8.921189	12.049917
24.5	15.574325	8.913366	12.038649
25.5	15.571965	8.905263	12.027062
26.5	15.569543	8.896832	12.015075
27.5	15.569484	8.896577	12.01468
28.5	15.569432	8.896339	12.014327
29.5	15.569382	8.896101	12.013974
30.5	15.569307	8.895862	12.013622
31.5	15.569226	8.895624	12.013269
32.5	15.569145	8.895386	12.012917
33.5	15.569066	8.895148	12.012564
34.5	15.568985	8.894909	12.012212
35.5	15.568903	8.894671	12.011859
36.5	15.56882	8.894433	12.011506
37.5	15.568734	8.894194	12.011154
38.5	15.568645	8.893956	12.010801

**Table D.2.** Coolant Loop 2 Axial Pressure Profile at Steady State

axial position (m)	$P$ (MPa) water cooled model	$P$ (MPa) helium cooled model	$P$ (MPa) carbon dioxide cooled model
0.5	15.600784	8.989802	12.153318
1.5	15.600728	8.989674	12.153117
2.5	15.600673	8.989546	12.152915
3.5	15.600617	8.989419	12.152712
4.5	15.600563	8.989293	12.152509
5.5	15.600508	8.989167	12.152306
6.5	15.600453	8.989041	12.152103
7.5	15.600398	8.988914	12.1519
8.5	15.600343	8.988788	12.151698
9.5	15.600288	8.988662	12.151495
10.5	15.600233	8.988536	12.151292
11.5	15.600178	8.98841	12.151089
12.5	15.600123	8.988284	12.150887
13.5	15.59821	8.984392	12.144966
14.5	15.596185	8.979279	12.136913
15.5	15.594138	8.973901	12.128532
16.5	15.592069	8.968258	12.119828
17.5	15.589976	8.962348	12.110803
18.5	15.587857	8.956168	12.101457
19.5	15.585712	8.949719	12.091789
20.5	15.583538	8.942998	12.081801
21.5	15.581334	8.936004	12.071493
22.5	15.579098	8.928734	12.060865
23.5	15.576825	8.921189	12.049917
24.5	15.574514	8.913366	12.038649
25.5	15.572132	8.905263	12.027062
26.5	15.569691	8.896832	12.015075
27.5	15.569617	8.896577	12.01468
28.5	15.569541	8.896339	12.014327
29.5	15.569459	8.896101	12.013974
30.5	15.569372	8.895862	12.013622
31.5	15.569283	8.895624	12.013269
32.5	15.569192	8.895386	12.012917
33.5	15.5691	8.895148	12.012564
34.5	15.569007	8.894909	12.012212
35.5	15.568914	8.894671	12.011859
36.5	15.568819	8.894433	12.011506
37.5	15.568724	8.894194	12.011154
38.5	15.568629	8.893956	12.010801

**Table D.3.** Coolant Loop 3 Axial Pressure Profile at Steady State

axial position (m)	$P$ (MPa) water cooled model	$P$ (MPa) helium cooled model	$P$ (MPa) carbon dioxide cooled model
0.5	15.600662	8.989801	12.153314
1.5	15.600585	8.989673	12.153113
2.5	15.600506	8.989546	12.152911
3.5	15.600427	8.989419	12.152708
4.5	15.600348	8.989292	12.152505
5.5	15.600268	8.989166	12.152302
6.5	15.600188	8.98904	12.152099
7.5	15.600108	8.988914	12.151897
8.5	15.600028	8.988788	12.151694
9.5	15.599948	8.988662	12.151491
10.5	15.599868	8.988535	12.151289
11.5	15.599787	8.988409	12.151086
12.5	15.599707	8.988283	12.150883
13.5	15.597758	8.984391	12.144963
14.5	15.595702	8.979279	12.13691
15.5	15.593626	8.973901	12.128529
16.5	15.59153	8.968258	12.119826
17.5	15.58941	8.962347	12.110801
18.5	15.587266	8.956168	12.101455
19.5	15.585096	8.949719	12.091788
20.5	15.582898	8.942998	12.0818
21.5	15.580669	8.936003	12.071492
22.5	15.578408	8.928734	12.060864
23.5	15.57611	8.921189	12.049917
24.5	15.573755	8.913366	12.038649
25.5	15.571337	8.905263	12.027063
26.5	15.568852	8.896832	12.015076
27.5	15.568775	8.896577	12.014681
28.5	15.568717	8.896339	12.014328
29.5	15.568667	8.896101	12.013975
30.5	15.568622	8.895862	12.013623
31.5	15.568582	8.895624	12.01327
32.5	15.568546	8.895386	12.012918
33.5	15.568512	8.895148	12.012565
34.5	15.568481	8.894909	12.012212
35.5	15.568451	8.894671	12.01186
36.5	15.568422	8.894433	12.011507
37.5	15.568393	8.894195	12.011155
38.5	15.568365	8.893956	12.010802



**Table D.4.** Coolant Loop 1 Density Pressure Profile at Steady State

axial position (m)	$\rho \left( \frac{kg}{m^3} \right)$ water cooled model	$\rho \left( \frac{kg}{m^3} \right)$ helium cooled model	$\rho \left( \frac{kg}{m^3} \right)$ carbon dioxide cooled model
0.5	749.59131	8.2115049	112.66197
1.5	749.59204	8.2114325	112.66013
2.5	749.59283	8.2113609	112.65829
3.5	749.59363	8.2112885	112.65646
4.5	749.59442	8.2112169	112.65464
5.5	749.59515	8.2111444	112.65286
6.5	749.59595	8.2110729	112.65111
7.5	749.59674	8.2110023	112.6494
8.5	749.59753	8.2109318	112.64773
9.5	749.59833	8.2108603	112.6461
10.5	749.59912	8.2107897	112.64451
11.5	749.59998	8.2107191	112.64297
12.5	749.60089	8.2106476	112.64146
13.5	741.44507	7.7462115	106.68672
14.5	733.11078	7.3306222	101.40847
15.5	724.58954	6.9569139	96.701103
16.5	715.87164	6.6190367	92.472862
17.5	706.94611	6.3120542	88.650116
18.5	697.80054	6.0318952	85.172218
19.5	688.42108	5.7751751	81.991524
20.5	678.79211	5.5390544	79.068924
21.5	668.896	5.321135	76.372017
22.5	658.73828	5.1193771	73.873695
23.5	648.43768	4.932034	71.55114
24.5	636.99835	4.7576032	69.384956
25.5	623.72675	4.5947824	67.358589
26.5	624.16803	4.592175	67.304459
27.5	624.35962	4.5921006	67.302818
28.5	624.48608	4.5920291	67.301353
29.5	624.58667	4.5919571	67.299866
30.5	624.65454	4.5918851	67.298378
31.5	624.729	4.5918126	67.296883
32.5	624.81256	4.5917397	67.295387
33.5	624.90332	4.5916662	67.2939
34.5	624.99866	4.5915918	67.292419
35.5	625.09546	4.591517	67.290932
36.5	625.19067	4.5914416	67.289459
37.5	625.2818	4.5913663	67.287979
38.5	625.39008	4.5912914	67.286507

**Table D.5.** Coolant Loop 2 Density Pressure Profile at Steady State

axial position (m)	$\rho \left( \frac{kg}{m^3} \right)$ water cooled model	$\rho \left( \frac{kg}{m^3} \right)$ helium cooled model	$\rho \left( \frac{kg}{m^3} \right)$ carbon dioxide cooled model
0.5	749.59125	8.2115049	112.66197
1.5	749.59204	8.2114325	112.66013
2.5	749.59277	8.2113609	112.65829
3.5	749.59357	8.2112885	112.65646
4.5	749.59436	8.2112169	112.65464
5.5	749.59515	8.2111444	112.65286
6.5	749.59589	8.2110729	112.65111
7.5	749.59668	8.2110023	112.6494
8.5	749.59747	8.2109318	112.64773
9.5	749.59827	8.2108603	112.6461
10.5	749.59912	8.2107897	112.64451
11.5	749.59998	8.2107191	112.64297
12.5	749.60089	8.2106476	112.64146
13.5	741.45154	7.7462115	106.68672
14.5	733.12238	7.3306222	101.40847
15.5	724.60541	6.9569139	96.701103
16.5	715.89124	6.6190367	92.472862
17.5	706.96918	6.3120542	88.650116
18.5	697.8269	6.0318952	85.172218
19.5	688.45081	5.7751751	81.991524
20.5	678.82526	5.5390544	79.068924
21.5	668.93274	5.321135	76.372017
22.5	658.78412	5.1193771	73.873695
23.5	648.32642	4.932034	71.55114
24.5	636.94574	4.7576032	69.384956
25.5	626.15955	4.5947824	67.358589
26.5	625.59027	4.592175	67.304459
27.5	625.26831	4.5921006	67.302818
28.5	625.0127	4.5920291	67.301353
29.5	624.88885	4.5919571	67.299866
30.5	624.87244	4.5918851	67.298378
31.5	624.92554	4.5918126	67.296883
32.5	625.01385	4.5917397	67.295387
33.5	625.11493	4.5916662	67.2939
34.5	625.2157	4.5915918	67.292419
35.5	625.30969	4.591517	67.290932
36.5	625.39471	4.5914416	67.289459
37.5	625.47052	4.5913663	67.287979
38.5	625.565	4.5912914	67.286507

**Table D.6.** Coolant Loop 3 Density Pressure Profile at Steady State

axial position (m)	$\rho \left( \frac{kg}{m^3} \right)$ water cooled model	$\rho \left( \frac{kg}{m^3} \right)$ helium cooled model	$\rho \left( \frac{kg}{m^3} \right)$ carbon dioxide cooled model
0.5	749.59143	8.211504	112.66194
1.5	749.59222	8.2114325	112.6601
2.5	749.59302	8.2113609	112.65826
3.5	749.59381	8.2112885	112.65643
4.5	749.5946	8.211216	112.65462
5.5	749.5954	8.2111444	112.65283
6.5	749.59625	8.2110729	112.65108
7.5	749.59705	8.2110023	112.64938
8.5	749.59784	8.2109308	112.6477
9.5	749.59869	8.2108603	112.64607
10.5	749.59955	8.2107897	112.64449
11.5	749.6004	8.2107182	112.64294
12.5	749.60132	8.2106476	112.64144
13.5	741.43506	7.7462087	106.68658
14.5	733.09613	7.3306174	101.40823
15.5	724.57355	6.9569073	96.700798
16.5	715.85614	6.6190295	92.472504
17.5	706.93201	6.3120456	88.649712
18.5	697.78839	6.0318861	85.171783
19.5	688.41107	5.7751651	81.991058
20.5	678.78442	5.5390439	79.068443
21.5	668.89075	5.3211241	76.371513
22.5	658.73846	5.1193657	73.873184
23.5	648.58887	4.932023	71.550613
24.5	636.48218	4.7575917	69.38443
25.5	620.33673	4.5947709	67.358055
26.5	622.14105	4.5921636	67.303925
27.5	623.42017	4.5920892	67.302284
28.5	624.16333	4.5920177	67.300819
29.5	624.62067	4.5919456	67.299332
30.5	624.89667	4.5918732	67.297844
31.5	625.06586	4.5918012	67.296349
32.5	625.17493	4.5917282	67.294861
33.5	625.2525	4.5916548	67.293373
34.5	625.3147	4.5915804	67.291885
35.5	625.3703	4.5915055	67.290405
36.5	625.42358	4.5914302	67.288925
37.5	625.47638	4.5913548	67.287445
38.5	625.55176	4.5912795	67.285973

**Table D.7.** Coolant Loop 1 Coolant Axial Temperature Profile at Steady State

axial position (m)	$T$ (K) water cooled model	$T$ (K) helium cooled model	$T$ (K) carbon dioxide cooled model
0.5	561.42859	527.04205	586.37018
1.5	561.42816	527.03918	586.37018
2.5	561.42773	527.03638	586.37012
3.5	561.42725	527.03357	586.37
4.5	561.42676	527.0307	586.36981
5.5	561.42627	527.02789	586.36951
6.5	561.42578	527.02509	586.36914
7.5	561.42529	527.02228	586.36865
8.5	561.42487	527.01941	586.36804
9.5	561.42438	527.0166	586.36725
10.5	561.42389	527.01373	586.36633
11.5	561.4234	527.01086	586.36523
12.5	561.42285	527.008	586.36395
13.5	565.7431	558.36285	612.98438
14.5	569.99231	589.68213	639.53473
15.5	574.16864	620.98657	665.99707
16.5	578.26727	652.27545	692.34894
17.5	582.28308	683.54797	718.5755
18.5	586.21063	714.80334	744.66663
19.5	590.04382	746.04083	770.61774
20.5	593.77618	777.25952	796.42731
21.5	597.40045	808.45862	822.09576
22.5	600.93976	839.63727	847.62518
23.5	604.24274	870.79468	873.01825
24.5	607.28094	901.92981	898.27869
25.5	610.61298	933.04193	923.41028
26.5	610.2605	932.685	923.26135
27.5	610.42108	932.67365	923.25562
28.5	610.50848	932.66309	923.25031
29.5	610.56616	932.65265	923.24487
30.5	610.57745	932.64233	923.23938
31.5	610.59247	932.63202	923.23383
32.5	610.60065	932.62183	923.22827
33.5	610.60498	932.61169	923.2226
34.5	610.60718	932.60156	923.21692
35.5	610.60815	932.59155	923.21118
36.5	610.60846	932.58154	923.20544
37.5	610.60858	932.57166	923.19965
38.5	610.61279	932.56171	923.19379

**Table D.8.** Coolant Loop 2 Coolant Axial Temperature Profile at Steady State

axial position (m)	$T$ (K) water cooled model	$T$ (K) helium cooled model	$T$ (K) carbon dioxide cooled model
0.5	561.42865	527.04205	586.37018
1.5	561.42822	527.03918	586.37018
2.5	561.42773	527.03638	586.37012
3.5	561.42725	527.03357	586.37
4.5	561.42676	527.0307	586.36981
5.5	561.42627	527.02789	586.36951
6.5	561.42584	527.02509	586.36914
7.5	561.42535	527.02228	586.36865
8.5	561.42487	527.01941	586.36804
9.5	561.42438	527.0166	586.36725
10.5	561.42395	527.01373	586.36633
11.5	561.4234	527.01086	586.36523
12.5	561.42291	527.008	586.36395
13.5	565.74615	558.36285	612.98438
14.5	569.99182	589.68213	639.53473
15.5	574.16547	620.98657	665.99707
16.5	578.26215	652.27545	692.34894
17.5	582.27643	683.54797	718.5755
18.5	586.2027	714.80334	744.66663
19.5	590.03491	746.04083	770.61774
20.5	593.76648	777.25952	796.42731
21.5	597.39001	808.45862	822.09576
22.5	600.9408	839.63727	847.62518
23.5	604.2934	870.79468	873.01825
24.5	607.39685	901.92981	898.27869
25.5	610.80914	933.04193	923.41028
26.5	610.53033	932.685	923.26135
27.5	610.54456	932.67365	923.25562
28.5	610.54559	932.66309	923.25031
29.5	610.54401	932.65265	923.24487
30.5	610.54498	932.64233	923.23938
31.5	610.54871	932.63202	923.23383
32.5	610.55414	932.62183	923.22827
33.5	610.5603	932.61169	923.2226
34.5	610.56659	932.60156	923.21692
35.5	610.57257	932.59155	923.21118
36.5	610.57813	932.58154	923.20544
37.5	610.58307	932.57166	923.19965
38.5	610.59015	932.56171	923.19379

**Table D.9.** Coolant Loop 3 Coolant Axial Temperature Profile at Steady State

axial position (m)	$T$ (K) water cooled model	$T$ (K) helium cooled model	$T$ (K) carbon dioxide cooled model
0.5	561.42859	527.04199	586.37018
1.5	561.42816	527.03918	586.37012
2.5	561.42767	527.03638	586.37006
3.5	561.42719	527.03351	586.36993
4.5	561.4267	527.0307	586.36975
5.5	561.42621	527.02789	586.36951
6.5	561.42572	527.02509	586.36914
7.5	561.42523	527.02222	586.36865
8.5	561.42474	527.01941	586.36804
9.5	561.42426	527.01654	586.36725
10.5	561.42377	527.01373	586.36633
11.5	561.42328	527.01086	586.36517
12.5	561.42279	527.008	586.36389
13.5	565.73407	558.36304	612.98492
14.5	569.98932	589.6825	639.53589
15.5	574.16846	620.98712	665.99872
16.5	578.26813	652.27612	692.3512
17.5	582.284	683.54883	718.57837
18.5	586.21106	714.80444	744.66998
19.5	590.04364	746.04205	770.62164
20.5	593.77533	777.26093	796.4317
21.5	597.39886	808.46027	822.10077
22.5	600.99274	839.6391	847.63068
23.5	605.22552	870.79663	873.02429
24.5	607.22723	901.93201	898.28522
25.5	610.55646	933.04431	923.41736
26.5	610.13501	932.68738	923.26843
27.5	610.33051	932.67596	923.2627
28.5	610.43427	932.66547	923.25739
29.5	610.4834	932.65503	923.25195
30.5	610.51825	932.64465	923.24646
31.5	610.54199	932.63434	923.24091
32.5	610.55817	932.62415	923.23529
33.5	610.56934	932.61401	923.22968
34.5	610.57745	932.60394	923.224
35.5	610.58362	932.59387	923.21826
36.5	610.58844	932.58392	923.21252
37.5	610.59241	932.57397	923.20673
38.5	610.5979	932.56409	923.20087

**Table D.10.** Coolant Loop 1 Axial Velocity Profile at Steady State

axial position (m)	$V \left( \frac{m}{s} \right)$ water cooled model	$V \left( \frac{m}{s} \right)$ helium cooled model	$V \left( \frac{m}{s} \right)$ carbon dioxide cooled model
0	3.5654278	45.199234	17.187021
1	3.5654354	45.199497	17.186945
2	3.565443	45.199944	17.187149
3	3.5654504	45.200386	17.187357
4	3.5654578	45.200829	17.187569
5	3.5654652	45.201275	17.187778
6	3.5654726	45.201717	17.187988
7	3.5654798	45.20216	17.188198
8	3.5654871	45.202599	17.188408
9	3.5654943	45.203033	17.188616
10	3.5655015	45.203472	17.188826
11	3.5655086	45.203911	17.189034
12	3.5655158	45.20435	17.189243
13	3.5655229	45.204784	17.189453
14	3.604763	47.91515	18.148886
15	3.6457603	50.631603	19.093521
16	3.6886497	53.351452	20.022984
17	3.7335842	56.074886	20.938517
18	3.780736	58.802101	21.841425
19	3.8303006	61.533287	22.733295
20	3.8825002	64.268646	23.615196
21	3.9375885	67.008362	24.488085
22	3.9958572	69.752655	25.352837
23	4.0578437	72.501717	26.210247
24	4.1225057	75.255753	27.061047
25	4.1920009	78.014969	27.905897
26	4.2655039	80.779572	28.745411
27	4.2624264	80.825485	28.768543
28	4.2614632	80.826851	28.769262
29	4.2605081	80.828156	28.769915
30	4.2828746	80.829475	28.770578
31	4.2821231	80.830795	28.771246
32	4.2813964	80.832115	28.771915
33	4.2807031	80.83345	28.772587
34	4.2800546	80.834793	28.773256
35	4.2794542	80.836151	28.773924
36	4.2789001	80.837517	28.774593
37	4.2783933	80.838882	28.775261
38	4.2779307	80.840248	28.77593
39	4.2773461	80.841614	28.776598

**Table D.11.** Coolant Loop 2 Axial Velocity Profile at Steady State

axial position (m)	$V \left( \frac{m}{s} \right)$ water cooled model	$V \left( \frac{m}{s} \right)$ helium cooled model	$V \left( \frac{m}{s} \right)$ carbon dioxide cooled model
0	3.5651295	45.199234	17.187021
1	3.5651371	45.199497	17.186945
2	3.5651443	45.199944	17.187149
3	3.5651517	45.200386	17.187357
4	3.5651588	45.200829	17.187569
5	3.5651658	45.201275	17.187778
6	3.5651729	45.201717	17.187988
7	3.5651798	45.20216	17.188198
8	3.5651867	45.202599	17.188408
9	3.5651937	45.203033	17.188616
10	3.5652006	45.203472	17.188826
11	3.5652075	45.203911	17.189034
12	3.5652144	45.20435	17.189243
13	3.5652211	45.204784	17.189453
14	3.6044588	47.91515	18.148886
15	3.6454549	50.631603	19.093521
16	3.688343	53.351452	20.022984
17	3.7332757	56.074886	20.938517
18	3.7804248	58.802101	21.841425
19	3.8299859	61.533287	22.733295
20	3.8821805	64.268646	23.615196
21	3.9372618	67.008362	24.488085
22	3.9955218	69.752655	25.352837
23	4.0575895	72.501717	26.210247
24	4.1233959	75.255753	27.061047
25	4.2041125	78.014969	27.905897
26	4.2826757	80.779572	28.745411
27	4.2815957	80.825485	28.768543
28	4.2801709	80.826851	28.769262
29	4.2791133	80.828156	28.769915
30	4.2780747	80.829475	28.770578
31	4.2770562	80.830795	28.771246
32	4.2761106	80.832115	28.771915
33	4.2752843	80.83345	28.772587
34	4.2745891	80.834793	28.773256
35	4.2740121	80.836151	28.773924
36	4.2735314	80.837517	28.774593
37	4.2731228	80.838882	28.775261
38	4.2727661	80.840248	28.77593
39	4.272336	80.841614	28.776598



**Table D.12.** Coolant Loop 3 Axial Velocity Profile at Steady State

axial position (m)	$V \left( \frac{m}{s} \right)$ water cooled model	$V \left( \frac{m}{s} \right)$ helium cooled model	$V \left( \frac{m}{s} \right)$ carbon dioxide cooled model
0	3.5664375	45.198975	17.186649
1	3.5664456	45.199242	17.186579
2	3.5664537	45.199684	17.186783
3	3.5664618	45.20013	17.186993
4	3.5664699	45.200573	17.187202
5	3.5664783	45.201019	17.187412
6	3.5664864	45.201462	17.187622
7	3.5664949	45.2019	17.187832
8	3.5665033	45.202339	17.188042
9	3.5665119	45.202778	17.18825
10	3.5665205	45.203217	17.188459
11	3.5665293	45.203655	17.188667
12	3.5665379	45.20409	17.188877
13	3.5665469	45.204529	17.189087
14	3.6057773	47.91489	18.148518
15	3.6467559	50.631348	19.093155
16	3.6896219	53.351196	20.022615
17	3.7345312	56.074631	20.938147
18	3.781657	58.801846	21.841053
19	3.8311958	61.533031	22.732922
20	3.8833694	64.268387	23.61482
21	3.9384322	67.00811	24.487707
22	3.9966753	69.752396	25.352455
23	4.0591254	72.501457	26.209866
24	4.1330438	75.255493	27.060661
25	4.2083883	78.014709	27.90551
26	4.2796893	80.779312	28.74502
27	4.2730894	80.825226	28.76815
28	4.2719831	80.826591	28.768869
29	4.2720132	80.827896	28.769522
30	4.2718778	80.829216	28.770185
31	4.2716689	80.830536	28.770855
32	4.2713981	80.831856	28.771524
33	4.271071	80.833191	28.772194
34	4.2706923	80.834534	28.772863
35	4.2702789	80.835892	28.773533
36	4.2698483	80.837257	28.7742
37	4.2694144	80.838623	28.77487
38	4.2689891	80.839989	28.775537
39	4.2685018	80.841354	28.776205

**Table D.13.** Heat Transfer Coefficients Axial Profile in Vessel at Steady State

axial position (m)	$V \left( \frac{m}{s} \right)$ water cooled model	$V \left( \frac{m}{s} \right)$ helium cooled model	$V \left( \frac{m}{s} \right)$ carbon dioxide cooled model
0.5	21869.58	3525.3315	2957.7214
1.5	22056.564	3575.9209	3003.7456
2.5	22257.854	3623.2297	3050.2505
3.5	22475.074	3667.5989	3096.4426
4.5	22709.891	3709.387	3141.9202
5.5	22963.777	3748.8918	3186.3704
6.5	23237.531	3786.3635	3229.6638
7.5	23530.195	3822.0139	3271.7051
8.5	23836.174	3856.0239	3312.4329
9.5	25247.863	3888.5488	3351.8542
10.5	28369.084	3919.7227	3389.9556
11.5	28629.84	3949.6626	3426.7681
12.5	90718.391	3978.4707	3462.3171
13.5	21891.168	3525.3315	2957.7214
14.5	22078.195	3575.9209	3003.7456
15.5	22279.541	3623.2297	3050.2505
16.5	22496.832	3667.5989	3096.4426
17.5	22731.721	3709.387	3141.9202
18.5	22985.689	3748.8918	3186.3704
19.5	23259.537	3786.3635	3229.6638
20.5	23552.324	3822.0139	3271.7051
21.5	23858.488	3856.0239	3312.4329
22.5	25388.85	3888.5488	3351.8542
23.5	30179.461	3919.7227	3389.9556
24.5	36130.691	3949.6626	3426.7681
25.5	85566.008	3978.4707	3462.3171
26.5	21826.607	3525.314	2957.6631
27.5	22013.67	3575.9033	3003.688
28.5	22215.027	3623.2124	3050.1934
29.5	22432.309	3667.5815	3096.386
30.5	22667.176	3709.3699	3141.864
31.5	22921.113	3748.8748	3186.3145
32.5	23194.932	3786.3464	3229.6082
33.5	23487.705	3821.9971	3271.6497
34.5	23793.918	3856.0071	3312.3774
35.5	26030.467	3888.5317	3351.7991
36.5	70058.648	3919.7058	3389.9004
37.5	27503.574	3949.6458	3426.7129
38.5	84490.914	3978.4539	3462.262

**Table D.14.** Beryllium Axial Temperature Profile in Vessel at Steady State

axial position (m)	$T$ (K) water cooled model	$T$ (K) helium cooled model	$T$ (K) carbon dioxide cooled model
0.5	598.31873	698.21509	776.9093
1.5	602.35339	727.46448	800.91479
2.5	606.3056	756.86908	824.88397
3.5	610.16998	786.40552	848.83075
4.5	613.9408	816.05219	872.75433
5.5	617.61212	845.79181	896.6532
6.5	621.17841	875.61011	920.52222
7.5	624.63495	905.49548	944.35797
8.5	627.97986	935.43817	968.15778
9.5	630.53424	965.43024	991.91803
10.5	631.32031	995.46497	1015.6375
11.5	632.94806	1025.5369	1039.3143
12.5	629.33258	1055.6411	1062.9474
13.5	598.3028	698.21509	776.9093
14.5	602.3349	727.46448	800.91479
15.5	606.28528	756.86908	824.88397
16.5	610.14838	786.40552	848.83075
17.5	613.91815	816.05219	872.75433
18.5	617.58881	845.79181	896.6532
19.5	621.15454	875.61011	920.52222
20.5	624.61066	905.49548	944.35797
21.5	627.9552	935.43817	968.15778
22.5	630.48578	965.43024	991.91803
23.5	630.89258	995.46497	1015.6375
24.5	630.1969	1025.5369	1039.3143
25.5	629.7796	1055.6411	1062.9474
26.5	598.33484	698.21588	776.91284
27.5	602.37134	727.46545	800.91882
28.5	606.32379	756.87018	824.88843
29.5	610.18762	786.4068	848.83563
30.5	613.95752	816.05365	872.75964
31.5	617.62781	845.79346	896.65906
32.5	621.19299	875.61194	920.5285
33.5	624.64838	905.49744	944.36469
34.5	627.99219	935.44031	968.16498
35.5	630.26703	965.43256	991.92572
36.5	625.53931	995.46747	1015.6457
37.5	633.13031	1025.5394	1039.3229
38.5	628.58875	1055.6439	1062.9565

# Bibliography

- [1] STEPHEN BAJOREK, E. A. (2017) *TRACE V5.0 PATCH 5 USER'S MANUAL Volume 1: Input Specification*, United States Nuclear Regulatory Commission.
- [2] (2013) "The nuke that might have been," .
- [3] (2018), "Nuclear Power Reactors," .
- [4] JENSEN, S. E. and E. NONBOL (1998) *Description of the Magnox Type of Gas Cooled Reactor (MAGNOX)*, *Tech. Rep. 87-7893-050-2*, nks.
- [5] KIM, S. (2015), "Chapter 1. Nuclear Reactor Systems," .
- [6] JOHN GIBBONS, E. A. (1984) *Nuclear Power in an Age of Uncertainty*.
- [7] (2018) "CO2 Corrosion," .
- [8] LEWARS, E. G. (2008) *Modeling Marvels*, Springer.
- [9] OF ENCYCLOPAEDIA BRITANNICA, T. E. (2018) "Carbon dioxide CHEMICAL COMPOUND," *Encyclopaedia Britannica*.
- [10] N.E. TODREAS, E. A. (2009) "Flexible conversion ratio fast reactors: Overview," *Nuclear Engineering Design*, **239**, pp. 2582–2595.
- [11] K. D. WEAVER, E. A. (2003) *Generation IV Nuclear Energy Systems – The Gas-Cooled Fast Reactor (GFR) Report on Safety System Design for Decay Heat Removal*, *Tech. rep.*, Idaho National Engineering and Environmental Laboratory.
- [12] CHENG, L.-Y. and T. Y. C. WEI (2009) "Decay Heat Removal in GEN IV Gas-Cooled Fast Reactors," *Science and Technology of Nuclear Installations*, **2009**.
- [13] AARON EPINEY, E. A. (2008) *Comparative transient analysis of the 2400 MWth GFR with the TRACE and CATHARE codes*, *Tech. rep.*

- [14] HE, X. (2016) *Validation of the TRACE Code for the System Dynamic Simulations of the Molten Salt Reactor Experiment and the Preliminary Study on the Dual Fluid Molten Salt Reactor*, Ph.D. thesis.
- [15] BALESTRI, D. (2014) *Benchmarking Thermal-hydraulic analysis code RELAP5/MOD3.2.2 beta for lead bismuth eutectic alloy on Nacie facility tests of natural and gas enhanced circulation*, Ph.D. thesis.
- [16] SCARLET, R. O. (2012) *Design of Complex Systems to Achieve Passive Safety: Natural Circulation Cooling of Liquid Salt Pebble Bed Reactors*, Ph.D. thesis.
- [17] CHENU, A. (2011) *Single- and Two-Phase Flow Modeling for Coupled Neutronics / Thermal-Hydraulics Transient Analysis of Advanced Sodium-Cooled Fast Reactors*, Ph.D. thesis.
- [18] HERBELL, H. (2009) *Multi-scale, coupled Reactor Physics / Thermal-Hydraulics system and applications to the HPLWR 3 Pass Core*, Ph.D. thesis.
- [19] LISOWSKI, D. (2013) *Thermal Hydraulic Analysis of an Experimental Reactor Cavity Cooling System with Water: Performance and Stability*, Ph.D. thesis.
- [20] S. P. SARASWAT, E. A. (2016) “Thermal Hydraulic and Safety Assessment of First Wall Helium Cooling System of a Generalized Test Blanket System in ITER Using RELAP/SCDAPSIM/MOD4.0 Code,” *ASME J of Nuclear Rad Sci*, **3**.
- [21] ASHUTOSHTIWARI, E. A. (2012) “Insertion of lead lithium eutectic mixture in RELAP/SCDAPSIM Mod 4.0 for Fusion Reactor Systems,” *Fusion Engineering and Design*, **87**, pp. 156–160.
- [22] JAYANTI, S. (2011) “HELICAL COIL BOILERS,” *THERMOPEDIA*.
- [23] (2018) “Superheated Steam,” *Nuclear Power*.
- [24] STEPHEN BAJOREK, E. A. (2017) *TRACE V5.0 PATCH 5 THEORY MANUAL Field Equations, Solution Methods, and Physical Models*, United States Nuclear Regulatory Commission.
- [25] FERZIGER, J. H. and M. PERIC (2002) *Computational Methods for Fluid Dynamics*, Springer.
- [26] DAVIES, T. (2011) “FOURIER’S LAW,” *THERMOPEDIA*.
- [27] LEMMON, E., M. HUBER, and M. MCLINDEN (2010) *NIST Standard Reference Database 23: Reference Fluid Thermodynamic and Transport Properties-REFPROP, Version 9.0*.

- [28] ET. AL., R. (2017) “Allowable heat load on the edge of the ITER first wall panel beryllium flat tiles,” *Nuclear Materials and Energy*, **12**, pp. 1067–1070.
- [29] (2012) “PRESSURE LOSS FROM FITTINGS AND EXCESS HEAD (K) METHOD,” *Neutrium*.
- [30] SLOUGH, J., G. VOTROUBEK, and C. PIHL (2011) “Creation of a high-temperature plasma through merging and compression of supersonic field reversed configuration plasmoids,” *Nuclear Fusion*, **51**.
- [31] BINDERBAUER, M. (2017) “The Heat is On,” .
- [32] WATSON, J. K. (2016) “Power Plant Simulation,” .
- [33] LI, Y. (2017) “Optimal control system for pressurizer in nuclear power plant based on NMGSA,” IEEE.
- [34] J. A. DAHLHEIMER, E. A. (1984) *the westinghouse pressurized water reactor nuclear power plant*, Westinghouse Electric Corporation Water Reactor Divisions, Nuclear Operations Division, P.O. Box 355, Pittsburgh, Pennsylvania 15230.
- [35] HAYNES, W. (2013-2014) *CRC Handbook of Chemistry and Physics*, 94 ed., CRC Press.
- [36] HWANG, G.-J. (1989) *transport phenomena in thermal control*, Hemisphere Publishing Corporation.
- [37] SHEA, J. (2011) *SEQUOYAH NUCLEAR PLANT FINAL SAFETY ANALYSIS REPORT UPDATE*, *Tech. Rep. 50-327 and 50-328*.
- [38] HOFFER, N. V., P. SABHARWALL, and N. A. ANDERSON (2011) *Modeling a Helical-coil Steam Generator in RELAP5-3D for the Next Generation Nuclear Plant*, *Tech. rep.*, Idaho National Laboratory.
- [39] A.R. RAFFRAY, E. A. (1989) “Helium-Cooled Solid Breeder Blanket for ITER,” *Fusion Technology*, **15**, pp. 858–863.
- [40] ZHU, Q. (2017) “Innovative power generation systems using supercritical CO<sub>2</sub> cycles,” *Clean Energy*, **1**, pp. 68–70.
- [41] OF STANDARDS, N. I. and TECHNOLOGY (2017), “NIST Chemistry WebBook, SRD 69,” .
- [42] R SCHULTZ, K., L. BROWN, G. E BESENBRUCH, and C. J HAMILTON (2003) “Large-scale production of hydrogen by nuclear energy for the hydrogen economy,” .

- [43] SOFTWARE, S. P. (2017) *Introduction to pipeline flow-induced vibration*.
- [44] SHIGEHIKO KANEKO, E. A. (2008) *Flow Induced Vibrations*, ELSEVIER.
- [45] BAXI, C. (1995) “Design, Fabrication and Testing of a Helium Cooled Module,” *Fusion Engineering and Design*, pp. 22–26.
- [46] JOHN H. ROSENFELD, E. A. (1993) “Test results from a Pumped Single Phase Porous Metal Heat Exchanger,” vol. 1997, SPIE.
- [47] GORDON, R. and J. COBONQUE (1963) “Heat Transfer Between a Flat Plate and Jets of Air Impinging On it,” *International Developments in Heat Transfer*, p. 454.
- [48] SHIMUZU, A. (1997) “Gas Solid Suspension Cooled Fusion Power Reactor Concept,” US-Japan Workshop on Fusion High Power Density Devices.
- [49] J. SCHLOSSER, E. A. (1991) “Development of High Heat Flux Components for Continuous Operation in Tokamaks,” 4th Symposium on Fusion Engineering.
- [50] S. KAKAC, E. A. (1987) *Handbook of Single Phase Heat Transfer*, J. Wiley and Sons.
- [51] C.B. BAXI, E. A. (1996) “Design and Fabrication of Helium Cooled Vanadium Module for Fusion Applications,” .
- [52] EDWARD J. PARMA, E. A. (2011) *Supercritical CO<sub>2</sub> Direct Cycle Gas Fast Reactor (SC-GFR) Concept*, Sandia National Laboratory.